Novel Protein Delivery Platforms to Modulate SDF-1α/CXCR4 Signaling in the Adult Cortex

by

Dipankar Dutta

A Dissertation Presented in Partial Fulfillment
of the Requirements for the Degree
Doctor of Philosophy

Approved July 2016 by the
Graduate Supervisory Committee:

Sarah Stabenfeldt, Chair
Jeffrey Kleim
Mehdi Nikkhah
Rachael Sirianni
Brent Vernon

ARIZONA STATE UNIVERSITY

August 2016

ABSTRACT

Stromal cell-derived factor-1α (SDF-1α) and its key receptor, CXCR4 are ubiquitously expressed in systems across the body (e.g. liver, skin, lung, etc.). This signaling axis regulates a myriad of physiological processes that range from maintaining of organ homeostasis in adults to, chemotaxis of stem/progenitor and immune cell types after injury. Given its potential role as a therapeutic target for diverse applications, surprisingly little is known about how SDF-1α mediated signaling propagates through native tissues. This limitation ultimately constrains rational design of interventional biomaterials that aim to target the SDF-1α/CXCR4 signaling axis. One application of particular interest is traumatic brain injury (TBI) for which, there are currently no means of targeting the underlying biochemical pathology to improve prognosis.

Growing evidence suggests a relationship between SDF-1α/CXCR4 signaling and endogenous neural progenitor/stem cells (NPSC)-mediated regeneration after neural injury. Long-term modulation of the SDF-1α/CXCR4 signaling axis is thus hypothesized as a possible avenue for harnessing and amplifying endogenous regenerative mechanisms after TBI. In order to understand how the SDF-1α/CXCR4 signaling can be modulated *in vivo*, we first developed and characterized a sustained protein delivery platform *in vitro*. We were the first, to our knowledge, to demonstrate that protein release profiles from poly(D,L,-lactic-*co*-glycolic) acid (PLGA) particles can be tuned independent of particle fabrication parameters via centrifugal fractioning. This process of physically separating the particles altered the average diameter of a particle population, which is in turn was correlated to critical release characteristics. Secondly, we demonstrated sustained release of SDF-1α from PLGA/fibrin composites (particles embedded in fibrin) with tunable burst release as a function of fibrin concentration. Finally, we contrasted the spatiotemporal localization of endogenous SDF-1α and CXCR4

expression in response to either bolus or sustained release of exogenous SDF-1α. Sustained release of exogenous SDF-1α induced spatially diffuse endogenous SDF-1/CXCR4 expression relative to bolus SDF-1 administration; however, the observed effects were transient in both cases, persisting only to a maximum of 3 days post injection. These studies will inform future systematic evaluations of strategies that exploit SDF-1α/CXCR4 signaling for diverse applications.

DEDICATION

For my parents who worked so hard to put me on this path, my brother for setting a good example, and my friends for making this such a fulfilling experience.

ACKNOWLEDGMENTS

First and foremost, I want to thank my advisor, Dr. Sarah Stabenfeldt, for giving me the opportunity to work in her lab and dedicating so much of her time and effort to me over the last few years. Her mentorship has allowed me to develop and be comfortable with most basic skills in science; experimental design, execution and communication. I appreciate how Sarah always made herself available for questions and guidance. She fostered an environment where her students were challenged, but never burdened. She consistently pushed me to perform at my best, but also allowed me to take some time off when I needed it. Her balanced approach towards her mentorship is an important reason I am able to reach this point.

I would also like to thank my committee members, Drs. Jeffrey Kleim, Mehdi Nikkhah, Rachael Sirianni, and Brent Vernon for their continued support and guidance. I am very fortunate to their collective expertise guiding the work I have completed. Special thanks to Dr. Rachael Sirianni who got me started with PLGA systems, which is the basis for a large part of this document.

I would like to thank the entire Stabenfeldt lab team. Specifically, Chase Fauer, Crystal Willingham and Mariama Salifu who have been instrumental in helping me finish up experiments leading up to this document. Crystal has put in many hours to making sure the animal experiments were finished following an expedited schedule. Chase and Mariama both started working with me since they began their undergraduate studies and have contributed immensely. Chase has put in countless dedicated hours into a lot of the work presented here, so special thanks to you. Thanks to Caroline Addington, Vimala Bharadwaj, Paul Song and William Marsh who have not only lent me their expertise when needed, but also have supported me with their friendship. I would also like to thank Dr. Jeff Kleim and Nagheme Thomas for training me with animal

surgeries, perfusion, behavioral assessments and allowing me liberal access to their surgical suite. I would like to thank Dr. Christine Pauken for her expertise with and training with cell culture and Dr. Sisouk Phrasavath for training me with the SEM.

This work was made possible using equipment at the John M. Cowley Center for High Resolution Electron Microscopy and William M. Keck Imaging Lab. I would like to thank Caroline Addington and Vimala Bharadwaj for assistance with confocal microscopy.

This work was funded by Arizona State University start-up funds, the National Institutes of Health, and the National Science Foundation. Travel funds to attend national and international conferences came from the School of Biological and Health Systems Engineering and the Graduate and Professional Student Association at the Arizona State University.

TABLE OF CONTENTS

Page

CHAPTER Page

LIST OF TABLES

Table Page

LIST OF FIGURES

Figure Page

PREFACE

The work represented in this dissertation document has been previously published in the form of two review articles (Chapters 1 & 2, *J. Polym. Sci. Part B, 2012* [1], & *Biomarker Insights*, *2015* [2]) and two original research articles (Chapters 3, 4, *J. Biomed. Mater. Res. A, 2015* [3], *& J. Mater. Chem., 2015* [4]). These published works have been expanded upon and adapted for use in this dissertation document.

CHAPTER 1

INTRODUCTION

The general public has a grasp of the overall function of stem cells during the developmental stages of life; they are self-renewing units that divide to create new and specialized cells. However, the reality that the majority of tissues in adult humans also contain populations of stem cells has yet to disseminate as widely. In fact, the idea of a stem cell originated in the 19th century as a hypothesis for how an adult can self-renew short-lived cells (i.e. skin, blood etc.) over an entire lifetime [5]. Although most of the stem cells found in adults are restricted to only certain cell types or lineages (i.e. they do not have the potency of an embryonic stem cell), they do have the capacity to: 1) self-renew perpetually and, 2) give rise to new, and fully differentiated cell types. One of their main functions in healthy adults is to, generate fully differentiated cells at the rate at which they are lost (i.e. maintain homeostasis).

Another complementary hypothesis beginning to gain favor is that stem cells in adults are also meant to help cope with environmental stresses. For example, injury or disease in adults activates/amplifies similar cellular signaling that guide stem cell-mediated tissue generation during development. The ligand, stromal cell-derived factor-1 (SDF-1) and its key receptor, CXCR4 has garnered significant attention due to its correlation with stem cell-mediated regenerative processes in the injured liver, muscle, heart, bone and central nervous system (CNS) [6]. This chapter will first introduce the SDF-1/CXCR4 cellular signaling cascade and its importance to tissue engineering as a whole. The work presented is in the context of traumatic brain injury (TBI), and thus the motivation and its pathophysiology will be discussed. Finally, this section will end with a discussion on bioengineering approaches for protein delivery centered on SDF-1/CXCR4 signaling in the CNS.

1.1 The Stromal Cell-Derived Factor-1α (SDF-1α) and CXCR4 Signaling Axis

1.1.1 Stromal Cell-Derived Factor-1: The Molecule and its Receptors

Stromal cell-derived factor-1 (SDF-1) is a chemoattractant cytokine (chemokine) with a molecular weight of ~8-14kDa and an isoelectric point of pH ~9.6 [4]. Chemokines are generally classified in four groups (CXC, CC, C, and CX3C); SDF-1 belongs to the CXC family and is also commonly known as CXCL12. Six splice variants of the SDF-1 gene have been identified. The two most studied isoforms are: 1) SDF-1α, an 89 amino acid protein that is the predominant isoform found in most tissues and, 2) SDF-1β, which has four additional amino acids at the C-terminus [7]. The remaining four isoforms have 1, 30, 31 and 51 amino acid extensions at the C-terminus and are known as, SDF-1ε, SDF-1γ, SDF-1δ, and SDF-1φ, respectively [8]. All alternate splice variants are expected to be functional and are differentially expressed throughout the body. The functional significance for the diversity in splicing variants and how their expression is regulated is unclear. SDF-1α has a short plasma half-life of 25mins and the extensions at the C-terminus may putatively provide protection from proteases (e.g. carboxypeptidase N) [9], [10]. However, quantitative analysis contrasting bioactivity and stability between all known SDF-1 isoforms is currently unavailable [9]. SDF-1α is the most common variant of SDF-1/CXCL12 used to conduct studies in literature thus far.

Chemokines interact with receptors of the G-protein-coupled seven-span transmembrane receptor (GPCR) superfamily. The first receptor discovered to interact with SDF-1 is the CXC receptor 4 (CXCR4). Similar to other GPCR receptors, SDF-1α/CXCR4 binding initiates mitogen-activated protein kinase (MAPK) signaling through the Akt and ERK1/2, and IP3 pathways that regulate intracellular calcium concentrations as well as, cell survival, proliferation, activation and chemotaxis [11]–[14]. In addition, β-arrestin pathway can also be activated to internalize the SDF-1α/CXCR4 complex.

Mechanisms controlling CXCR4 internalization and subsequent recycling is not clear, but may provide means for tuning sensitivity to extracellular SDF-1α [11], [13]. Recent studies have shed light on a second receptor, CXC receptor 7 (CXCR7) that is also implicated in regulating SDF-1α-mediated signaling [15]. CXCR7 is an atypical chemokine receptor thought to be incapable of transducing any intracellular signaling characteristic of chemokine receptor activation (i.e. intracellular calcium mobilization, MAPK signaling etc.) [16]. Thus, some reports characterize CXCR7 as a decoy receptor with the role of sequestering SDF-1 [17], [18]. Conflicting reports propose mechanisms for CXCR7-mediated intracellular signal transduction and regulation through heterodimerization with CXCR4 among other mechanisms [19], [20]. Others studies indicate CXCR7-mediated signaling may be more important for regulating angiogenesis in tumor development [17], [21]. The full extent of interactions and interplay between SDF-1α, CXCR4 and CXCR7 remains to be determined. However, the SDF-1α/CXCR4 signaling axis, and the directed migration of CXCR4+ cells are more widely characterized.

1.1.2 Function and Regulation in Healthy Tissues

Morphogenesis requires migration of precursor cells to reach developing organs where they undergo proliferation and differentiation. SDF-1/CXCR4 signaling is instrumental in orchestrating the migratory patterns and organization of stem/progenitor cells during development. CXCR4 is expressed in several types of precursor cells that include embryonic pluripotent stem cells as well as, multipotent stem cells (e.g. neural, skeletal lineages etc.) [6]. In addition, to CXCR4 expression, these precursor cells also have the capacity to migrate down SDF-1 gradients [22]. Genetic knockout of either SDF-1 or CXCR4 genes in mice is lethal, causing embryonic death in utero due to anomalous organ structures [23]. Multiple studies have shown that critical

developmental processes such as, hematopoiesis, organogenesis (cardiac, cerebellar, renal, gastro- intestinal tract etc.), angiogenesis, B-cell development and others are at least partly guided by the SDF-1/CXCR4 signaling axis [6], [22]–[25].

After development, populations of (multi- or uni-potent) stems cells in healthy adults are found ubiquitously in organs throughout the body in specialized microenvironments termed, niches [26], [27]. Stem cell activity in their niches is highly regulated and varies depending on the type/function of tissue. An important role of SDF-1α/CXCR4 signaling in adults is to direct these populations of stem cells towards maintaining organ homeostasis. For example, the turnover rate for blood cells is high relative to cells in other types of tissues. As such, hematopoietic stem cells in adult bone marrow continuously produce new cells at a complimentary rate [23]. Similarly, proliferation and cellular turnover is also high in the epidermis and the intestinal epithelium compared to the central nervous system (CNS) or liver, where the stem cells are retained in a more quiescent state [26]. The SDF-1/CXCR4 signaling axis plays important roles specific to the modulation of endogenous stem cells.

1.1.3 Function and Regulation during Pathology

The SDF-1/CXCR4 signaling axis has a hand in perpetuating a number of pathological states. Migration of cancer stem cells (CSC) is important in tumor growth and metastasis. Populations of CSCs are documented for leukemia, and tumors in the brain, breast, lungs, prostate and others [6], [28]–[32]. CSCs in most (if not all) of these cases are CXCR4+ and respond to a SDF-1 gradients [6]. As a result, several studies indicate chemoattraction of CSCs towards organs with relatively high SDF-1 levels [28], [29], [32]. For example, CXCR4+ CSCs from, breast and prostate cancers selectively metastasize to the bones and/or lymph nodes, presumably in an SDF-1 gradient-dependent manner [29], [32]. Aberrant expression of SDF-1/CXCR4 is also associated to

several CNS disorders such as dementia, multiple sclerosis, among others [14]. SDF-1/CXCR4 signaling controls homing of systemic immune cells and may also be implicated in autoimmune disorders such as adhesion and chemotaxis of autoimmune lymphocytes [33], [34]. Furthermore, CXCR4 is one of the primary receptors that mediate infectivity of human immunodeficiency virus-1 in leukocytes [35].

On the other hand, SDF-1/CXCR4 signaling plays a key role in managing the endogenous repair response after injury. Secretion of SDF-1 has been detected by stromal and endothelial cells of the brain, heart, liver, kidney, skeletal muscle and others [22]. In fact, evidence suggests that proliferative, migratory and differentiation cues are upregulated to mobilize endogenous stem cells after injury across diverse systems of the body. For example overexpression of SDF-1 is detected in damaged tissues that include the brain [36], skin [37], heart [38], liver [39], bone [40], and damage due to chemotherapy [22], [41]. Local overexpression of SDF-1 acts as a homing beacon for local and systemic CXCR4+ stem cells that migrate specifically to areas of injury. CD34+ stem cells in the peripheral circulatory system migrate across the basal lamina of the endothelium after local activation of cell-adhesive integrins to follow a SDF-1 source in the parenchyma of injured tissue, such as the brain [21], [42], [43]. Once at the site of injury, stem/progenitor cells promote regeneration, not only by providing trophic support, but also through differentiation and integration to replace lost tissues [2]. This form of stem cell homing through SDF-1/CXCR4 signaling is observed for diverse tissues throughout the body and is thus considered a promising therapeutic target for regeneration. The adult CNS has its own stem cell niche(s) and there are ongoing efforts to regulate its function in the context of various pathological conditions such as stroke, Alzheimer's disease, cancer, etc. Our interest in SDF-1/CXCR4 signaling within the CNS

specifically relates to the activity of endogenous neural progenitor/stem cells after traumatic brain injury (TBI).

1.2. Epidemiology of Traumatic Brain Injury (TBI)

Approximately 5.3 million individuals are affected by traumatic brain injury (TBI) annually, within the US alone [44], [45]. Among them, 43% of TBI survivors report having sustained and/or progressive disabilities one year after injury [46]. TBI is also correlated to the development of other disorders such as chronic traumatic encephalopathy, dementia, depression, epilepsy and Alzheimer's disease [47], [48]. Moreover, the incidence of TBI has been on the rise in recent years largely attributed to military conflicts as well as increasing popularity of football, soccer and other forms of contact-sports [45]. As such, TBI accounts for an estimated $76.5 billion strain on U.S. healthcare and economy each year [2]. TBI represents a substantial public health concern that has garnered public attention in recent years.

1.3. Pathophysiology of Traumatic Brain Injury

Trauma to the brain is classified in two categories based on etiology and the resulting biochemical sequelae. Acute injury refers to concussions, mild-to-moderate TBI, as well as catastrophic, or severe TBI brain injury that may lead to death [49]. Chronic injuries on the other hand, is characterized by sustained and progressive neurodegenerative disorders such as chronic traumatic encephalopathy (CTE) [50]. Acute injuries also increase the risk factor of developing chronic disorders. For example, CTE is correlated to repeated concussions and/or mild TBIs prevalent in contact sports such as boxing, ice hockey etc. [50]. The outcome of mild-to-severe TBI is further dependent on two disparate phases of injury. The first phase known as, the primary injury, is defined as damage to neural tissues and its vasculature caused directly by a mechanical insult. The magnitude, location and directionality of forces (blast, linear

and/or rotational forces) dictate the effects of the primary damage (i.e. focal, diffuse, severity etc.). Primary injuries cause contusion(s), laceration(s), intracranial hemorrhaging, ischemia and neuronal death (by necrosis) [2]. The primary injury subsequently sets off a complex series of biochemical signaling cascades that propagate at the cellular and sub-cellular scales resulting in secondary injury. This prolonged phase of the injury is due to imbalances in the metabolic and ionic homeostasis, as well as, inhibitory autocrine and paracrine signaling between CNS and systemic cell types [51], [52]. Secondary injury is characterized by breakage of the blood-brain-barrier (BBB), chronic inflammation and upregulation of apoptotic/necrotic pathways. The sustained effects of secondary injury may persist for weeks causing progressive functional and cognitive impairments.

1.3.1. TBI Injury Progression

A period of hyperglycolysis begins immediately after the primary insult around the injury site that lasts for 0.5 - 4hours in animal models [53], [54]. Unregulated release of excitatory neurotransmitters, such as glutamate and aspartate, is thought to be a contributing factor [55]. Glutamate-mediated generation of sustained action potentials (leading to excitotoxicity) greatly increases the metabolic rate of the affected area(s) through the activity of ion pumps attempting to maintain adequate ion concentration gradients [51], [55], [56]. Non-excitable cells such as astrocytes also contribute to post-TBI hyperglycolysis. In addition to providing structural and metabolic support, astrocytes aid neurons by maintaining ionic homeostasis and regulating neurotransmitter concentrations [57]. Increased rates of neuronal firing after injury causes a massive efflux of ions (such as potassium) into the brain extracellular matrix (ECM) which in-turn activates astrocytic ion (and glutamate) pumps [57]. This action increases the overall metabolic demand to unsustainable levels in the injured tissue since

damage to the vasculature leads to inadequate rates of both, nutrient and waste product exchange [51]. As a result, cellular ATP stores eventually deplete and increases the concentrations of ADP, AMP, lactic acid and eventually uric acid as well as reactive oxygen species [58]. Glutamate also causes overstimulation of calcium ion channels, increasing intracellular calcium concentration [56]. High calcium levels combined with reactive oxygen species formation begins catabolic metabolism processes that include increased (plasma and mitochondrial) membrane permeability, DNA structural changes and eventually, activation of apoptotic signaling [51].

At the cellular level, the primary injury initiates neuroinflammation comprised of complex cellular interactions and phenotypic changes. Moreover, infiltrating systemic leukocytes and macrophages (mobilized by upregulation of adhesion molecules and chemokines) may also participate in the inflammation after TBI [59]. A number of proinflammatory factors are upregulated within minutes after injury and may also include proteases, lipid peroxidases and vasoconstrictors that further aggravates the injury microenvironment [2], [51]. Aberrant neurotransmitter and soluble signaling factor concentrations activates microglia, the resident immune cells and phagocyte of the CNS [52]. Activated microglia act to insulate the injury area form healthy tissue through: 1) directed movement of its processes and 2) migrating to the injury site, if necessary [47]. In the acute phase of injury, activated microglia, release more glutamate as well as, pro- and anti-inflammatory cytokines [51], [52]. Disruptions in metabolic and ionic homeostasis plays a role in cellular influx of Ca^{2+}, Na^{+} and K^{+} ions, where Ca^{2+} influx is thought to be initiate astrogliosis (adopting the reactive astrocyte phenotype) after brain injury [51], [60], [61]. In addition, rises in intracellular Ca^{2+} also induces astrocytes to release vasoconstrictors (endothelin-1), matrix metallopeptidase 9 (degrades ECM) and more glutamate [62].

At the tissue level, neural injury immediately leads to a disparity in cerebral blood flow and metabolic need due to either hypo- (causing ischemia) or hyperperfusion (increasing intracranial pressure). Focal or global ischemia (hypoperfusion) may occur after TBI where the ischemic brain volume is directly associated with overall neurological outcome [51]. Osmotic imbalance caused by breakdown of autoregulatory processes often leads to edema formation (and increases intracranial pressure) after TBI. Disruption of blood vessels activates the coagulation cascade leading to deposition of intravascular thrombi in the pericontusional brain tissue. This post-traumatic coagulation process occludes venules and, possibly arterioles leading to further reductions in local blood flow [63]. Neural injury invariably leads to the breakage of the BBB where TBI severity is correlated to the extent of BBB breakage [64]. Additionally, catabolic/proteolytic processes, infiltration of systemic cells, neuroinflammation, oxidative stress and other factors have shown to exacerbate BBB permeability post-injury [65]. The cumulative inhibitory signaling and auto-regulatory failure may lead to further long term neuronal loss and as a result, degradation of motor and cognitive functions, well after the primary injury.

1.3.2. Duality of Signaling Molecule and Cellular Function

An important consideration for the injury microenvironment is the duality in function of the majority of signaling mediators after injury. For example, interleukin factor 1 (IL-1) is a pro-inflammatory factor synthesized mainly by activated microglia in the CNS. IL-1 acts synergistically with tumor necrosis factor alpha (TNF-α), another pro-inflammatory factor, to orchestrate the immune response and exacerbate glutamate mediated neuronal excitotoxicity [66], [67]. Interestingly, IL-1 interaction with astrocytes also shows an upregulation of the neurotrophic factor, nerve growth factor (NGF), a well-known neuroprotective agent [68]. In fact, this type of dual-role behavior

is observed for several cytokines [52], including the anti-inflammatory signal, IL-6, which on one hand, inhibits TNF-α and stimulates angiogenesis, but on the other, upregulates chemotactic signaling and adhesion molecule production that promotes recruitment of monocytes from the systemic circulation [69], [70]. Another example is SDF-1α, a potent chemotactic agent important in regulating the endogenous regeneration after injury, but it also has been correlated to a tumorigenic potential (mobilization of cancer stem cells) and neuropathic pain [71].

The same duality in activity that some cytokines seem to exhibit is also true for certain CNS cell types. For example, although astrocytes play a pivotal role during the acute injury phase (metabolic support, production of neurotrophic factors), they are also heavily involved in the process of glial scar formation later on; a process that is thought to inhibit neural regeneration [72]. As mentioned earlier, microglia are involved in excitotoxicity of neurons, release of pro-inflammatory cytokines and other inhibitory functions. At the same time, they have also been shown to release neurotrophic factors, degrade cellular debris/non-functional proteins from dead or dying cells and modulate neural plasticity by helping to incorporate new neurons into existing networks [73], [74]. This functional duality of cellular/molecular mediators in the injury microenvironment may be one reason why current clinical treatments for TBI do not yet address the underlying biochemical pathology.

1.3.3. Current Treatment Practices & Clinical Trials

Lack of effective treatments for TBI is considered one of the greatest unmet needs in modern medicine [75]. Immediately after the patient's arrival to a hospital due to a moderate to severe TBI, the first priority is rapid patient resuscitation (if needed) and stabilization. Subsequently, standard protocols involve only management of symptoms rather than treatment of underlying pathologies. The intracranial pressure and cerebral

blood flow is monitored and if necessary, a craniotomy may be performed to address increased intracranial pressure [76]. Additionally, there are no reliable means of preventing worsening of symptoms, only addressing them as they manifest. For example, anticonvulsant treatments are administered if the patient develops post-traumatic seizures [76]. For the sub-acute and chronic phases on injury, treatment is usually limited to behavior/cognitive therapy that include therapeutic exercise, psychological interventions, sleep management etc. [76]. No phase III clinical trials for neuroprotective agents have shown a significant benefit after TBI [75].

1.4. The Role of Neural Progenitor/Stem Cells (NPSC) after TBI

Until a few decades ago, neurogenesis in adults from endogenous sources was thought to be unlikely, if not impossible. In the 1960's, several studies began to challenge that notion, notably with the discovery of immature neurons in the dentate gyrus of the hippocampus [77], [78]. Today, the community has established a degree of understanding about the maintenance, migration, differentiation and integration of neuronal precursors in the CNS during normal and pathological conditions.

1.4.1. The Neurogenic Niche in the Healthy Adult Brain

The neurogenic niches for neural progenitor/stem cells (NPSC) are located near the subgranular zone (SGZ) in the dentate gyrus of the hippocampus and the subventricular zone (SVZ) of the lateral ventricles. Their normal functions include continuous generation of neuroblasts in the SVZ that migrate along the rostral migratory stream reaching the olfactory bulb (OB). Once at the OB, they are capable of differentiating into interneurons and integrating into existing circuitry (Figure 1A) [2], [79]. In rodents, this process is thought to give rise to approximately 30,000 immature neurons in the olfactory bulb, per day [79]. Neuronal precursors produced in the SGZ, on the other hand, is associated with hippocampal neuroplasticity. Altogether, the activity of

NPSCs in adult brains is indispensable for learning, memory tasks and maintenance of CNS homeostasis.

1.4.2. NPSC Response to Neural Injury

After neural injury (e.g. stroke and TBI), proliferation rates in NPSC niches increases significantly, particularly in the SVZ. The niche physically increases in size to accommodate a greater number of cells [2], [80]. Furthermore, migrating NPSCs deviate from the RMS and undergo vasophilic migration to selectively accumulate forming ectopic niches at the site of injury (Figure 1B) [2], [36], [81]. NPSCs subsequently participate in modulating the signaling milieu in the injury site by secreting neurotrophic and anti-inflammatory factors; presumably in an effort for neuroprotection and regeneration. Moreover, NPSC-mediated neurogenesis in adults is not restricted simply to the SGZ, SVZ, olfactory bulb and the hippocampus. After injury to the CNS, NPSC-derived immature neurons have been detected in otherwise non-neurogenic areas of the brain such as the cortex and the striatum [4]. NPSCs also assist in preserving synaptic connectivity in the injury area [82]. As such, ablation of endogenous NPSC populations before induction of neural injury significantly exacerbates its cognitive impairments [83]. Moreover, neurogenesis in the cortex have been reported up to 4 months post-stroke in a rodent model; indicating a sustained regenerative effort from endogenous NPSCs after injury [84]. However, it is also important to note that even with such a complex endogenous repair response after injury, its effectiveness is quite low especially when compared to other tissues in the body (e.g. liver).

1.4.3. Soluble Signaling Factors that Regulate NPSC Activity after Neural Injury

SDF-1α expression increases within the injury penumbra within 24 hours after TBI and persists to approximately 3 days before reaching basal levels [81], [85]. Both *in*

vitro and *in vivo* data indicate that local increases in SDF-1α is mediated by endothelial cells, perivascular astrocytes, as well as reactive astrocytes in the peri-lesion site after neural injury [36], [85], [86]. Unpublished data from our lab largely agrees with literature where SDF-1α within the injury penumbra peak at 1-3 days post injury (DPI) and returns back to basal between 7-14 days following a rodent controlled cortical impact (CCI). Similar to pattern of SDF-1α overexpression in the injured cortex, NPSC migratory response peaks at 1-3 DPI and decreases dramatically, although not completely, by two weeks post injury [87]. SDF-1α also has a role in increasing NPSC proliferation *in vitro*, however this relationship is not as well defined in the context of TBI [2].

A number of other critical signaling factors play an important role on NPSC recruitment after neural injury [2]. Vascular endothelial growth factor (VEGF) may act directly and indirectly to induce NPSC migration and proliferation [2]. Epidermal growth factor (EGF) and fibroblast growth factor (FGF) are other both implicated in the increased proliferation of NPSCs in their niches after injury [2], [88]. Brain-derived neurotrophic factor (BDNF), on the other hand plays a more critical role in controlling NPSC differentiation and survival [89]. Overexpression of the above signaling mediators that mobilize NPSCs after injury are usually short-lived (especially for SDF-1α, VEGF, FGF & BDNF) [2]. Their concentrations reach basal levels only days post injury, coinciding with the transient migratory response of NPSCs after neural injury [2]. In addition to modulating NPSC activity, these factors directly and indirectly act on a myriad of other cells and signaling cascades [2]. Thus, from an engineering point of view, carefully modulating the bioavailability of these proteins may be a means for achieving a therapeutic effect after neural injury [2].

1.5. Strategies for Modulating the Injury Microenvironment

The injury site is inundated with a myriad of soluble and immobilized signaling factors that have complex interplay and cross-talk. We are beginning to understand how some of the intracellular signaling overlap of different signaling mediators may be of therapeutic benefit [12]. In addition to events in the molecular scale, the diversity in cell-types that participate in regulating the injury microenvironment adds to its intricacy. More importantly, many of the critical parameters in the injury microenvironment (pH, ionic stress, expression of signaling mediators & enzymes, cell types & their phenotype, BBB leakage, etc.) are dependent on the type of primary injury and are dynamic spatially, temporally. Despite this complexity, tuning the injury microenvironment may still be possible to bias the overall signaling milieu towards neuroprotection and neuro/angiogenesis. This goal may be achieved through delivery of proteins [2], agonist/antagonists [90]–[93], soluble receptors [94], [95], exogenous stem cells and amplifying the endogenous NPSC recruitment. The following sections will specifically explore how proteins may be used to modulate the injury microenvironment.

1.5.1. Stem Cell Transplants

Cellular therapy has gained considerable attention as potential means for treating diverse disorders in the CNS [96]–[99]. A wide range of studies in the CNS have tested various cell types, mesenchymal stem cells (MSCs) [100] & NSCs [101]; gene-modified stem cells [102], [103]; stem cells encapsulated in hydrogels [104]; as well as, how, where and when they are delivered [101], [105]–[109]. Several authors have reported functional improvements using these therapeutic systems employed in animal models [108], [110]–[112]. However, positive results have been mostly elusive in human trials [96], [113]**.** Cumulative results of stem cell therapy in animal models indicate that survival, retention and neuronal differentiation of implanted stem cell is <5% [2]. Such a low rate of implant survival indicates that functional improvements seen in animal models cannot

solely be attributed to implant-derived generation and integration new neurons. Instead, implants of exogenous stem cells are correlated to an increase in the concentration of neurotrophic factors (e.g. SDF-1α, BDNF, VEGF, FGF and others) and anti-inflammatory cytokines available to injury microenvironment [114]–[116]. Stem cell implants can therefore be considered to also function as a depot for releasing complex cocktails of proteins that tune the biochemical milieu of the injury microenvironment. Additionally, stem cell encapsulation in hydrogels, genetic modified and "priming" could not only produce more resilient phenotypes, but may also better bolster their capacity to provide trophic support [2], [104].

Although exogenous stem cell transplants hold great therapeutic potential, their transition to the clinic may be limited by scarcity of cell sources, high costs and possible regulatory hurdles [117]. Modulation of the endogenous populations of stem cells is thus an important alternative, which has yet to receive the same degree of attention as the field of exogenous cell implants. Moreover, cellular signaling that regulates injury response of endogenous stem cells (e.g. the SDF-1α/CXCR4 signaling axis) has overlap across diverse systems of the body. The following sections will discuss protein delivery in the CNS with a focus on proteins that regulate NPSC activity after injury.

1.5.2. Protein Delivery: Challenges in the CNS

A quick look at the pathophysiology of TBI indicates that increased bioavailability of specific signaling mediators may be used to regulate processes or biochemical cascades of interest to affect injury outcome. To that extent, a variety of different types of therapeutic approaches have been proposed which include protein (neurotrophic factors)[118]–[124],[125],[126], agonist/antagonist[90]–[93], soluble receptor delivery[94], [95] using several forms of carrier systems[94], [125], [127]. As discussed in the earlier sections, the cellular mechanisms for endogenous neurotrophic support and

neurogenesis exist even in non-neurogenic areas of the brain, like the cortical tissues, after TBI or stoke. An important (yet, often overlooked) avenue for tissue engineering is to modulate/amplify this innate capacity of NPSCs for: 1) directed, long-distance migration, 2) for their ability to provide trophic support in the injury area and, 3) even neuronal differentiation as well as integration. Protein delivery to modulate NPSC activity will need to first address some CNS-specific challenges.

1.5.2.1. Developing & Testing Biomaterials for the CNS

Recapitulating the complexity of the injury microenvironment *in vitro* to test the efficacy of biomaterials is exceedingly difficult. For example, if natural, biodegradable hydrogel-based systems are implanted, the effect of proteolytic enzymes that maybe overexpressed is difficult to model. Degradation of non-bioinert components and protein deposition may affect the mechanical properties of an implant. Materials will also be exposed to aberrant ionic concentrations and pH levels, which is especially relevant in biodegradable, poly-ester-based systems. In addition, specific and non-specific adsorption of cargo with components in the injury micro-environment may add to discrepancies between expected *in vitro* and effective *in vivo* release profiles [128]. Activated immune cells also present a special problem for nanoparticle-based systems. Initiation of phago/endocytosis cascades in the presence of nanometer scale particles is common and may also contribute to attenuating the protein concentration gradients for protein release applications [14].

1.5.2.2. The Blood-Brain-Barrier (BBB)

In addition to difficulties of modeling the injury environment in the CNS, another formidable challenge is access to the CNS. The BBB is made of specialized brain microvessel endothelial cells (BMEC), pericytes and astrocytes that maintains exquisite

control over molecular and cellular transport between blood and the CNS [2]. BMECs are characterized by the presence of an unusually low concentration of pinocytic vesicles at the luminal side and tight junctions between adjacent cells that prevent cell migration and virtually eliminate passive and paracellular transport of molecules through simple diffusion into the CNS [64]. On the parenchymal side, glial cells that make intimate contact with the BBB where normal function is regulated by paracrine/autocrine signaling of perivascular astrocytes and microglia [130]. These morphological and functional properties of the BBB represent a challenge for engineers looking to deliver therapeutic agents (especially lipid-insoluble molecules) to the CNS.

1.5.2.3. Routes of Delivery to the CNS

Intravenous (i.v.) or subcutaneous administration of proteins are subjected to a number of factors such as rapid clearance/degradation from the serum, and limited to no penetration of the BBB, especially of large proteins/peptides [131]. As a result, one study reports brain uptake of FGF was only about ~0.01% of the total injected dose [132]. Brain injury (i.e. TBI or stroke) may cause the BBB to be permeable for up to 3 days after injury [64]. This disrupting represents a potential time window where therapeutic agents (proteins and carriers such as, nanoparticles) can accumulate at relatively high concentrations in the brain interstitium. However, a global biodistribution of injected agent may increase risks of unwanted side effects. Intravenous injections may be applicable in cases where BBB is being “tricked” into letting the therapeutic agents pass into the CNS by mimicking properties of molecules that have the ability to traverse the BBB [133].

Intranasal delivery has garnered attention due to its ability to bypass the BBB in a non-invasive fashion and its patient-friendly nature. The exact mechanism(s) for its action is yet to be elucidated but one hypothesis states that following adsorption to the

nasal mucosa, the nerves from the nasal passages facilitate in transport to the olfactory bulb, spinal cord and cerebrospinal fluid [120]. Intranasal delivery appears to cause greater accumulation of drug in the olfactory bulb immediately after infusion, followed by diffusion-based transport to the rest of the brain [120], [134]. It is important to note that this can result in uneven and possibly sub-therapeutic concentrations of drug in certain areas of interest.

Intrathecal injections are made directly in the subarachnoid space of the spinal cord and thus bypass the BBB to access the CSF. Intrathecal route can be used in conjunction with a slow infusion device for sustained release of therapeutic agents. However, intrathecal injections can be risky; improper needle or catheter placement can cause serious patient complications [135].

Intracerebroventricular (i.c.v.) and intracortical injections are infusions directly in the ventricles or in the cortical interstitium, respectively. These forms of injections require surgical intervention and thus have associated risks. Infusion through the i.c.v. route means that the protein/drug has to pass the ependymal lining and in combination with slow diffusion, causes high drug accumulation at the ventricle lining relative to deeper in the brain parenchyma. The CSF in the ventricles are constantly renewed (every ~5 hrs in humans) and thus investigators will also need to consider the rate at which infused drugs will be cleared back out into the systemic circulation [135]. Intracortical injections allow for a significantly higher dose of drug/protein to be delivered to the cortex. However, in addition to risks associated with its invasive nature, diffusion is the rate limiting means of transport and thus injected agents usually only penetrate in the order of millimeters (or less) from its source [136].

1.5.3. Protein Delivery: Rational Design Criterion

Although, administration of proteins has long been assessed experimentally for their potential of neuroprotective and regenerative effects for a wide variety of CNS conditions, no commercially available solutions have survived the scrutiny of clinical trials. All modes bypassing the BBB subject proteins to one or more factors such as 1) rapid clearance from the serum/CSF, 2) degradation and/or loss of activity due to protein half-life and 3) limited to no penetration of the BBB, especially of large proteins/peptides [2]. Moreover, for cases where the BBB is bypassed, diffusion limited penetration of drug/protein into the brain parenchyma poses another significant hurdle [136]. As a result, maintaining an appropriate local concentration of a therapeutic agent over a desired time window is especially challenging in the CNS.

1.5.3.1 Spatio-temporal Presentation of Proteins Affect the Biological Response

Precise control over the concentration and localization of biomolecules is a pre-requisite for much of cellular signaling at multiple size and time scales. In addition to immobilized components such as ECM and lipid rafts in plasma membranes [137], evidence for organization also exists for freely soluble components such as transmembrane ion gradients. and spatial gradients of proteins involved in transduction of intracellular signaling [138] as well as extracellular concentration gradients of chemotactic signals [71], [81]. While the amount/concentration of exogenous protein delivered is a critical design parameter, the spatio-temporal bioavailability is thus also important (Figure 1.2). For example, intraventricular bolus injection of EGF after the fluid percussion injury model in rodents induces preferential differentiation of NPSCs towards an astroglial cell fate in the dentate gyrus and the SVZ [139]. However, epi-cortical sustained release of EGF after cortical ischemia led to a higher number of NPSCs differentiating into neurons in the SVZ [140]. In this case, data suggests controlled release of EGF is likely to be a more efficacious means of promoting neurogenesis.

Another study found that sustained release of BDNF *in vitro* affects the terminal phenotypes of differentiated NPSCs relative to daily BDNF supplementation in soluble form [141].

In other cases, sustained release of drug does not always produce a greater benefit compared to one of multiple bolus injections. Nutropin Depot® (Genentech, San Diego CA, and Alkermes, Cambridge, MA) was designed for controlled release of human growth hormone (HGH) to improve compliance in patients with growth hormone deficiency. Sustained release failed to show a significant improvement in therapeutic outcome relative to daily dosage [142]. Another example indicates that the antidepressant-like effects of BDNF when delivered over a short period of time (2 days) could not be replicated when BDNF was delivered over 10 days [143]. Additionally, receptor desensitization/downregulation due to over and/or continuous stimulation is another well-known phenomenon that may be applicable in controlled release devices [144], [145]. These are some indications that delayed or pulsed release may be more beneficial to achieve a therapeutic benefit for specific applications. One important example is how pulsatile release of insulin performs significantly better compared to sustained release at a constant concentration [146]. Thus, the same bioactive factor, when presented differently (spatially and/or temporally) may be expected to change the overall biochemical response. However, there is a paucity of studies looking to systematically contrast how protein release profiles affects the biological outcome. Development of a range of protein release platforms to have better spatial and/or temporal control may therefore be instrumental in understanding how a system of interest may be modulated efficiently.

1.5.3.2. Delivery of Multiple Growth Factors

Co-delivery and/or orchestrated delivery of proteins is an idea that is gaining traction in the field due to its potential for inducing an enhanced or even synergistic effect on functional recovery. Kojima and Tater report that co-delivery of EGF and FGF-2 intrathecally after SCI increased proliferation rates, migration of ependymal cells (may give rise to NPSCs) and spare white matter; whereas delivery of either of the two factors alone did not elicit the same response [147], [148]. Additional studies looking at neurotrophin co-delivery indicate feasibility in the CNS after injury [127], [149], [150]. Delayed release, or orchestrated release of proteins is another strategy of interest in applications where spatio-temporal presentation of proteins is critical for a desired outcome. For example, a sequential release profile of two, or more proteins that mimic biological patterns is hypothesized to stimulate angiogenesis [151]. In other cases, delayed or pulsed protein release could be especially useful for systems susceptible to protein desensitization [144], [145].

1.5.4. Protein Delivery: Protein Carriers for the CNS in Literature

Withstanding the above limitations, delivery of proteins has been proposed for and tested in pre-clinical CNS injury/disease models. The cumulative data from such studies indicate that exogenous delivery of bioactive components can 1) elicit desired biological responses in the CNS and 2) produce positive therapeutic outcomes as measured by histological and/or behavioral outcomes. The sub-sections below will summarize broad categories of biomaterials-based approaches to deliver bioactive proteins in the CNS.

1.5.4.1. Hydrogels

Hydrogels are hydrated polymeric constructs that maintain viscoelastic properties from physical and/or chemical crosslinks. Due to their high water content,

possibility for modification/functionalization (especially in synthetic polymers) and inherent similarities to biological tissues, hydrogels are an attractive class of materials for biological applications in drug/protein delivery. Due to its hydrated nature, water soluble biomolecules can simply be mixed into the gel matrix and delivered locally, often in injectable form [1]. A simple mixing process to encapsulate proteins in an aqueous environment is more likely to preserve protein structure and thus, its bioactivity. Subsequent release of cargo occurs through four major mechanisms: 1) diffusion-mediated 2) swelling-mediated 3) chemical reaction-mediated and 4) a combination of mechanisms 1, 2 and/or 3 [152]. Additionally, cargo-carrier interactions may significantly affect release rates [4], [153]. In general, diffusion is commonly the rate-limiting mechanism controlling release of encapsulated cargo from hydrogels. Thus, achieving sustained release of hydrophilic proteins (e.g. chemokines like SDF-1α) for extended periods of time (weeks) is unlikely using hydrogel-based systems [4]. Systems that have been investigated for protein delivery to the brain include fibrin (VEGF), alginate (VEGF), agarose (BDNF), collagen (VEGF, BDNF, FGF), poly(ethylene glycol)-derivatives (BDNF), 2-hydroxyethyl methacrylate (FGF), chitosan (FGF), hyaluronan/methylcellulose blends (EGF) and others [4], [140], [154]–[161]. Cumulative results for these devices indicate increased bioavailability of cargo through controlled release [154], control over NPSC phenotype in vitro & in vivo [140][155] as well as, increased NPSC proliferation and migration [156].

1.5.4.2. Polyester-Based Biomaterials

Polyester-based biodegradable materials hold the capacity for sustained protein release over longer periods of time relative to hydrogels. Poly(D,L,-lactic-*co*-glycolic) acid (PLGA) and polylactic acid (PLA) are two examples that are FDA-approved for use in humans. Protein release form PLGA-based systems is mediated by a combination of

cargo diffusion and bulk degradation of the PLGA carrier [129]. However, release is generally thought to be limited by polymer degradation rate and thus extended release (over months) has been widely reported [3], [4], [162]. Release profiles can be tuned by modulating properties of the polymer (e.g. molecular weight, copolymer ratio, end group functionalization), as well as characteristics of the carrier (e.g. size, morphology etc.) [129], [163]. Examples in literature include, achieving sustained release of FGF using PLGA nanoparticles [158]. Fon et. al. NPSCs along the migratory pathway originating from the SVZ to the OB (via the RMS) can be redirected towards poly ε-caprolactone (PCL) implants loaded with a short BDNF-mimetic ligand [164]. In a similar study, the orientation of the BDNF-loaded PCL nano-fibers affects NPSC proliferation and differentiation, indicating both physical and chemical cues can be used to modulate NPSC behavior [159]. Sustained release of BDNF from PLGA-poly(L-lysine)-polyethylene glycol (PEG) microspheres have also been proposed [165]. Composite materials that include both hydrogels and polyester-based devices are beginning to be explored to exploit/combine characteristics of both systems. For example, loaded into FGF-loaded PLGA nanoparticles dispersed within the HAMC to achieve a long-term, linear release rate with low burst release [166].

1.5.5. Exogenous SDF-1α Delivery in the CNS

Intracortical delivery of SDF-1α after lateral fluid percussion model of TBI showed some efficacy in inducing $CD34^+$ stem cell–mediated angiogenesis [167]. SDF-1 treated groups exhibited increased local expression of CXCR4, which colocalized with $CD34^+$ cells in the injury area. SDF-1 increased microvessel density in treated animals and behavioral tests corroborated histological findings with improvements in functional outcome [167]. Moreover, blocking SDF-1α/CXCr4 signaling through injection of a soluble antibody significantly decreased microvessel density and aggravated functional

outcome, suggesting an important link between $CD34^+$ stem cell mediated angiogenesis and the SDF-1α/CXCR4 signaling axis. In a different study, intracortical administration of soluble SDF-1α, 24h post TBI led to a lower degree of BBB disruption, decrease in brain edema, lower expression of pro-inflammatory cytokines and attenuated neuronal apoptosis in the area surrounding the injury [168]. Other studies show SDF-1α infusion into the lesion site after spinal cord injury (SCI) promotes axonal sprouting that is correlated to plasticity-associated functional recovery [71], [169].

A growing body of evidence supports the therapeutic efficacy of prolonged SDF-1α delivery for various applications such as wound healing[170], [171], [172], skeletal regeneration [173], [174] and myocardial infractions [175], [176], [177], [178]. These studies demonstrate the viability of recruiting progenitor cells through exogenous infusion of SDF-1α. However, there is a lack of studies that specifically elucidate the *in-vivo* effects and feasibility of local, bolus/controlled release of SDF-1α in the context of TBI/stroke. Sustained release of exogenous SDF-1α to attract/amplify the number of endogenous NPSCs appearing at the injury site after TBI or an ischemic insult *in-vivo* has yet to be demonstrated. A number of devices have been proposed that hopes to achieve controlled release of SDF-1α over different time periods that include SDF-1α loaded star PEG-heparin hydrogels [179], PLGA microparticles [180], chitosan-tripolyphosphate based nanoparticles [181], poly(lactide ethylene oxide furmate) hydrogels [182], as well as a composite gelatin/dextran and poly(N-isopropylacrylamide)-based stimuli sensitive hydrogel [183]. The above systems have been characterized *in-vitro* and seems to maintain bioactivity of encapsulated SDF-1α to various degrees. However, no such device for the sustained release of SDF-1α has been evaluated *in-vivo* after TBI or stroke to our knowledge.

1.6. Objective and Specific Aims

The innate recruitment of NPSCs from their neurogenic niches to the site of neural injury (e.g. after stroke or TBI) is correlated to a local increase in SDF-1α concentration and CXCR4 expression acutely in the injury penumbra [36], [81]. However, local SDF-1α concentrations subsequently reach baseline sub-acutely, and is presumably a key factor contributing to a significant decrease observed in NPSC homing [81], [87]. Increased bioavailability of SDF-1α from exogenous sources is thus expected to amplify and sustain NPSC recruitment [4], [36], [81].

Despite a large preponderance of evidence that suggests a link between SDF-1α/CXCR4 signaling and NPSC recruitment, previous studies conducted using various rodent models of has only focused on immune-modulation, neuroprotection and angiogenesis in response to bolus treatments of SDF-1α [21], [168], [184]. SDF-1α release devices has been proposed for various applications, but they lack tunability of release profiles and have inherently short (diffusion-limited) release periods of 7-14 days [170], [171], [173], [178]. Thus, many of these previous designs (based on alginate, collagen, gelatin, star PEG–heparin etc.) do not significantly extend bioavailability of SDF-1α past what is observed for endogenous SDF-1α in the injury penumbra. Since NPSC activity in the injury penumbra has been observed, months after neural injury, long-term release of SDF-1α is believed to have therapeutic merit [84]. To achieve sustained release of SDF-1α for longer periods, others have employed biodegradable polyesters to achieve sustained release for 40-70days [172], [180], [185]. However, the priority of these studies was to explore the feasibility of encapsulating SDF-1α rather than modulation of the release profile and *in vivo* testing. Our first goal was to develop tunable controlled release devices capable of sustained release of bioactive SDF-1α on the order months.

Our second goal aims to address gaps in our understanding of the *in vivo* spatiotemporal interplay between endogenous SDF-1α/CXCR4 expression in response to exogenous SDF-1α. As such, rational design of biomaterials that mediate predictable and long-term manipulation of endogenous SDF-1α/CXCR4 signaling axis is not yet feasible. Our approach is to contrast sustained release of SDF-1α with the biochemical effects of bolus injections. We utilized CXCR4-EGFP transgenic mice to probe the effects of fluorophore-tagged, exogenous SDF-1α [186]. This animal model allows us to distinguish spatiotemporal localization of endogenous SDF-1α/CXCR4 as opposed to exogenous SDF-1α. The long-term goal of the proposed research is to harness the regenerative potential of endogenous NPSCs with clinically translational protein-based therapies that reduce motor and cognitive deficits after TBI. Our *central hypothesis* is that local spatiotemporal bioavailability of exogenous SDF-1α mediates differential endogenous SDF-1α expression and temporal autoregulation of CXCR4. Our *rationale* for these studies is to inform and enable future systematic evaluations of strategies that exploit SDF-1α/CXCR4 signaling to amplify and/or sustain the innate NPSC migration after injury. The results may confirm or challenge the overall inclination of the community to focus heavily on devices that mediate sustained release of proteins rather than other types of release profiles, for example one that exhibits "on/off" release characteristics. The experimental approach included the following specific aims:

1.6.1. Specific Aim 1: Validate platform for controlled release of proteins with tunable release profiles.

Tuning the size distribution of a population of poly(D,L,-lactic-co-glycolic acid) (PLGA) nanoparticles (NP) alters the overall protein release profile.

1.6.2. Specific Aim 2: Explore composite release systems to modulate sustained release of bioactive SDF-1α.

PLGA NPs are hypothesized to sustain release of bioactive SDF-1α. Additionally, the positive net surface charge & heparin-binding properties of SDF-1α can be exploited through non-covalent SDF-1α/hydrogel interactions to further tune the release profile from SDF-1α-loaded PLGA NPs.

1.6.3. Specific Aim 3: Determine spatiotemporal expression of endogenous SDF-1/CXCR4 after administration of exogenous SDF-1 in the intact mouse cortex.

Hypothesis 3a: Endogenous SDF-1/CXCR4 expression will increase acutely after exposure to both bolus and controlled release of exogenous SDF-1. *Hypothesis 3b:* Bolus administration leads to transient overexpression of SDF-1/CXCR4. *Hypothesis 3c:* Sustained release of exogenous SDF-1α leads to downregulation of CXCR4 expression overtime.

Specific aim (SA) 1 explored various means of achieving a tunable sustained protein release platform. PLGA-based particulate devices were the most promising due to its 1) versatility, and 2) ability to sustain protein release over the period of months. During this process we developed novel means of tuning protein release profiles from PLGA particles without altering their fabrication parameters. SA2 validated and characterized SDF-1α encapsulation and release from PLGA nanoparticles. In addition, we reported novel protein-affinity based tuning SDF-1α burst release from fibrin/PLGA nanoparticle composites. Finally, SA3 aimed to compare the two most common forms of protein delivery, bolus and sustained release and contrasted how spatiotemporal presentation of exogenous SDF-1α affected the endogenous SDF-1α/CXCR4 signaling axis.

1.7. Figures

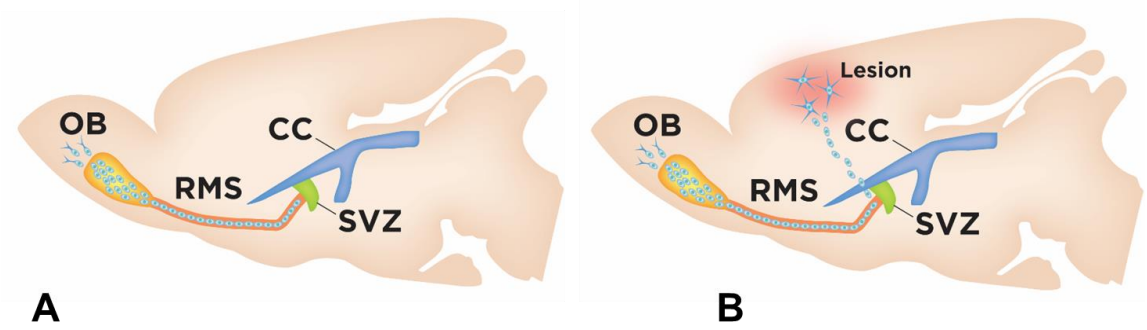

Figure 1.1: NPSC migratory behavior in the (A) normal and (B) injured brain. In normal conditions, NPSCs originating from the subventricular zone (SVZ) migrate using the rostral migratory stream (RMS) to reach the olfactory bulb where they participate in neural turnover. After TBI, migrating NPSCs deviate off of the RMS to selectively accumulate at the site of injury where they exert trophic support and hold the capacity for neuronal differentiation.

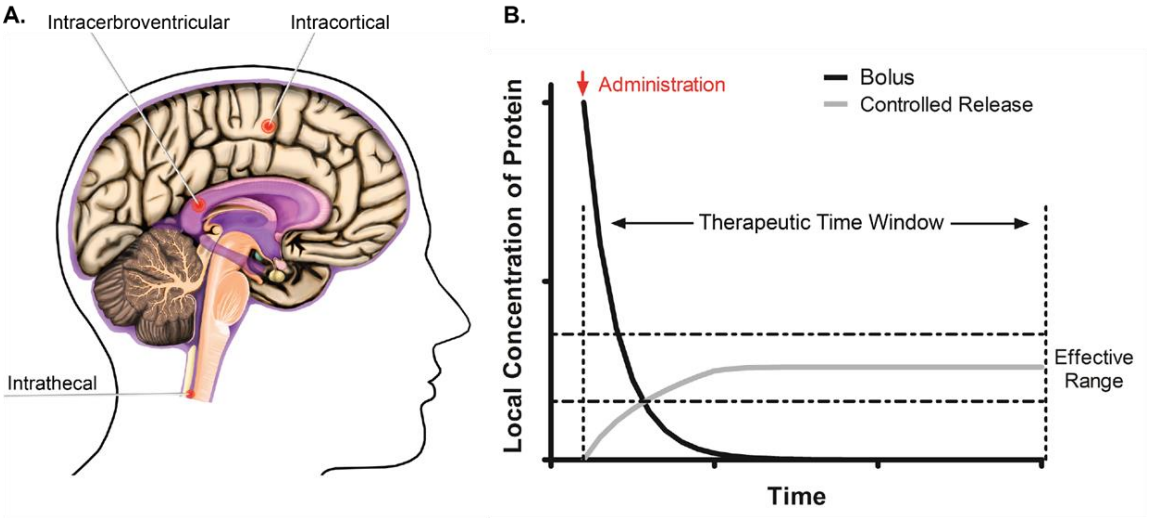

Figure 1.2: The route of delivery to the central nervous system plays a critical role in determining the spatial and temporal distribution of infused agents. (A) Demonstrates conventional means of bypassing the blood–brain barrier, which includes the

intracortical, intracerebroventricular, and intrathecal routes. Each route of delivery has its own strengths and weaknesses, and thus outcome of therapy depends heavily on proper selection of the means of administering the therapeutic agent/construct. Intrathecal injections are made directly in the subarachnoid space of the spinal cord, whereas intracerebroventricular and intracortical injections refer to infusion of drugs directly into the ventricles or into the cortical interstitium, respectively. Efficiency of drug accumulation in the CNS is very low, even in the cases where the blood–brain barrier is bypassed. This is especially a challenge for applications where high drug concentrations are required in a specific portion of the brain. (B) Bolus injections of a therapeutic have rather transient effects with minimal time in the therapeutic threshold window; however, (idealized) controlled release of bioactive molecules may achieve sustained biochemical effects throughout the therapeutic time window.

CHAPTER 2

TAILORING RELEASE PROFILES OF PROTEIN-LOADED SUB-MICRON PLGA PARTICLES USING CENTRIFUGAL FRACTIONING

2.1. Introduction

The popularity of the FDA-approved biodegradable polymer poly(D,L-lactic-*co*-glycolic acid) (PLGA) for drug delivery applications is not surprising due to the versatility of PLGA. Specifically, PLGA can encapsulate both water-soluble and insoluble molecules, facilitates tunable cargo release profiles, holds the potential for direct injection into target tissues, and consists of metabolizable degradation products [1], [187]–[190]. Moreover, PLGA matrices maintain prolonged, localized bioavailability and may aid in protecting the encapsulated cargo from degradation, a critical parameter for protein-based cargo [187], [191], [192]. Sub-micron PLGA particles are of particular interest due to the potential engineering opportunities for deeper tissue infiltration, improved cellular internalization and ability to circulate and accumulate in target tissues [187], [189], [193]–[195]. However, utility of PLGA particle systems can be compromised by undesirable release profiles, such as the characteristic large burst phase, which is followed by the desired steady state release profile. Therefore, mechanisms to tailor and refine specific aspects of the release profile are highly desirable for drug delivery applications.

One of the most common fabrication methods for PLGA particles is emulsion with solvent evaporation. Here, the fabrication parameters largely dictate the resulting particle morphological characteristics and thus play a critical role in determining cargo loading capacity and the resulting release profile (see reviews [163], [196], [197]). Previous studies have evaluated the influence of the fabrication parameters on the cargo loading and release from PLGA particles to provide general formulation trends on

obtaining broad release profile characteristics [188], [198], [199]. However, seemingly simple changes in the PLGA particle formulation may ultimately lead to a loss of desirable attribute(s) [197], [200]. For example, altering the polymer concentration in the organic phase reportedly affects both particle size and porosity, which in turn influences the encapsulation efficiency and initial burst release[201], [202]. In another example, varying the emulsifier concentration significantly affects particle size, zeta potential and encapsulation efficiency [202], [203]. Each particle formulation must therefore be thoroughly characterized to verify the final release properties. As a result, fine-tuning release profiles based solely on altering formulation parameters may prove substantially challenging and highly laborious.

Here, we describe modulation of sub-micron PLGA particle s properties via a centrifugal fractioning technique to refine the initial poly-dispersed population to refine particle sub-populations. The significance of this approach is that we have applied it to study encapsulation and release of protein for particles of varying diameter that were otherwise prepared identically. We hypothesized that the average particle diameter would directly affect protein loading and subsequent release characteristics. This post-fabrication approach is the first, to our knowledge, to directly evaluate the effect of PLGA particle size on critical release parameters while holding all fabrication parameters constant. Bovine serum albumin (BSA)-loaded sub-micron particles were fabricated with identical formulation conditions and then subjected to centrifugal fractioning. We observed particle size-dependent effects on the encapsulation efficiency, burst release, subsequent protein release rate and total release period. The results from this report significantly impact future PLGA micro/nanoparticle studies that may employ this technique as an additional tool to tune and achieve a desired release profile without altering baseline fabrication formulation parameters.

2.2. Experimental Methods

2.2.1. PLGA Particle Formulation

Sub-micron PLGA particles were synthesized via a W/O/W emulsion technique adopted from a method further described by McCall et al [204]. In short, the organic phase comprised of 100 mg/mL PLGA (PLGA; 50:50 ester-terminated; inherent viscosity = 0.55-0.75dL/g; Lactel, Birmingham, AL, USA) in ethyl acetate (Alfa Aesar; Ward Hill, MA, USA). The first emulsion was generated by vortexing the organic phase with a phosphate-buffered saline (PBS) solution containing 20mg/mL BSA (total protein content of 2.0% w/w of PLGA; Sigma-Aldrich, St. Louis, MO, USA). The above mixture was added dropwise to a 3.6x volume excess of an aqueous solution containing 2% (w/v) d-α tocopheryl polyethylene glycol 1000 succinate (TPGS; Sigma-Aldrich) under heavy vortex. The second emulsion was produced by ultrasonicating on ice for three consecutive 15s periods (Omni Ruptor 4000; Omni International; Kennesaw, GA, USA). The emulsion was then quickly transferred to a stirring aqueous bath containing 0.2% TPGS (10x volume excess; 300rpm) and left undisturbed for 3hrs to undergo solvent evaporation. The particles were washed three times by replacing the supernatant with deionized water after being centrifuged (Beckman Counter; Allegra 25R; Pasadena, CA, USA) at 15,000g for 15mins. The particles were frozen with 25% (w/w) D-(+)-trehalose dihydrate; Sigma-Aldrich) and recovered via lyophilization.

2.2.2. Centrifugal Fractioning

Following solvent evaporation, PLGA particles were subjected to centrifugal fractioning to obtain separate pellet and supernatant sub-groups (Figure 1). A total of six groups were used for the study. Fractioning (with varying parameters; Table 1) was performed on five groups, whereas the remaining was left unfractioned. Freshly fabricated PLGA particles (35.0mg) were resuspended in 0.5mL of deionized water and

carefully added atop of 5.5% (w/v) glucose solution with a density of 1.055g/cm^3 (5mL; Acros Organics, Geel, Belgium). The particles were then size fractioned (Centra CL3R; Thermo Fisher Scientific; Waltham, MA, USA) at specified centrifugal forces and spin times (Table 2.1). The supernatant and pellet fractions were separated and washed three more times with deionized water prior to lyophilization. Subsequent particle size analyses, loading and release assays were conducted for all pellet and supernatant sub-groups and compared to the unfractioned group.

2.2.3. Particle Size Analysis

Particle size analysis was performed via scanning electron microscopy (SEM). Briefly, particle samples were extracted from each group after the final deionized water rinse and mounted on to carbon tape after lyophilization. They were then coated with a gold/palladium sputter coater (108-Auto, Cressington Scientific; Watford, UK) to achieve a 5-10nm thick layer of Au/Pd. Samples were subsequently imaged with a 3-5kV electron beam (Phillips XL-30; San Francisco, CA, USA). A minimum of seven regions was imaged per particle group. ImageJ (National Institutes of Health, Bethesda, MD, USA) was employed to measure the diameter of at least 85 particles for each SEM image; thus at minimum 595 particles were measured per sample group that make up the size distribution plots. The particle polydispersity index (PDI) was approximated as the square of the standard deviation divided by the mean diameter of each group.

2.2.4. Encapsulation Efficiency

Total protein loading was determined by complete dissolution of the particles in dimethyl sulfoxide (DMSO; American Bioanalytical, Natick, MA, USA). The DMSO-polymer solution was then diluted 1:15 in 2.5% (w/v) sodium dodecyl sulfate (Sigma Aldrich) + 0.1N sodium hydroxide. The mixture was thoroughly vortexed prior to

completing a micro bicinchoninic assay (BCA; G Biosciences; St. Louis, MO, USA) to quantify protein using manufacturer's protocols. Standards were prepared with known amounts of soluble BSA supplemented with blank PLGA particles (i.e., no protein encapsulated, but produced using identical formulation/fractioning protocols). Encapsulation efficiency (EE) was calculated based on the ratio of total protein measured versus the total protein added during fabrication.

2.2.5. Protein Release Assays

Lyophilized particles were resuspended in PBS supplemented with 0.01% Tween 80 and 0.01% NaN_3 (8mg/mL) and incubated at 37°C under constant agitation. At specified time points, the particle suspensions were centrifuged at 14,000g for 15mins and supernatant was removed then replaced with fresh PBS. Release media samples were collected at the following time points: 1hr, 6hrs, 11hrs, 24hrs, 3d, and subsequently at every five days until day 83. The release media from all groups and time points was then quantified for protein content using the BCA assay following manufacturer's protocols.

2.2.6. Statistics

All results are depicted as the mean ± one standard deviation, unless otherwise noted. Statistical analyses were performed in PRISM (GraphPad Prism, La Jolla, CA) to evaluate differences between groups using analysis of variance (ANOVA), and multiplicity adjusted p-values are reported for Tukey post-hoc comparisons for significance value of $\alpha = 0.05$.

2.3. Results

2.3.1. Centrifugal Fractioning Does Not Affect Particle Morphology and Yield

The SEM micrographs indicate that the formulation protocol yields spherical particles with a smooth surface morphology and minimal batch-to-batch variability (Figure 2.1) [4], [204]. The fractioning protocol did not affect the structural integrity of the particles; qualitative differences in particle shape or surface morphology were not observed across any of the groups. Total yields for all fractioned sub-groups (pellet + supernatant) ranged between 58.5-65.7% relative to 65.1% for the unfractioned group indicating that the fractioning process also did not lead to a substantial loss of yield (Table 2.1). Collectively, average diameters for all groups evaluated in the study ranged between 211-707nm with a PDI between 0.18 - 0.74 (Table 2.1).

2.3.2. Centrifugal Fractioning Significantly Modulates Particle Size Distribution

The initial, unfractioned particles exhibited an average diameter of 341nm with a poly-dispersity index (PDI) of 0.74. The particle diameters ranged between 60nm and 2600nm with approximately 93% of the population less than 750nm in diameter (Figure 2.1A). Upon centrifugal fractioning, we observed a marked change in particle diameter distribution (Figure 2.1B). For example, exposing the initial particle population to 550g for 10mins resulted in a significantly smaller population in the supernatant with an average diameter of 224nm (PDI = 0.33) where 90% of the particles were less than 400nm in diameter (Figure 2.1B). In contrast, the pellet population for this same fractioning protocol exhibited an average particle diameter of 617nm (PDI =0.47) with 90% of the particles less than 1200nm in diameter (Figure 2.1B). Across the board, significant differences in size distributions were observed between the unfractioned population and all fractioned sub-groups (pellets and supernatants) with the exception of supernatant collected from the lowest centrifugal force with the shortest spin time (550g and 2min 15s; Table 2.1). The combination of low spin force (550g) and time (2min 15s) likely resulted in an insufficient pellet mass to significantly affect the size

distribution in the supernatant. The low pellet yield also meant further analysis of size distribution, EE and release profiles were not possible for the 550g, 2:15 pellet group (Figure 2.2A).

2.3.3. Importance of Centrifugation Parameters on Particle Size Distribution

Five different fractioning protocols were evaluated in this study, resulting in 10 different particle sub-groups. To compare the size distributions within each sub-group, we generated stacked frequency distribution bar graphs to directly visualize specific population ranges (Figure 2.2 & 2.3). Nearly half of the population in the unfractioned group exhibited diameters below 250nm. Fractioning at a centrifugal force of 550g for times ranging from 2:15 to 10:00mins resulted in a significant decrease in the 0-250nm particle sub-population in the pellet groups (15-20%; Figure 2.2A). Not surprisingly, we observed that the pelleted sub-populations were dominated by particles greater than 500nm (50-60%; Figure 2.2A). The shift in particle sub-populations resulted in approximately doubling of average pellet diameters (ranging between 607-707nm) relative to the unfractioned group (341nm). Conversely, we observed a steady increase in the smallest 0-250nm sub-population within the supernatant with respect to spin time (Figure 2.2B). Specifically, the 10min supernatant fraction had a population distribution that was significantly different compared to both unfractioned and shorter spin time sup-population groups (Figure 2.2B). Here, we observe the 0-250nm sub-population increase by 30%, while less than 5% of the particles were greater than 500nm in diameter. Collectively, this population shift resulted in an average diameter of 224nm compared to 341nm for the unfractioned group.

Altering centrifugal force between 550g (‘Low G’) and 1600g (‘High G’) while maintaining a constant spin time (10:00mins) yielded significant difference in particle size distributions between the pelleted fractions due to nuanced changes in NP sub-

populations (Figure 2.3A). Specifically, we observed a concurrent shift in two sub-populations: 250-500nm and greater than 750nm particles. The High G pellet sub-group shifted to contain a larger portion of 250-500nm particles (13%) compared to the Low G pellet sub-group (Figure 2.3A). Concurrently, the Low G pellet sub-group contained a greater number of particles larger than 750nm. No difference in average diameter was observed between the supernatant groups (Figure 2.3B). Yet, the PDI was noticeably lower for the High G supernatant (0.18) compared to the Low G supernatant fraction (0.33; Figure 2.3B) due to the lack of particles greater than 1000nm within the High G sub-populations.

2.3.4. Average Particle Diameter Affects Protein Loading and Release Characteristics

Upon demonstrating that centrifugal fractioning yields significant differences in particle populations, we next investigated the functional effects of average diameter on protein loading (encapsulation efficiency) and cargo release profile of our model protein, BSA. We observed marked differences in the encapsulation efficiencies among the particle groups, ranging from 36.4% and 49.4% (Table 2.1) with a direct relationship between average diameter and the encapsulation efficiency. Additionally, we observed a profound impact of particle size distribution on the resulting protein release profile. Release profiles for all particle sub-groups described in Figures 2.2 and 2.3 were collected and compared; for simplicity, we will conduct three main comparisons to highlight the impact of particle size (Figure 2.1 & 2.6) on release profile (Figure 2.4). First, we compared fractioned sub-groups with the largest difference in average diameter as illustrated by the cumulative frequency plots (Figure 2.6). The unfractioned group exhibited a high burst release of 30.3% of total protein in the first 24hrs followed by sustained release for 57days (Figure 2.4A). Particle populations with the smallest average diameter resulted in higher burst release (49.1%) and shorter total release period

(43days; Figure 2.4A). Conversely, the largest average diameter sub-group resulted in a lower burst release (15.8%) and longer protein release period (~78days; Figure 2.4A). Secondly, the fractioned group with average diameter and size distributions (Figure 2.6B) most similar to the unfractioned group exhibited comparable release profiles (Figure 2.4B). Thirdly, fine-tuning of the release profile based on modest yet statistically significant particle diameter distributions (Figure 2.6C) was also achieved (Figure 2.4C). The High vs Low G pellet sub-groups exhibited altered burst release (15.8% vs 22.9%, respectively) and significant difference in protein release period (63days vs 78days, respectively; Figure 2.4C).

2.3.5. Dependence of Loading and Release Characteristics on Particle Size

To highlight the key findings from this study, we probed for overarching trends in the encapsulation efficiency, burst release, release rate after burst and protein release period as a function of average particle diameter (Figure 2.5). Here, encapsulation efficiency and protein release period were directly related to average particle diameter, whereas, burst release and subsequent protein release rate was inversely proportional to average diameter. These findings provide tangible data regarding the direct impact particle size alone has on specific release characteristics. Thus, similar fractioning techniques may be employed to fine-tune release characteristics without altering sub-micron PLGA particle formulation parameters.

2.4. Discussion

PLGA is one of the most commonly investigated biodegradable polymers for applications in drug and protein delivery, where tailoring release profiles for different cargo/application settings is critical [187], [205]. In surveying methods to selectively tailor release characteristics, one is typically limited to adjusting particle formulation parameters to tune specific particle properties (e.g., size, porosity, surface

charge/coatings)[163], [190], [196], [197]. Optimization of the release characteristics is thus timely and laborious as a minor change in formulation parameters may result in a drastic shift in the release profile. Therefore, methods that modulate PLGA particle-based release properties without changing formulation parameters, such as the protocol described here, will reduce time and energy to obtain the desired controlled release system.

Previous studies have reported similar correlations in the encapsulation efficiency and release profile relative to PLGA particle average diameter [196], [200], [206]–[208]. However, these studies acquired different particle sizes by modifying particle formulation parameters that could be expected to confound encapsulation and release characteristics. Here, the PLGA particle characteristics were based solely on differences in particle size by employing centrifugal fractioning to formulation conditions previously established to yield consistent particle size distributions with minimal batch-to-batch variability [4], [204]. Our data revealed a direct relationship between average particle diameter, encapsulation efficiency and burst release; we also observed an inverse relationship between average diameter, protein release rate after burst and total release period (Figure 2.5). An example of these trends is illustrated in a comparison of the two fractioned sub-groups with a large difference in average diameter (High G supernatant and pellet sub-groups). Here, the smaller sub-group (average diameter: 211nm) exhibited the lowest observed encapsulation efficiency of 36.4% as opposed to 49.4% for the larger particle sub-group (average diameter: 541nm; Table 2.1). These results corroborate previous studies that systemically modulated formulation parameters to alter average particle diameter where they also report a positive correlation between encapsulation efficiency and average diameter[196], [206], [207].

Encapsulation efficiency is heavily dependent on the interaction of encapsulated agent with the polymer and water during the solvent evaporation stage. Here, the cargo is mobile within the dispersed oil (polymer+organic solvent) phase and is thus free to diffuse into the continuous aqueous phase [200]. Due to the higher surface area to volume ratio of smaller oil droplets, diffusion of hydrophilic proteins across the aqueous/organic interface is expected to lower encapsulation efficiency relative to larger droplets. As such, the amount of protein encapsulated is expected to relate directly to particle diameter, as we observed (Figure 2.5A). Our maximum encapsulation efficiency of near 50% is lower than previously reported PLGA micro/nanoparticles that obtained 80%, however, these studies altered the emulsifier concentration to increase the amount of protein loaded, whereas we held this parameter constant throughout the study [196], [208].

The release profiles reported here exhibit an initial burst release followed by a roughly zero-order release rate (Figure 2.4). Reported *in-vitro* release profiles from PLGA micro/nano-particles vary greatly, ranging from zero-order to monophasic, biphasic and triphasic shapes [188]. Cargo release profiles depend on interactions within the particle (i.e., cargo/polymer, cargo/cargo, etc.) and release mechanisms (i.e. diffusion, bulk/surface erosion, etc.) that are unique to each particle formulation and release conditions [188], [198]. Formulation parameters, such as the type of PLGA polymer (i.e., MW, end-group, lactide:glycolide ratio, etc.) and the resulting initial particle morphology (i.e., size, porosity and density), determine which mechanisms dominate control release rate[197]. Previous studies indicate that reversible interactions between BSA and PLGA, particularly for carboxyl end-capped polymers, dominate protein encapsulation and release rate properties [188]. Irreversible aggregation or adsorption to PLGA polymers/oligomers result in BSA instability and incomplete release

[191]. Evaluating protein stability/degradation of released BSA was beyond the scope of this study, yet the release assays reliably accounted for at least 90% of the encapsulated protein over the course of the release assays (Figure 2.4). In addition to particle morphology, population distribution (PDI) is also an important factor in determining the overall release profile. For example, Berkland et al. combined particles of various sizes to shift the population PDI, resulting in a switch in the release profile of a small, water-soluble molecule from Fickian to zero-order release[209]. Here, we observed similar linear release rates after burst for our particle groups, potentially due to the high PDI (PDI <0.1 is considered monodisperse; Table 2.1). In addition, a number of other studies report similar release profiles (semi-linear release profile after a burst phase) from micro- and nanoparticles[210], [211].

During the early release phase when PLGA particles undergo hydration and wetting of the polymer matrix, diffusion dominates the protein release profile. Surface adsorbed and loosely immobilized cargo diffuse out rapidly, resulting in the burst release[188]. This phase of the release profile is largely correlated with the initial particle porosity, cargo properties (size, effective diffusivity, charge, hydrophillicity, etc.) and hydration rate of the particle[198]. In addition, particle size also plays a significant role in affecting the initial burst release[200]. Increased surface area to volume ratio of smaller particles results in a higher burst release, since a greater percentage of the cargo is likely to be loosely surface adsorbed and/or pore immobilized in close proximity to the surface. Our data support this model whereby we observed a marked increase in burst release from the smallest and largest average particle diameter groups (Figure 2.5B). Conversely, comparing two NP groups with an average diameter and population distribution most similar to each other demonstrated no significant difference in release profile (Figure 2.4B). These results suggest that average particle diameter and diameter

distributions of particle formulated using identical parameters plays a significant role in modulating the burst release. The inverse relationship between burst release and the average particle diameter corroborates with general trends reported in literature where different micro/nanoparticle sizes were achieved by altering formulation parameters[200], [207], [212].

Probing further aspects of the release profile, we revealed relationships between the average diameter, the total release period and the release rate of BSA after the burst phenomenon (Figure 2.5C & D). Release of encapsulated cargo from PLGA particles occurs by three mechanisms: 1) transport through the polymer, 2) transport through water-filled pores and 3) transport-independent dissolution of encapsulated cargo [188]. The rate of water penetration into PLGA matrices is fast relative to the rate of polymer hydrolysis, and thus micro/nanoparticles are primarily degraded via bulk instead of surface processes [162]. Cargo diffusion through the PLGA matrix is assumed to be negligible for all but small, hydrophobic molecules [213]. Thus, after the burst phase and particle hydration, release of hydrophilic proteins such as BSA (MW = 66kDa) is mediated by diffusion through water-filled pores and is thought to be limited by the rate of PLGA degradation/erosion that produces these pores [188]. Specifically, release is attributed to the formation, dilation and coalescence of nano-pores (forming mesopores) inside the PLGA matrix. Effective protein diffusivity is directly correlated to the size, interconnectivity and tortuosity of the pore network, as well as protein/polymer and protein/protein interactions[198], [214]. Subsequent diffusion of proteins through these pores driven mainly by concentration gradients determines the overall release profile following the initial burst. We observed an overall decrease in the rate of protein release rate as the average particle diameter increased (Figure 2.5C) potentially due to: 1) additional time required to form an interconnected pore network (assuming identical

particle porosity & density) and 2) significantly longer diffusion lengths to reach the release medium in relatively large particles. Blanco et. al. generated sub-micron PLGA particles with diameters ranging between 320-523nm and found that protein release rate range between 0.49-1.45% cumulative release per day after burst [207]. Although their protein release rates are similar to the ranges reported here (1.01-1.36% cumulative release/day), they did not report any discernable trends; likely due to the confounding effects of altering formulation parameters.

Increasing the average diameter of a particle population also led to a longer protein release period, most likely due to principles outlined above (Figure 2.5D). In our study, the detectable protein release period ranged from 38 days to 75 days relative to the unfractioned group that released protein for 57 days (Figure 2.5D). It is important to note that the longer diffusion paths of large particles may also result in accumulation of acidic PLGA degradation products near the core of the particle, leading to pH-driven autocatalytic polymer degradation[198]. The heterogeneous rate of polymer degradation and erosion is a proposed mechanism to describe relatively fast cargo release rates for some large microparticles and, in some cases, shorter release periods than smaller particles [215]. The effects of autocatalytic polymer degradation is much less pronounced in smaller particles and does not seem to play an appreciable role for the sub-micron particles used in this study[198].

2.6 Conclusion

Due to the complexity and the number of interactions involved in determining PLGA particle properties, changing formulation parameters to achieve desired loading and release characteristics may be time consuming. The methods outlined here demonstrate a direct relationship between release properties and the particle population size characteristics (distribution and average diameter). Encapsulation efficiency and

several parameters of the release curve (burst release, protein release rate and protein release period) correlated to the average diameter of the particle population. Thus centrifugal fractioning represents a potential tool for tuning sub-micron PLGA particle properties without modifying formulation parameters. Subsequently, centrifugal fractioning is useful tool in achieving a desired release profile (such as reducing burst release) without potentially compromising other particle attributes due to changes in formulation parameters.

2.6. Figures

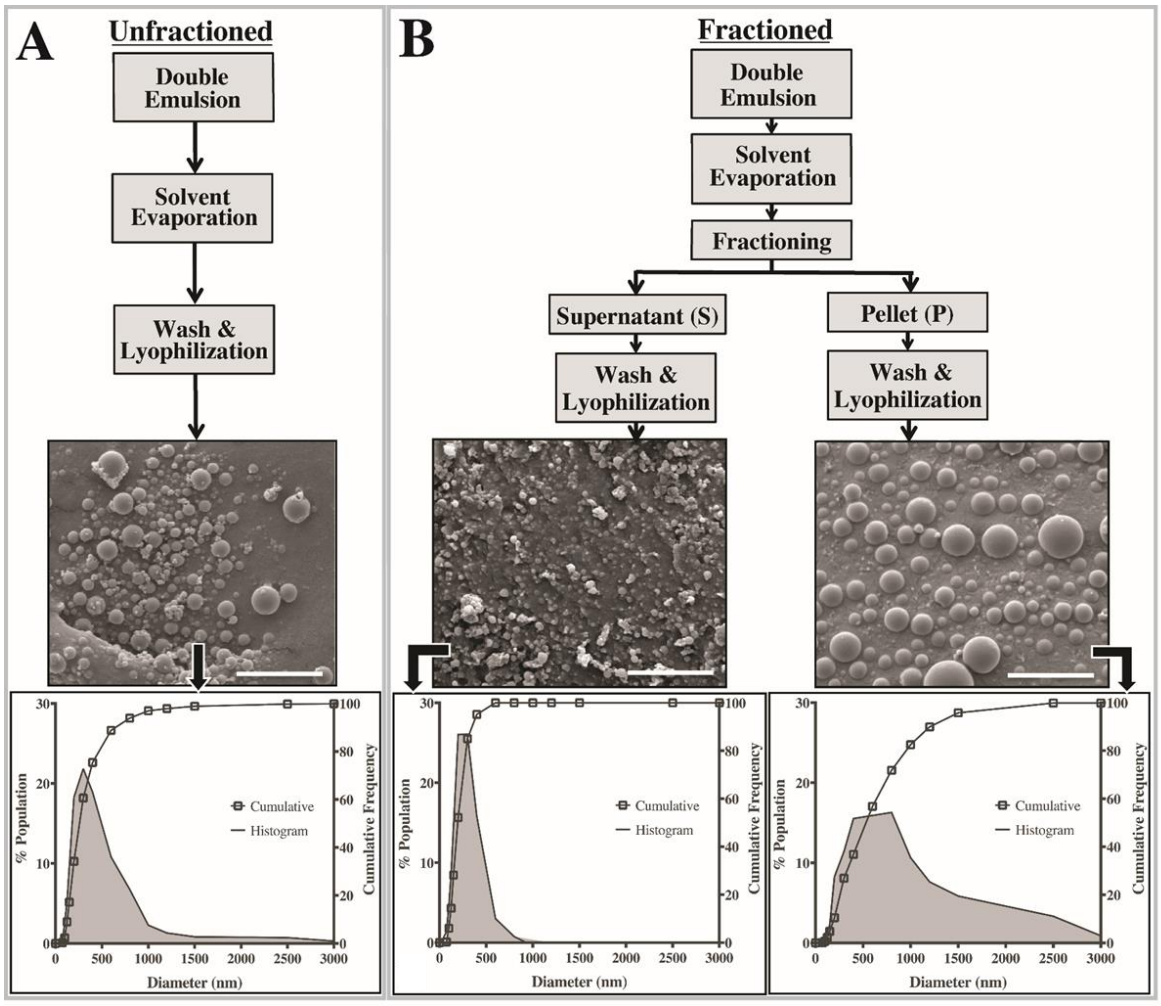

Figure 2.1: Schematic outlining particle preparation protocols and their resulting size distributions. A) Unfractioned sub-micron PLGA particles were generated using a standard double emulsion technique. B) For the fractioned groups, particles were subjected to a centrifugal size fractioning prior to the washing steps where relatively small particles comprised the supernatant sub-groups, and larger particles formed the pellet sub-groups. Cumulative frequency plots along with their respective histograms illustrate significant differences in particle size distributions were achieved without necessitating changes to any formulation parameters. All scale bars represent 5µm.

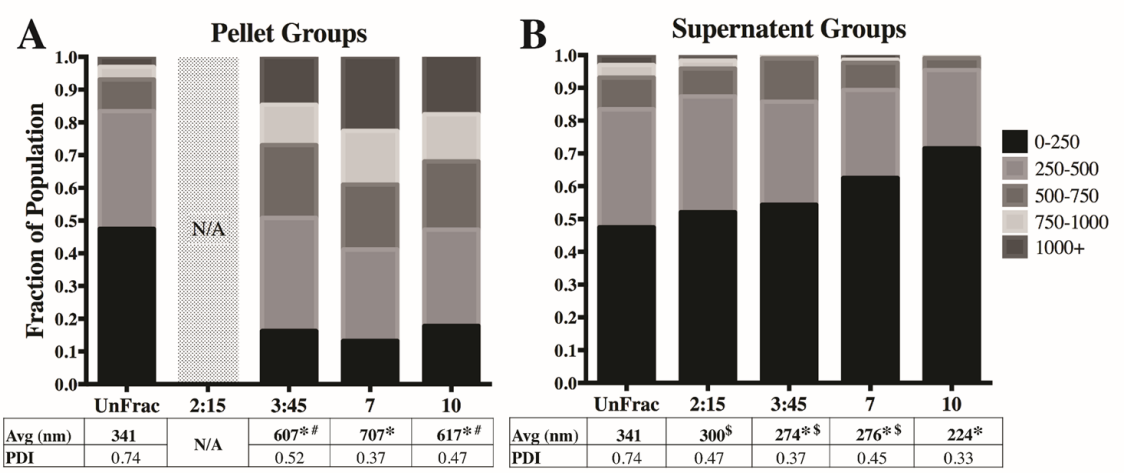

	UnFrac	2:15	3:45	7	10
Avg (nm)	341	N/A	607*#	707*	617*#
PDI	0.74		0.52	0.37	0.47

	UnFrac	2:15	3:45	7	10
Avg (nm)	341	300$	274*$	276*$	224*
PDI	0.74	0.47	0.37	0.45	0.33

Figure 2.2: Spin time alters average diameter and diameter distributions. A) All fractioned pellet sub-groups (constant spin force of 550g; Low G) had significantly larger diameter distributions relative to unfractioned (UnFrac). Size analysis for the 2:15min group was not conducted due to low yield. B) All Low G supernatant sub-groups were significantly different relative to Unfrac, except for the 2min 15s group. The 10min supernatant group was significantly different compared to the rest of the fractioned groups. (* - $p<0.01$ compared to unfractioned; # - $p<0.05$ compared to 7min pellet; $ - $p<0.05$ compared to 10min supernatant).

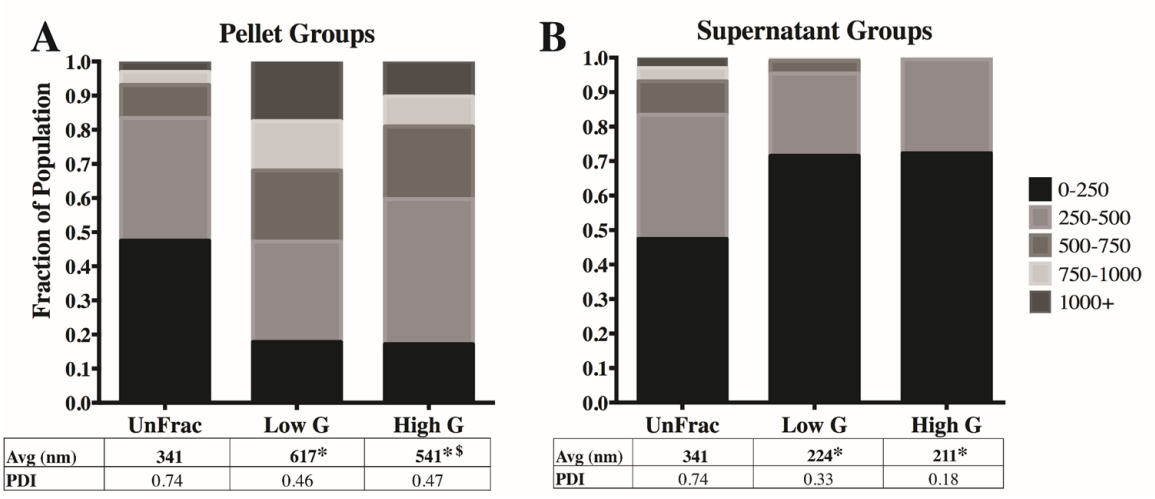

	UnFrac	Low G	High G
Avg (nm)	341	617*	541*$
PDI	0.74	0.46	0.47

	UnFrac	Low G	High G
Avg (nm)	341	224*	211*
PDI	0.74	0.33	0.18

Figure 2.3: Spin force affects average diameter and diameter distributions. A) Fractioning at 550g (Low G) and 1600g (High G) leads to significant changes between Low G and High G pellet sub-groups. B) The supernatant size distributions for both the Low and High G groups were significantly different from UnFrac. Although the differences between the Low and High G supernatant sub-groups were not statistically significant, the PDI is reduced from 0.33 to 0.18. (* - $p<0.01$ compared to unfractioned; $ - $p<0.05$ compared to 10min supernatant).

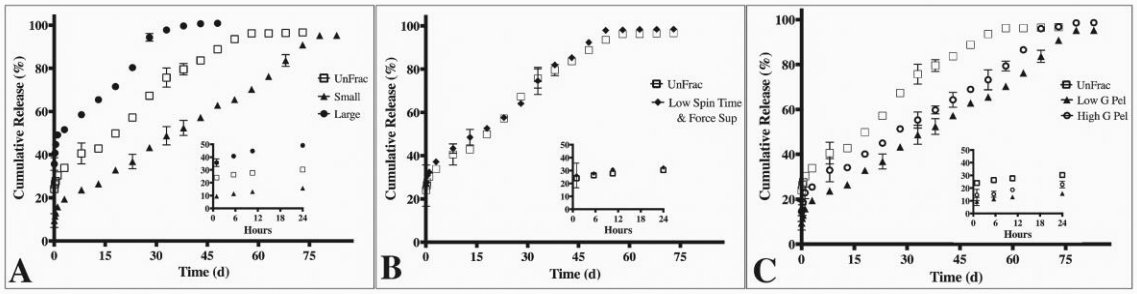

Figure 2.4: The protein release profile is dependent on the particle size distribution. A) Compares two sub-groups “Small” (1600g supernatant) and “Large” (Large; 550g, 7min pellet) with the most significant differences average diameters relative to unfractioned (UnFrac). The corresponding release profile from Small exhibited a 50% burst release and 40day release period. Large exhibited an 18% burst release followed by a 75day

release period. In contrast, UnFrac exhibited a burst release of 30.3% with sustained release for 57days. B) Groups with similar particle size distributions also exhibit comparable burst release, protein release rate and release period. “Low Spin Time & Force Sup” represents the 550g, 2:15min supernatant sub-group. C) Modest, yet statistically significant differences in particle size distribution also affects the release profile. Significant differences in cumulative protein release were observed at all time-points except for hours 1, 6 & 11 and days 3, 33 & 48 ($p>0.05$).

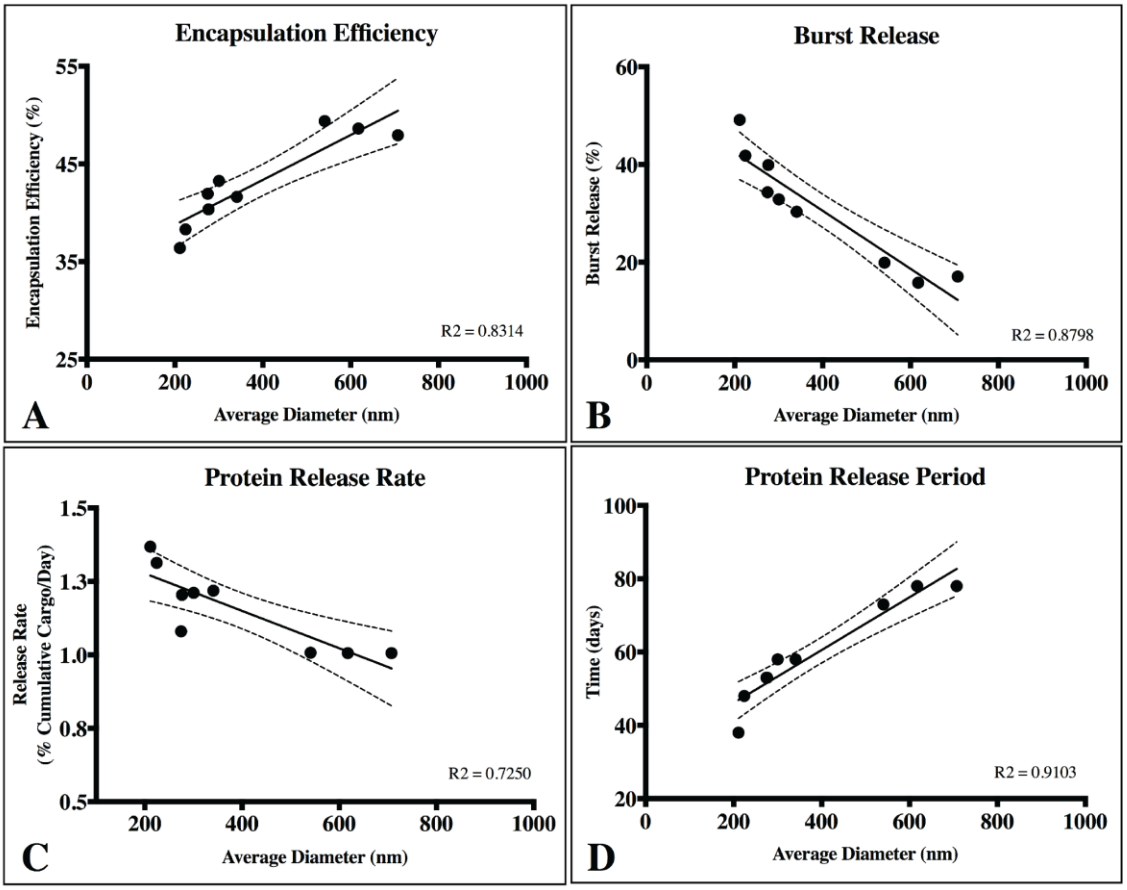

Figure 2.5: Average particle diameter affects (A) encapsulation efficiency, (B) burst release, (C) protein release rate after the burst phase, and (D) and total protein release period. Encapsulation efficiency and release period was directly proportional to the average particle diameter (A and D). Conversely, the magnitude of the burst release and

the rate of protein release subsequently were inversely related to average particle diameter (B and C). The dotted lines represent 95% confidence interval for all cases and a linear regression was used to empirically model the trends for each case.

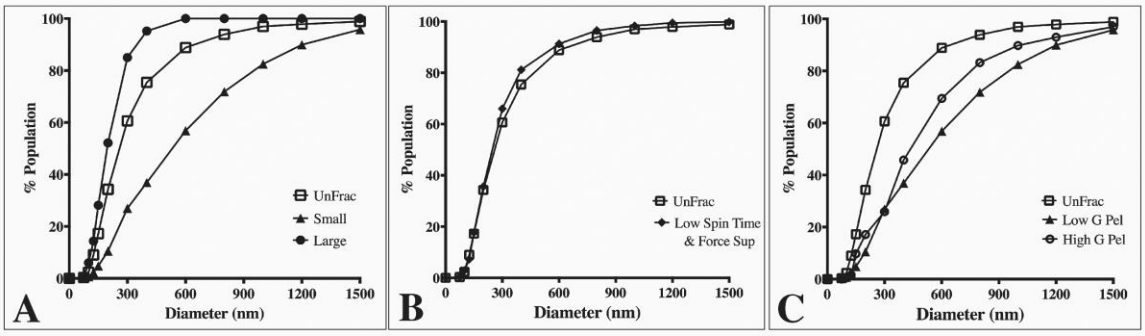

Figure 2.6: A) Compares the particle size distributions of groups with the most significant differences in average diameters. The smallest average diameter particle group (Small; 1600g supernatant) contains 90% of the particle population below 400nm. The largest average diameter particle group (Large; 550g, 7min pellet) contains 90% of the particle population below 1200nm. B) Compares the particle size distributions of the two most similar groups; unfractioned (UnFrac) and 550g, 2:15min supernatant (Low Spin time & Force Sup). C) Illustrates the modest, yet statistically significant differences in particle diameter distributions of High G and Low G pellet sub-groups.

Table 2.1: Average particle diameters and protein encapsulation efficiencies (EE) are significantly altered as a function of centrifugation force and time. Total particle yields (pellet+supernatant) was not significantly affected due to the fractioning process. (* and # represent $p<0.05$ in comparison to unfractioned).

Unfractionated		Average Diameter (nm)	PDI	Yield (%)	EE (%)					
		341	0.74	65.1	41.8 ±1.6%					
		Supernatant				**Pellet**				
Centrifugal Force	**Spin Time (min:s)**	**Average Diameter (nm)**	**PDI**	**Yield (%)**	**EE (%)**	**Average Diameter (nm)**	**PDI**	**Yield (%)**	**EE (%)**	**Total Yield (%)**
500 (Low)	2:15	**300**	0.47	52.7	43.2±0.4%					
	3:45	**274***	0.37	48.0	41.1±1.1%	**607***	0.52	14.0	44.6±0.5%	62.0
	7:00	**276***	0.45	38.4	40.4±1.5%	**707***	0.37	20.3	48.0±1.1%#	58.7
	10:00	**224***	0.33	41.3	38.3±1.0%	**617***	0.47	24.4	48.6±0.2%#	65.7
1600 (High)	10:00	**211***	0.18	17.3	36.4±0.5%#	**541***	0.47	41.2	49.4±0.1%#	58.5

CHAPTER 3

TUNABLE CONTROLLED RELEASE OF BIOATIVE SDF-1α VIA PROTEIN-SPECIFIC INTERACTIONS WITHIN FIBRIN/NANOPARTICLE COMPOSITES

3.1. Introduction

The studies presented in Chapter 2 employed the model protein, BSA, to validate protein encapsulation and release from poly(D,L,-lactic-*co*-glycolic) acid (PLGA) particulate devices. The process of developing this generalized protein release platform aided in the rational design for the PLGA nanoparticle fabrication protocol best suited for SDF-1α encapsulation and release. For example, the protein encapsulation efficiency was found to be directly proportional to emulsifier (TPGS) concentration, whereas the polydispersity index (PDI) of particle populations was inversely proportional to emulsifier concentration. Thus the PLGA particles generated for studies conducted in Chapter 2, protein encapsulation efficiency was sacrificed to yield particle populations with higher PDI to directly evaluate the relationship between protein release properties and the particle population size characteristics. In this current chapter, the focus transitioned to optimization and tuning release profiles from SDF-1α loaded PLGA particles where the principal difference was an increase of TPGS concentrations both in the second emulsion (2.0% vs. 5.0% w/v) and the solvent evaporation phase (0.2% vs 0.4% w/v). The second major change included the addition of 1.25% (w/v) sodium chloride in the solvent evaporation phase that was hypothesized increase in protein encapsulation due to osmotic effects [216].

Traumatic brain injury (TBI) is a leading cause of death and disability around the world with over 50,000 deaths and an estimated $60 billion in direct and indirect economic costs every year, in the United States alone[45]. Although current treatment practices have demonstrated some efficacy in treating its long-term effects, there are no

means of directly addressing the underlying pathophysiology of TBI [217]. Recent studies have reported the activation of endogenous neural progenitor/stem cell (NPSC)-mediated neurotrophic support and neurogenesis after injury events (e.g. stroke or traumatic brain injury) [2], [81], [218]. NPSCs originating from the two adult neural stem cell niches (subventricular zone, SVZ; and subgranular zone of hippocampus dentate gyrus) selectively migrate to the injury penumbra forming ectopic niches, even within non-neurogenic areas of the brain (such as adult cortical tissues)[81], [219]. The concentration of the chemokine, stromal cell-derived factor-1α (SDF-1α), and the expression of its receptor, CXCR4, increases significantly in the injury penumbra and is implicated as a key regulator of directed NPSC recruitment after neural injury[2], [81]. However, increased SDF-1α levels subside by 14days post injury, in most reports, coinciding with a diminishing number of NPSCs (observed at the injured area) [2], [81], [220], [221]. Building on this inherent injury-stimulated signal, we postulate that increased and sustained bioavailability of SDF-1α locally in the injury penumbra would augment NPSC recruitment and bolster the capacity for endogenous regeneration.

With this in vivo application in mind, this study focused on developing a drug delivery device for local, sustained release of SDF-1α with the following attributes: 1) injectable, 2) biodegradable, 3) prolonged release well past 14days and 4) maintenance of SDF-1α levels within the therapeutic concentration range. The most basic form of delivering therapeutics is systemic bolus administration. Drawbacks of this method include a lack of control over biodistribution due to physiological barriers (i.e. endothelial barrier) and rapid systemic clearance[2]. Direct, local injection in the target tissue affords control over dosage, but negates temporal control or payload degradation leading to only transient therapeutic benefits. Conventional means for local, sustained delivery to control both dosage and temporal concentration profile involve bulky,

invasive minipump systems that are linked to infections, bleeding and neurologic injury [222]. Injectable biomaterials for the controlled release of therapeutics (i.e. hydrogels and biodegradable plastics) hold the capacity to overcome the common limitations of drug delivery (i.e. dosage, temporal concentration, biocompatibility & patient compliance)[1]. Release devices for local and sustained delivery of SDF-1α have been explored in several different physiological applications including neural regeneration, myocardial infarctions, skeletal regeneration and wound healing[170], [173], [179], [223]. However, many of these previous designs were based on hydrogels (such as, alginate, collagen, gelatin, star PEG-heparin etc.) and provided sustained SDF-1α for less than 14days. Therefore, we sought to tailor a controlled release system that fits the aforementioned design criterion, ultimately for neural applications.

PLGA, a FDA-approved biodegradable polyester, has long been studied for diverse applications in the central nervous system[224], [225]. In addition tunable release profiles, a significant benefit of PLGA carriers is insulation of encapsulated cargo from the local microenvironment, limiting specific and non-specific degradation and leading to increased protein half-life [187]. With a half-life of 25mins in blood, maintaining SDF-1α bioactivity was an important parameter for this study [226]. Sustained delivery of SDF-1α has been achieved with macro-scale PLGA scaffolds and microparticles [172], [180], [185]. Yet, the utility of such macro-to-micro-scale systems for minimally invasive delivery is limited. As such, novel nanoscale SDF-1α PLGA-based devices are of great interest.

The release profiles of encapsulated cargo from PLGA-based particles vary greatly (zero-order, monophasic, biphasic and triphasic) depending primarily on formulation parameters and typically includes a burst release within the first few hours [188]. The PLGA burst phase is problematic since supra-therapeutic concentrations may

result in undesired biological consequences. Mechanisms to address the burst issue range multilayer coatings to composite system embedding PLGA particles within hydrogel matrices. The biologically-derived matrix fibrin has been investigated as a carrier for protein delivery [227], [228]. Numerous studies report engineered fibrin-derivatives crosslinkers to mediate and enhance affinity-based interactions for controlled release of a multitude of biologics (e.g. nerve growth factor (NGF), neurotrophin-3, glial-derived neurotrophic factor, genetic material) [229]–[232]. As a natural extracellular matrix (ECM) protein, fibrin possesses inherent ability to bind and sequester soluble signaling factors, predominately through a heparin-like binding domains that mediate immobilization of small, highly basic (and heparin-binding) proteins such as basic fibroblast growth factor (FGF) [233] [153], [234]. Here in this study, we hypothesized that embedding SDF-1α-loaded NPs within fibrin matrices will modulate the burst release phase due to specific protein-protein interactions between SDF-1α and fibrin. The key objectives for this study were to 1) characterize SDF-1α-loaded NPs, 2) probe the mechanism of SDF-1α/fibrin(ogen) interactions and 3) determine the effect of SDF-1α/fibrin(ogen) interactions on SDF-1α release from PLGA NPs. Collectively, we report a composite fibrin/PLGA system with the capacity to achieve long-term (60 days), bioactive SDF-1α release and the means to independently tune protein release during the burst phase.

3.2. Experimental Methods

3.2.1. Materials

Poly(lactic-*co*-glycolic) acid (PLGA; 50:50 ester-terminated; inherent viscosity = 0.55-0.75dL/g) was purchased from Lactel (Birmingham, USA). Recombinant mouse stromal cell-derived factor-1 α (SDF-1α) were acquired from PeproTech (Rocky Hill, USA). B27 growth supplement, DAPI nuclear stain, tetramethylbenzidine (TMB)

substrate and Dulbecco's modified eagle medium were acquired from Life Technologies (Carlsbad, USA). Glucose was obtained from Acros Organics (Geel, Belgium). High-binding 96-well enzyme-linked immunosorbent assay (ELISA) plates were acquired from Greiner Bio-One (Frickenhausen, Germany). The organic solvent ethyl acetate was acquired from Alfa Aesar (Ward Hill, USA) and dimethyl sulfoxide (DMSO) from American bioanalytical (Natick, USA). Human fibrinogen (Plasminogen, von Willebrand Factor and Fibronectin Depleted), human α-thrombin, human factor XIIIa (FXIII) and human plasmin were acquired from Enzyme Research Laboratories (South Bend, USA). All other materials and chemicals were purchased from Sigma-Aldrich (St. Louis, USA) and used without further modification or purification.

3.2.2. Formulation of SDF-1α Loaded Nanoparticle

SDF-1α loaded PLGA nanoparticles were synthesized using a water/oil/water (W/O/W) emulsion technique adapted from a previously published protocol[204]. Briefly, the first emulsion (W/O) was obtained by vortexing the oil phase (100 mg/mL PLGA in ethyl acetate) with PBS buffer solution (pH = 7.4) containing 20.0mg/mL bovine serum albumin (BSA; 2.0% w/w of PLGA) and 2.0mg/mL SDF-1α (0.2% w/w of PLGA). The above solution was added dropwise to a 3.6x volume excess of an aqueous 5.0% (w/v) d-α tocopheryl polyethylene glycol 1000 succinate (TPGS) and the second emulsion (W/O/W) was produced by ultrasonicating (Omni Ruptor 4000; Omni International; Kennesaw, USA) the solution for two consecutive 15sec periods in an ice bath (120W power with a 90% duty cycle). The emulsion was then quickly transferred to a stirring (300RPM) aqueous bath containing 0.5% TPGS + 1.25% (w/v) NaCl (10x volume excess) and left undisturbed for 3hrs for solvent evaporation. The particle suspension was washed three times with deionized water by centrifugation at 15,000g for 15min in between rinses (Beckman Counter; Allegra 25R; Pasadena, USA). The

particles were supplemented with 25% (w/w) D-(+)-trehalose dihydrate and recovered through lyophilization. Particle size analyses were performed by scanning electron microscope (SEM; Phillips XL-30; San Francisco, USA) using a 3-5kV electron beam. Lyophilized particle samples were prepared for SEM analysis via gold/palladium sputter coater (108-Auto, Cressington Scientific; Watford, UK) to achieve a 5-10nm thick layer. A minimum of 7 images were captured per group and were processed using ImageJ to determine the size distributions. At least 85 sampling points were required for each image and thus size distribution histograms are comprised of a minimum of 595 measurement points in total.

3.2.3. Protein Loading & Release Assays

Total protein loading was determined by complete dissolution of a known amount of particles (10 mg/mL) in dimethyl sulfoxide (DMSO). The DMSO solution was then diluted 1:15 using 2.5% (w/v) sodium dodecyl sulfate and 0.1N NaOH in deionized water. The mixture was thoroughly agitated, being careful not to introduce bubbles. Known amounts of soluble BSA added to blank particles (no protein encapsulated; synthesized using identical synthesis protocols) were used to generate calibration curve. Protein quantification was performed using bicinchoninic assay (BCA; G Biosciences; St. Louis, USA) in triplicates following manufacturer's protocols. Encapsulation efficiency and loading capacity were calculated using the following:

$$Encapsulation\ efficiency\ (\%) = 100 * (\frac{Total\ encapsulated\ protein\ (mg)}{Total\ protein\ added\ (mg)})$$

$$Loading\ Capacity\ (\%) = 100 * (\frac{SDF\ content\ in\ NPs\ (mg)}{Amount\ of\ NPs\ (mg)})$$

For the release assays, lyophilized particles were resuspended in 1 mL of buffer release media (1x PBS supplemented with 0.01% tween 80 and 0.01% NaN_3) at

3.5mg/mL and incubated at 37°C under constant agitation. At specified time points, the supernatant was collected by centrifuging the particle suspension at 14,000g for 15mins, collecting 90% of the supernatant and replenishing with fresh buffer release media. Extracted buffer release media samples were stored at -80°C for subsequent protein analysis. To specifically determine the SDF-1α content, a known concentration (500ng/mL) was incubated alongside the NP suspension as a positive control for subsequent analysis using ELISA-based detection (R&D systems; Minneapolis, USA). NPs with no encapsulated SDF-1α served as the negative control.

3.2.4. SDF-1α Bioactivity Assay

3.2.4.1. Neural Progenitor/Stem Cell Harvest and Culture

Murine fetal derived neural/progenitor stem cells (NPSCs) were isolated from the medial and lateral germinal eminences of E14.5 C57BL/6 mice based on previously published protocols and in accordance with approval by the Institutional Animal Care and Use Committee at Arizona State University[235]. The germinal eminences were harvested, mechanically disassociated and cultured in NPSC medium (Dulbecco's modified eagle medium (DMEM:F12) with 2.4mg/mL sodium bicarbonate ($NaHCO_3$), 6 mg/mL glucose, 5mM HEPES, 62.9 ng/mL progesterone, 9.6 μg/mL putrescine, 1.83 μg/mL heparin, 1X B27 growth supplement, 20 ng/mL epidermal growth factor (EGF), 5 ng/mL FGF, 5 μg/mL insulin, 5 μg/mL transferrin, and 5 ng/mL sodium selenite). NPSCs were cultured as non-adherent neurospheres and used for experimentation between passages 3-6.

3.2.4.2. Modified Boyden Chamber Assay

NPSC chemotaxis in a modified-Boyden chamber assay was used to determine SDF-1α bioactivity as previously described[12]. In short, disassociated NPSCs were

plated (70,000 cells/cm^2) on laminin-coated transwell inserts with 12μm pore diameter (Millipore, Temecula, CA). Growth factor-free NPSC medium (no EGF or FGF) with 0 or 250ng/mL SDF-1α (negative and positive control, respectively) was added in the bottom chamber. NPSCs were then allowed to undergo chemotaxis for 24hrs in an incubator (37^{o}C and 5% CO_2). Subsequently, cells on the top side of the transwell membrane were removed using a cotton swab whereas migrated cells that reached the bottom were fixed, underwent a DAPI nuclear stain and imaged. NPSC nuclei have diameters of approximately 20μm[236]. After intensity thresholding, nuclei count was quantified using a particle count algorithm in ImageJ where stained nuclei 10-30μm in diameter were counted as individual cells. Nuclei count was determined by imaging and quantifying whole transwell membranes.

3.2.4.3. Bioactivity of Encapsulated SDF-1α

The bioactivity of the encapsulated/released SDF-1α from PLGA NPs was evaluated at two timepoint intervals (day 0-1 and day 20-22) via the modified Boyden chamber assay described above. Release samples were acquired from blank and SDF-1α-loaded NPs resuspended in cell culture release media (DMEM:F12 supplemented with 2.4mg/mL $NaHCO_3$); the NP concentration for day 0-1 interval was 9.0mg/mL versus 17.5mg/mL for day 20-22 to account for variation in the amount of SDF-1α released during the burst or sustained release phases. The NP suspensions were incubated at 37^{o}C with agitation, taking precautions to maintain sterility. For the day 20-22 interval, the cell culture release media was exchanged every 3days until day 20. After the specified incubation period, NPs were centrifuged (14,000g for 15mins) to collect the supernatant, and the modified Boyden chamber assay was carried out immediately. NP cell culture release media was diluted 1:10 and 1:2 for day 0-1 and day 20-22 samples, respectively, with growth factor-free NPSC media to achieve a SDF-1α concentration in the NPSC

chemotactic range (Figure 3.2). The dilution factors were estimated via a preliminary total protein release profile (data not shown). A minimum of 4 replicates per group performed for all migration assays.

3.2.5. SDF-1α-Fibrin(ogen) Binding Detection ELISAs

SDF-1α-fibrinogen interaction were probed by adapting a previously described modified ELISA[153]. SDF-1α, BSA and basic fibroblast growth factor (FGF) were coated on high-binding ELISA plates by incubating the soluble factors at 100nM (in 100mM carbonate buffer; pH 9.6) for 3hrs at 37°C. All growth factor (GF) coated wells were blocked using 2.0% (w/v) fat-free powdered milk in PBS for 1hr at room temperature (RT). Fibrinogen (35μg/mL; depleted of fibronectin, plasminogen, and von Willebrand factor) was incubated for 1hr at RT. The primary antibody (rabbit anti-fibrinogen; EMD Millipore; Darmstadt, Germany) was then added for 1hr at RT, followed by the secondary antibody (HRP conjugated goat anti-rabbit IgG; Thermo Scientific; Waltham, USA), also under the same conditions. Detection was carried out TMB substrate following manufacturer's protocols. Four washes were performed in between each of the steps mentioned using PBS with 0.01% Tween-20 (PBS-T). Heparin competition ELISAs were also performed with various concentrations (0.75 – 200μg/mL) of soluble heparin (17-19kDa), which was supplemented in the fibrinogen solution after the blocking step mentioned above[153]. All subsequent steps were kept identical.

The next modified ELISA probed SDF-1α interactions with fibrin. A previously described protocol was adapted to generate a thin layer of fibrin network on high-binding ELISA plates[237]. In short, fibrinogen (depleted of fibronectin, plasminogen, and von Willebrand factor) was incubated at 100μg/mL for 1hr at RT. After rinsing three times with Tris-buffered solution (10mM Tris + 150mM NaCl), the wells were blocked using 1.0% (w/v) BSA for 20mins at RT. After rinsing, human thrombin (2.5 NIH U/mL)

and human FXIIIa (0.5 NIH U/mL) was added and incubated for 15mins at RT. Fibrin coating was completed after washing and subsequent incubation with fibrinogen (500μg/mL), anti-thrombin-III (50μg/mL) and heparin (60μg/mL) for 1hr at RT. The plates were then washed and stored with 2.0% (w/v) powdered milk in PBS overnight at 4°C. Control groups included wells that were coated with heparin (70μg/mL; positive control) or BSA (1.0 mg/mL; negative control) in PBS, overnight at 4°C. Surface-modified wells were then exposed to various concentrations of SDF-1α (0-20μg/mL) for 1hr and relative levels of SDF-1α binding were measured using rabbit anti-SDF-1α (Abcam; Cambridge, USA), HRP-conjugated goat anti-rabbit and TMB substrate. A minimum of n=3 was used for all ELISAs.

3.2.6. SDF-1α Release from Fibrin Matrices

Release of soluble SDF-1α from fibrin matrices was conducted as described previously[153]. In short, fibrin gels were generated with fibrinogen (3 or 25mg/mL), human thrombin (5U/mL), human FXIIIa (2.5U/mL), calcium chloride (5mM) and SDF-1α (500ng/mL) in TBS. The fibrin matrices (150μL) were polymerized (by combining separate fibrinogen and thrombin solutions) for 1hr at 37°C under sterile conditions in ultra-low binding 24-well plates. After the polymerization, 700μL of TBS (with 0.1% w/v BSA) was added to initiate the release assay. The release buffer was extracted, stored in -80°C and replaced with fresh TBS every 24hrs for 7days. On Day 7, the fibrin matrices were digested with plasmin (0.5U/mL) to quantify the remaining SDF-1α. A control group consisted of soluble SDF-1α (500ng/mL) where 30μL was extracted for every timepoint and also underwent the plasmin treatment. SDF-1α content was determined via SDF-1α ELISA. All groups were measured in triplicates.

3.2.7. Release Assay from SDF-1α-Loaded NPs Embedded in Fibrin

Fibrin gels (3, 10, 25mg/mL) were formed using the same procedure as above where free SDF-1α was replaced by PLGA NPs (blank and SDF-1α-loaded NPs) with a final concentration of 1mg PLGA NPs/1mL of fibrin gel. Similar to the previous release assay, fibrin matrices (150µL) were formed in ultra-low binding 24-well plates for 1hr at 37°C under sterile conditions, after which 700µL of TBS (with 0.1% w/v BSA) was added. The release media was extracted, replaced and stored at hours 1, 3, 6, 12, 24 48 and 72 after initiating the release assay. SDF-1α content in all timepoints were quantified via ELISA. A 500ng/mL SDF-1α group as served as the control groups, where similar to before, 30µL was extracted at every timepoint. All groups were tested in triplicates.

3.2.8. Physical Characterization of Fibrin/NPs Composite

Fibrin polymerization was monitored with time-dependent optical density measurements (Epoch; Biotek; Winooski, USA). Control (native fibrin clots with no NPs) and NP-embedded gels (0.1, 1 & 10mg/mL) were prepared using the same parameters as mentioned earlier. Three different fibrinogen (3, 15 & 30mg/mL) groups were tested where optical density (OD) was measured every 30sec for 2hrs in triplicate per group. Terminal clot turbidity refers to the OD at the end of 2hrs.

Percent clottable protein was quantified for control and experimental fibrin gels (with NPs; 0.1, 1 & 10mg/mL; n= 3). The fibrinogen content before polymerization was compared to the remaining soluble fibrinogen that remained following fibrin gel formation (40min) [238]. Fibrinogen (FBN) content in the remaining solution (clot liquor), taking into account the presence of additional enzymes, was measured using BCA where percent clottable protein (CP) is defined as the following:

$$CP(\%) = 100 * \left(\frac{FBN_{Initial}\left(\frac{mg}{ml}\right) - FBN_{Clot\ Liquor}\left(\frac{mg}{ml}\right)}{FBN_{Initial}\left(\frac{mg}{ml}\right)}\right)$$

The mechanical properties of the fibrin gels were also analyzed with an oscillatory parallel-plate geometry rheometer (MCR 101; Anton Paar; Ashland, USA). Fibrin clots (3 & 30mg/mL) with and without NPs (0.1, 1, 10 mg/mL) were generated with identical protocols as described above. The fibrin gels (0.4mL) were polymerized within a 400μm gap between the top and bottom plates (1hr at 37°C under high humidity). A strain sweep (0.01 to 100%) was performed to determine the linear viscoelastic regime for all concentrations of fibrin and strain amplitude of 1% was chosen for all subsequent frequency sweep tests (0.01-100Hz) to determine storage (G') and loss (G") modulus (n = 2)

3.2.9. Statistics

Statistical analysis was performed on all quantitative assays. All results are depicted as the mean ± one standard deviation, unless otherwise stated. Statistical analyses (GraphPad Prism, La Jolla, CA) evaluated differences between groups using analysis of variance (ANOVA) followed by Tukey post-hoc tests to determine statistical significance with $p < 0.05$ considered significant. Multiplicity adjusted p-values are reported for Tukey post-hoc comparisons.

3.3. Results and Discussion

3.3.1. Characterization of SDF-1α Loaded NPs

SDF-1α was successfully encapsulated in PLGA NPs using a double emulsion method. Characterization assays included size analyses via SEM micrographs, total protein encapsulation efficiency as well as quantification of SDF-1α release profile (Figure 3.1). Resulting NPs were spherical in shape and had smooth surface morphology with an average diameter (± standard error of mean; SE) of 288.9 ± 19.2 nm, comparable to previously reported PLGA NPs[204], [239]. The reported average NP

diameter was an average of 5 separately prepared batches. The NP population distribution for each batch consistently ranged between 100-1500nm with 90% of the NPs falling within 200-600nm (Figure 3.1C). NP size distributions were statistically consistent between batches and NP yields ranged between 57-65%, indicating minimal batch-to-batch variability. The total protein (BSA+SDF-1α) encapsulation efficiency for the resulting NPs was 61.7% ± 2.8%. Attempts to determine SDF-1α loading using conventional methods requiring dissolution of NPs in an organic solvent followed by protein extraction and quantification via SDF-1α ELISA proved unreliable due to protein denaturation and degradation; this issue was also previously reported by Cross et. al. [180]. As a result, we estimated total encapsulated SDF-1α via cumulative values from the SDF-1α ELISA release profile (Figure 3.1D). SDF-1α content measured during the release assay amounted to a total SDF-1α loading capacity of 293ng of SDF-1α/1mg of PLGA (i.e. 0.029±0.00076% (w/w) PLGA NPs). Furthermore, the NPs exhibited a tri-phasic release profile, frequently observed in PLGA-based release devices[188]. We observed sustained release of SDF-1α for 60 days following an initial burst release and a lag phase approximately between days 2 and 6 (Figure 3.1D). In the first day, the NPs release 67ng SDF-1α for every 1mg of PLGA NPs, which translates to a burst release of 23% total released SDF-1α as determined by ELISA.

PLGA-based release systems devices are unique since cargo release rate is largely controlled by polymer degradation rate and thus is not purely diffusion-mediated[188]. The release profile is a result of various interactions (i.e. cargo/polymer, cargo/cargo etc.) and release mechanisms (i.e. diffusion, bulk erosion etc.) that are relevant to a particular set of particles[145][144](Hines and Kaplan, 2013)[9]. After the burst release, the mechanism of release for hydrophilic proteins is attributed to the formation, dilation and coalescence of nano-pores (forming mesopores) inside the PLGA matrix [162]. The

effective protein diffusivity is directly correlated to the properties of the pore network and protein/polymer interactions. Thus prolonged release in the later stages is mediated by polymer degradation and erosion as well protein diffusion. As a result, choice of PLGA was a rational decision considering our goal for achieving long-term, sustained and bioactive SDF-1α release.

Previous studies demonstrated the feasibility of encapsulating and releasing bioactive SDF-1α (as tested by *in vitro* mesenchymal stem cell migration) from PLGA microparticles to achieve controlled release over 40-70days [180], [185]. However, both studies report relatively low SDF-1α loading. The PLGA microparticles in one study indicated a loading capacity of approximately 0.0018% (w/w) of PLGA, whereas the other had a theoretical maximum of 0.002% (w/w) SDF-1α relative to PLGA polymer. A low loading capacity equates to a requirement of high amounts of PLGA. Thus achieving adequate, therapeutic levels of SDF-1α may conflict with the accumulation of acidic byproducts that affects the local pH[163]. In comparison, we report PLGA nanoparticles with loading capacities of SDF-1α an order of magnitude higher at 0.029% (w/w) PLGA. Additionally, we achieved SDF-1α controlled release for 60 days, meeting our initial design criterion (Figure 3.1D).

3.3.2. NPSC Migration Assays Indicate Release of Bioactive SDF-1α

Modified-Boyden chamber migration assays were utilized to measure functional SDF-1α bioactivity (Figure 3.2A, B). SDF-1α is known to elicit a biphasic migratory response *in vitro* with a number of cell types (NPSCSs, mesenchymal stem cells; MSCs, leukocytes, hematopoietic cells etc.) over a wide range of concentrations (10-1000ng/mL) [12], [36], [41], [241]–[243]. This biphasic migratory response reportedly relates to the internalization of CXCR4 upon interaction with SDF-1α. Overstimulation from high concentrations of SDF-1α may lead to desensitization to the chemokine[241],

[244]. In our hands, the maximal NPSC migration response occurred at 250ng/mL after 24hrs and revealed a biphasic relationship to SDF-1α concentration where 1000ng/mL did not elicit any chemotactic response above the basal media levels (Figure 3.2B). The biphasic response of SDF-1α on NSCs suggests control over SDF-1α dosage and its temporal concentration profile is required to achieve a desired biological response.

The W/O/W double emulsion synthesis for PLGA NPs inherently involve harsh conditions such as water-oil interfaces, ultrasonication, freeze thaw cycles and lyophilization, known to affect the structural integrity and the biological properties of proteins[191]. Additionally, detection of SDF-1α via ELISA does not necessarily equate to functional bioactivity since the epitope recognition site for ELISA can vary from the biologically relevant site(s). As a result, the Boyden chamber assay described above was used to measure functional bioactivity of SDF-1α encapsulated in and released from the NPs. For each time interval (day 0-1 & days 20-22), 250 ng/mL SDF-1α and 0ng/mL served as the positive and negative controls for NPSC chemotaxis, respectively. In addition, release media from blank NPs were used as a control for confounding affects from PLGA degradation products.

The release media from day 0-1 elicited a robust migratory response that was significantly higher than both the negative control (no SDF-1α; $p = 0.0007$) and the blank NP group (Figure 3.3A, B; $p = 0.0201$). No adverse effects on NPSC chemotaxis were observed with the blank NP group for the 24hr incubation period, agreeing with previously published results with MSCs[180]. The data suggests that bioactivity of SDF-1α is not significantly altered with the NP synthesis protocol. The day 0-1 release media is largely composed of the burst phase that accounts for loosely adsorbed SDF-1α on the NP surface that diffuse out rapidly upon particle hydration. However, preservation of protein bioactivity in the first day does not indicate sustained release of bioactive

protein. Local pH within the particles have been reported to be <pH 3 and during release, the cargo can undergo aggregation, non-reversible adsorption and degradation leading to further loss in bioactivity and incomplete release[191]. Thus release media from day 20-22 was also evaluated to validate maintenance of bioactive SDF-1α (Figure 3.3A, C). Here, NPSC migration significantly increased in the SDF-1α-loaded NP group relative to blank NPs, which controlled for potential confounding affects from the acidic PLGA degradation products ($p<0.05$). A similar trend was observed in the pairwise comparison to the negative control, though not statistically significant ($p=0.0599$). In summary, encapsulation of SDF-1α in the NPs maintained the long-term bioactivity of SDF-1α. Moreover, encapsulated cargo is insulated from biological proteolytic factors in future in vivo applications. Thus we postulate this device has the potential to improve SDF-1α half-life (25mins in blood) as shown with other proteins *in vitro* and *in vivo* [187], [191].

3.3.3. Protein-protein Interactions between SDF-1α and Fibrin(ogen)

The high burst release from the NPs within the first hours is a concern considering biphasic response to SDF-1α (i.e. decreased NPSC migration; Figure 3.2). Moreover, high SDF-1α concentrations *in vivo* reportedly initiate systemic immune cell recruitment and infiltration [25]. Modest decrease of NP burst release magnitude may be achieved through alterations of the NP formulation parameters [200], [245]. However, changes in synthesis conditions create complex, multifaceted interactions that affect several particle properties at once. For example, changing polymer concentration not only affects encapsulation efficiency and loading capacity, but it also influences particle size and porosity, key factors determining release rate and duration [200], [246]. Therefore, we pursued a composite system as it affords the ability to independently tune

the release profile without compromising the desired attributes already attained by the NPs (sustained release of bioactive SDF-1α).

Composite biomaterials with drug carriers embedded in hydrogels has been explored for a number of applications [158], [247], [248]. One relevant example includes basic fibroblast growth factor (FGF)-loaded nanoparticles embedded in fibrin to achieve tunable ,zero-order release with the ability to reduce/eliminate the burst phenomenon [158]. The presence of heparin-like binding domains in the structure of native fibrin and its monomer, fibrinogen, is correlated to specific binding with highly basic, heparin-binding proteins such as FGF, vascular endothelial growth factor (VEGF), placenta growth factor-2 (PIGF-2) and insulin-like growth factor-binding protein-3 [153], [234], [249]. Due to the similarities in molecular weight, isoelectric point and heparin binding capacities between known fibrin-binding proteins such as, FGF, and SDF-1α, we probed the existence of fibrin(ogen)/SDF-1α interactions.

Fibrin(ogen)/SDF-1α interactions were determined using three modified ELISAs that probed both fibrin/fibrinogen affinity as well as, mechanistic competition with soluble heparin (Figure 3.4). First, the fibrinogen binding assay consisted of investigating soluble fibrinogen binding to adsorbed soluble factors (BSA, negative control; FGF, positive control; or SDF-1α). The results demonstrated a significant increase in fibrinogen binding/retention on SDF-1α-coated wells relative to BSA-coated wells (Figure 3.4A, B; $p<0.05$). More importantly, the fibrinogen retention levels for SDF-1α were comparable to the positive control FGF-coated wells, suggesting a binding interaction between SDF-1α and fibrinogen (Figure 3.4A, B).

The second ELISA assay probed the mechanism of SDF-1α/fibrinogen interaction. The heparin-like binding domain in fibrinogen is located in the first 66 amino acid residues of the Bβ chain [153], [250]. The high concentration of arginine and

lysine residues in that region allows promiscuous binding to both soluble factors and heparin [153]. Thus, a competition ELISA was performed where known amounts of soluble heparin (0.75-200μg/mL) was added to compete with the heparin-like binding domains on fibrinogen. The results indicate significant attenuation of signal with increasing heparin concentration for both FGF and SDF-1α–coated plates (Figure 3.4C). Conversely, signal from the BSA-coated wells do not exhibit a similar dependence on heparin content. The trends observed in Figures 3.4B and 3.4C agree with data from similar assays reported for other known fibrin-binding proteins [153]. Thus, the observed fibrinogen/SDF-1α interaction cannot be attributed to non-specific interactions, but most likely due to specific SDF-1α/fibrinogen interactions via the heparin-binding domain.

The final ELISA probed SDF-1α interactions with the insoluble, polymerized fibrin after a thin layer was deposited on ELISA plates [237]. Concentration dependent retention of SDF-1α on both, heparin-coated (positive control) and fibrin-coated wells relative to BSA-coated negative controls, indicate that specific SDF-1α/fibrinogen interactions are maintained when fibrinogen polymerizes to form fibrin (Figure 3.4D, E). Collectively, the results from these modified ELISA assays indicate specific protein-protein interactions between SDF-1α and fibrin(ogen) exists primarily via SDF-1α interactions with the heparin binding domain.

3.3.4. Fibrin Sequesters Free SDF-1α

Affinity-based interactions via the heparin-like binding domains on fibrin(ogen) is hypothesized to play a major role in determining growth factor release profile. For example, soluble heparin binding factors such as PIGF-2, FGF and VEGF exhibit prolonged release and sequestration in native fibrin matrices while, $VEGF_{121}$ (isoform lacking the heparin-binding domain) and NGF are released in a more diffusion-limited

manner [153], [228], [234]. Although fibrin density, fiber length and fiber aspect ratio are important determinants of release profile, evidence of immobilization/ sequestration (slow or no protein release) is a key indicator for affinity-based interactions playing a dominant role in determining release rate. For example, PIGF-2-loaded fibrin gels release ~15% of cumulative cargo in the first 2 days, whereas the remaining cargo was sequestered in the fibrin matrix for at least 7 days[153]. In contrast, NGF (low fibrinogen binding affinity) encapsulated in an identical fibrin matrix exhibited 100% cumulative release within 2 days [153]. Additionally, Wong et al. reported a similar release profile for FGF and concluded that diffusion-only release mechanism cannot account for cargo sequestration observed [234].

Building on the SDF-1α-fibrin(ogen) ELISA assays (Figure 3.4), we conducted SDF-1α release assays from fibrin gels to evaluate ability of the protein-protein interactions to sequester SDF-1α within three-dimensional fibrin matrices. We also evaluated the effects of fibrin density on SDF-1α release profile with the hypothesis that altering the number of available binding sites will dictate the maximal amount of sequestered SDF-1α within fibrin matrices [251]. We must note that altering fibrin density also modifies various matrix morphological properties and thus diffusion-limited cargo release profile; however, our experiment was designed to focus specifically on the sequestration of SDF-1α within a short 7 day release period (Figure 3.5). Thus, two concentrations of fibrin were evaluated, 3mg/mL (physiologically relevant concentration) and 25mg/mL gels loaded with a constant mass of SDF-1α (500ng/mL). The release study indicates that 90% of the encapsulated SDF-1α was released after 2 days in the 3mg/mL group whereas only 20% of the SDF-1α was released from the 25mg/mL group within that same time frame (Figure 3.5A). More interestingly, SDF-1α release between days 2-7 was undetectable using ELISA, suggesting sequestration of

residual SDF-1α not immediately released within the first 2 days. After 7 days, fibrin clots were digested with plasmin, a serine protease, to liberate immobilized SDF-1α for quantification. Cumulative detection of released SDF-1α in combination with SDF-1α recovered after fibrin digestion was similar to the initial payload for both groups (Figure 3.5B). Thus, the plateau in the SDF-1α release profile after the first 2 days strongly suggests that SDF-1α was captured and sequestered in fibrin matrices. The amount of SDF-1α sequestered was proportional to fibrin density as expected, where the 3mg/mL group was only able to sequester roughly 10% of the encapsulated SDF-1α. Additionally, The SDF-1α release profile from fibrin was comparable to previously reported for release kinetics for soluble FGF from fibrin [153], [234].

3.3.5. Fibrin Modulates SDF-1α Burst Release from PLGA NPs

Given the interaction uncovered between SDF-1α and fibrin(ogen), we evaluated potential modulation of NP release profile. Specifically, we aimed to determine the effect of embedding SDF-1α-loaded NPs in different fibrin densities on the burst release in an idealized *in vitro* release assay. This experiment only focused on the first 72hrs to fully capture the kinetics of the burst phenomena. The same concentration of NPs (1mg of PLGA / 1mL of fibrin) was embedded within three different fibrin clot densities (3, 10 & 25mg/mL). The resulting SDF-1α release profiles were strongly dependent on the fibrin concentrations (Figure 3.6A). Specifically, NPs embedded in 25mg/mL clots reduced the amount of detected SDF-1α by ~55% after 24hrs compared to NPs freely suspended in buffer. The total cumulative released SDF-1α was significantly reduced in the 10mg/mL ($p<0.01$) and 25mg/mL ($p<0.01$) groups after 72hrs in comparison to free NPs (Figure 3.6B). Additionally, difference in total protein released between the 25mg/mL, and both 3mg/mL ($p<0.01$) and 10mg/mL ($p<0.01$) groups was also statistically significant. Although, total SDF-1α detected in the 3mg/mL group was not significantly different

(compared to free NPs) after 72hrs, cumulative SDF-1α dosage was 25% lower after the first 10hrs upon addition of fibrin. Therefore, these data suggest the following, 1) amplitude of the NP burst may be tuned by exploiting SDF-1α/fibrin interactions and 2) embedding the NPs within fibrin gels of varying concentrations controls the amount of SDF-1α released within the first 72hrs *in vitro*, under idealized conditions.

3.3.6. PLGA NPs Do Not Significantly Alter Fibrin Polymerization

Fibrin (with and without NPs) matrices were assessed by measuring clottability of fibrinogen monomer, end-point turbidity and rheological characterization of viscoelastic properties. Our data suggests that the presence of NPs (up to 10mg/mL) does not significantly disrupt the formation of fibrin (Figure 3.7A). As a result, end-point turbidity of fibrin clots was also similar between native and NP-embedded gels for the 15 & 30mg/mL fibrin groups (Figure 3.7B). The differences observed for the 3mg/mL group was due to the presence of the NPs themselves (data not shown). Rheological studies further support that fibrin clot integrity was maintained upon addition of NPs (Figure 3.7C and D). The low-frequency plateau in the storage modulus (G') of both 3 & 30mg/mL fibrin groups indicate polymerization of fibrinogen to form viscoelastic fibrin (Figure 3.7C) [252]. Additionally, the overall characteristics of the storage and loss moduli was not altered upon adding 10mg/mL NPs in either 3 or 30mg/mL fibrin matrices (Figure 3.7C). The overall strength of fibrin was not dependent on NP content for the 3mg/mL fibrin group. Although statistically significant changes in G' was observed for 30mg/mL fibrin group with 1 & 10mg/mL NP (Figure 3.7D), the two-way ANOVA indicates that overall, NP concentration is not a significant determinant of fibrin storage modulus ($p=0.086$). Overall values for G' acquired for the fibrin groups were similar to other reports in literature for native fibrin [252]–[254].

3.5. Conclusion

Here, we report successful encapsulation of SDF-1α within PLGA NPs to achieve controlled release over 60days. Functional bioactivity of encapsulated and released SDF-1α was demonstrated through *in vitro* NPSC chemotactic migration assays. However, careful control over time-dependent SDF-1α concentration is crucial in eliciting desired therapeutic outcome. We determined that SDF-1α was successfully sequestered in fibrin clots and that NPs embedded in different concentrations of fibrin controlled the magnitude of the burst release profile without negatively affecting fibrin matrix properties. These results are significant in potentially obtaining local and sustained release of SDF-1α in a neural injury site to amplify and/or sustain NPSC-mediated endogenous repair response.

3.6 Figures

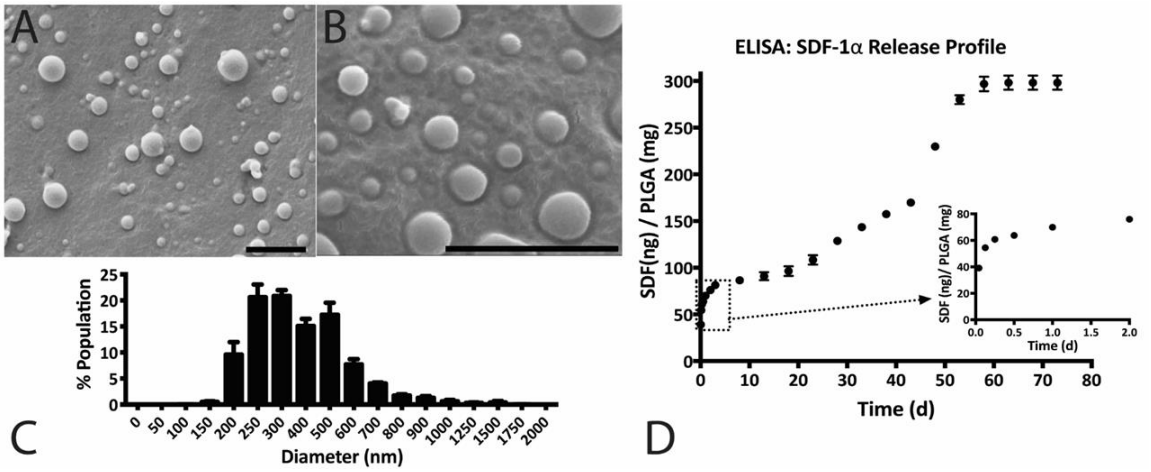

Figure 3.1: SDF-1α NP Characterization: (A, B) Representative SEM images of SDF-1α loaded NPs depicting smooth, spherical particles; scale bars = 2μm. (C) Histogram illustrating the size distribution of NPs with a range between 100-1500nm and where 90% of the population is between 200-600nm in diameter. (D) In vitro release assay measured with SDF-1α ELISA demonstrated sustained SDF-1α release for 60 days. The inset illustrates the initial burst release of 23% of total measured SDF-1α within the first 24hrs.

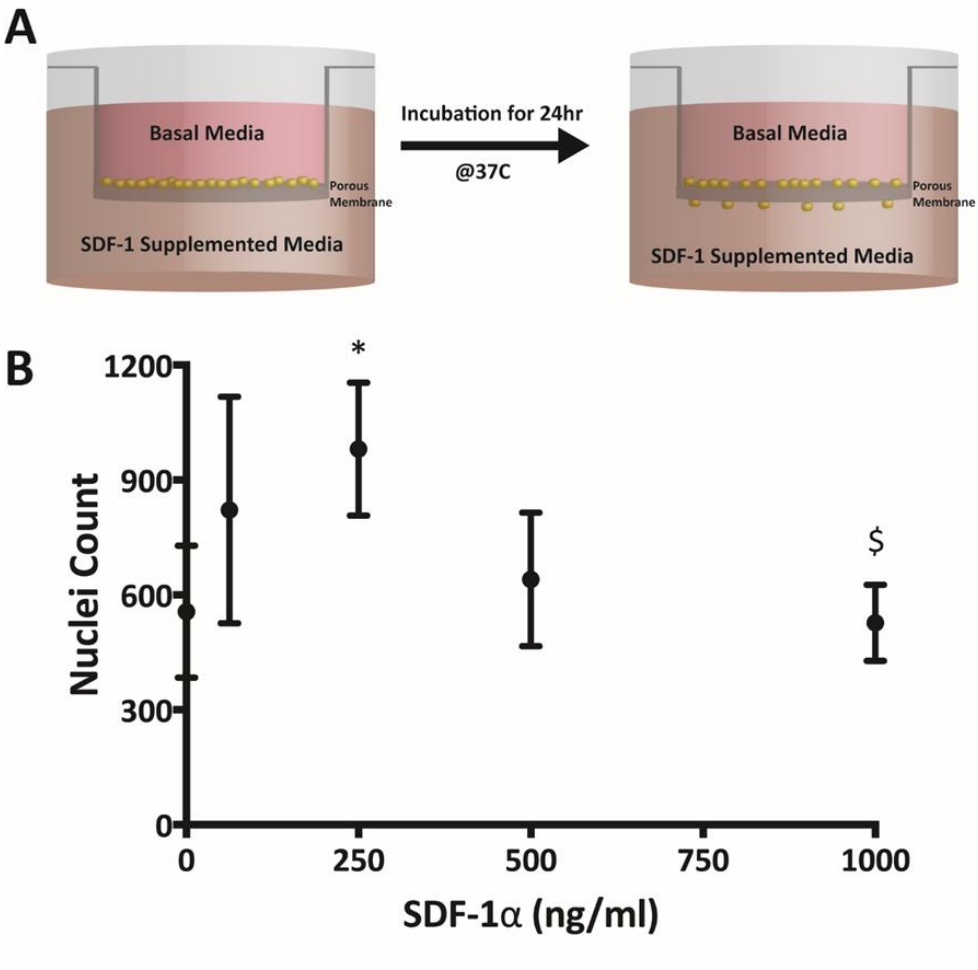

Figure 3.2: Soluble SDF-1α elicited a biphasic migration response in a Boyden chamber assay. (A) Schematic depicting the Boyden chamber setup where cells that were seeded in the top chamber migrates to reach the bottom side through chemotactic migration after 24hrs. (B) NPSC chemotactic migration demonstrates a biphasic response where the 250ng/mL group is significantly different compared to both to baseline and 1000ng/mL SDF-1α group. (* represents $p<0.05$ relative to 0ng/mL SDF-1α); $ represents $p<0.05$ relative to 250ng/mL).

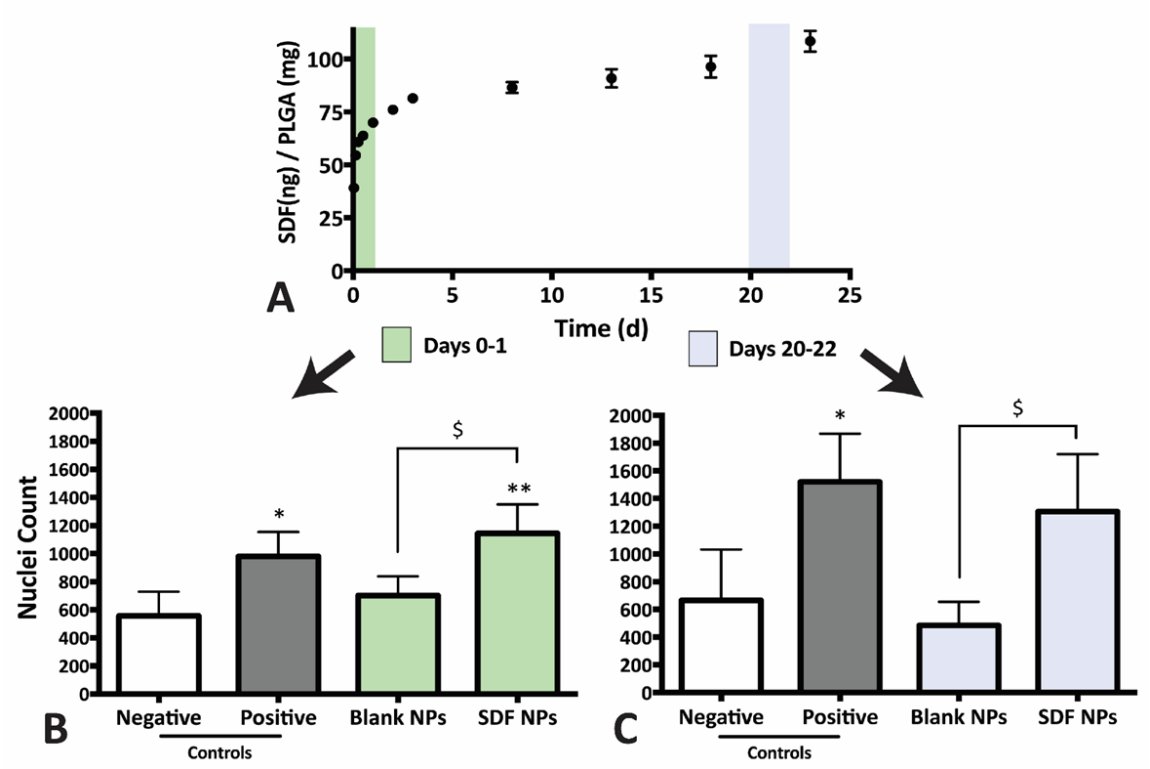

Figure 3.3: Bioactive SDF-1α Released from NPs. (A) Release media from day 0-1 and 20-22 were evaluated for bioactivity via NPSC chemotaxis assay. (B) Chemotactic response from NPSCs incubated with release media from day 0-1. SDF-1α-loaded NPs ('SDF NP') elicits a significant increase in nuclei count relative to both blank NPs and the negative control. (C) NPSC migration in response to release media from days 20-22. Although SDF-1α-loaded NPs were able to increase nuclei count significantly relative to blank NPs, the difference was not statistically significant in comparison to the negative control. (* & ** represents $p<0.05$ and $p<0.001$ respectively, relative to negative control and $ represents $p<0.05$ relative to blank NPs).

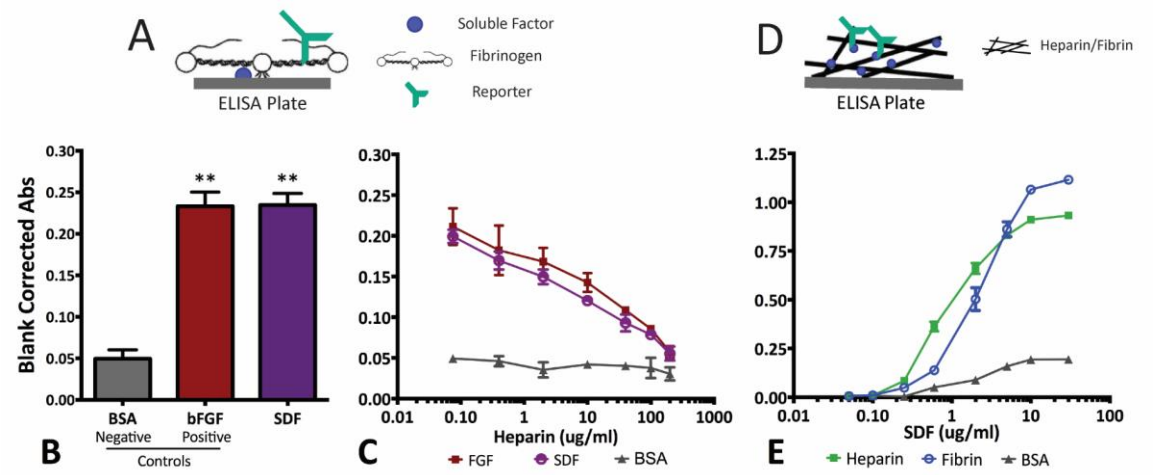

Figure 3.4: Specific protein-protein interactions exist between SDF-1α and fibrin(ogen). (A) Schematic depicting fibrinogen binding assay that consisted of high-binding ELISA plates coated with the soluble factors, bovine serum albumin (BSA; negative control), FGF (positive control) and SDF-1α ELISA setup used to measure fibrinogen binding affinity. (B) Signal from SDF-1α coated wells were significantly higher compared to negative controls (BSA) and comparable to the positive control (FGF) suggesting a specific interaction between SDF-1α and fibrinogen. (C) Increase in signal from fibrinogen binding is attenuated for FGF and SDF-1α-coated wells in a dose-dependent manner due to competition from soluble heparin. In contrast, BSA-coated wells do not exhibit heparin-dependant change in signal. (D) ELISA designed to probe fibrin interactions with SDF-1α where high-binding ELISA plates were coated with a thin layer of fibrin, BSA (negative control), and heparin (positive control). (E) A concentration-dependent increase in signal was observed for the fibrin-coated wells, similar to the trend observed for the positive control suggesting SDF-1α interactions persist in the polymerized form of fibrinogen, fibrin. (** represents $p<0.001$ relative to negative BSA control).

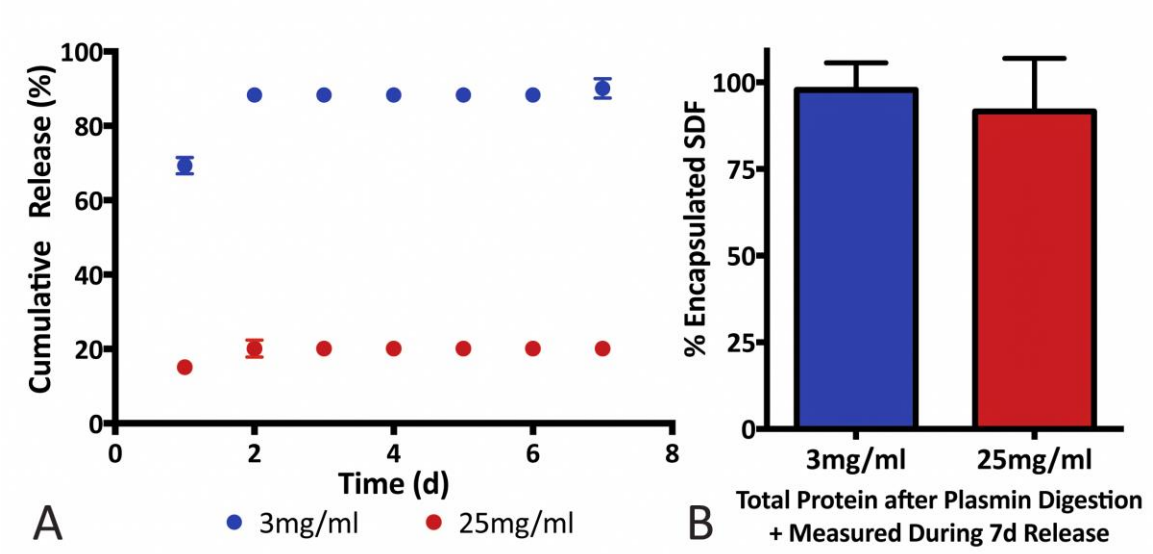

Figure 3.5: SDF-1α sequestered in fibrin matrices. (A) Release profile of free SDF-1α was significantly altered by encapsulation in different densities of fibrin. The 25mg/ml group showed a release of 20% after 2days, with no detectable SDF-1α released up to day 7. In contrast, the 3mg/ml released 90% of its cargo within the first 2days. (B) To ensure that the differences seen in the release profile were not due to problems with SDF-1α detection, the fibrin matrices were digested using plasmin and the total protein detected was similar to the initial payload for both groups.

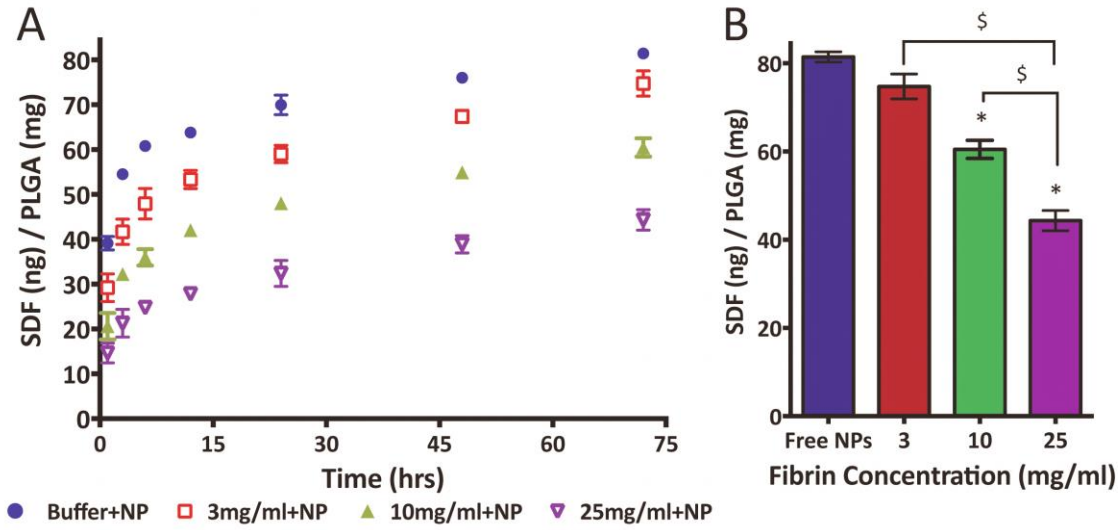

Figure 3.6: Magnitude of burst release from SDF-1α-loaded NPs was modulated with fibrin. (A) SDF-1α release from first three days was significantly modulated by embedding NPs in different concentrations of fibrin. After 24hrs, the 25mg/ml group was able to reduce SDF-1α detected in the release media by 60% relative to free NPs. B) Total SDF-1α detected was significantly different between the free NPs and 10mg/ml, as well as the 10 and 25mg/ml groups. Although the total SDF-1α detected after 72hrs in the 3mg/ml group was not significantly different, at 24hrs cumulative SDF-1α is decreased by 25% in the fibrin group. (* represents $p<0.05$ relative to free NPs; $ represents $p<0.05$ relative to 25mg/ml fibrin group).

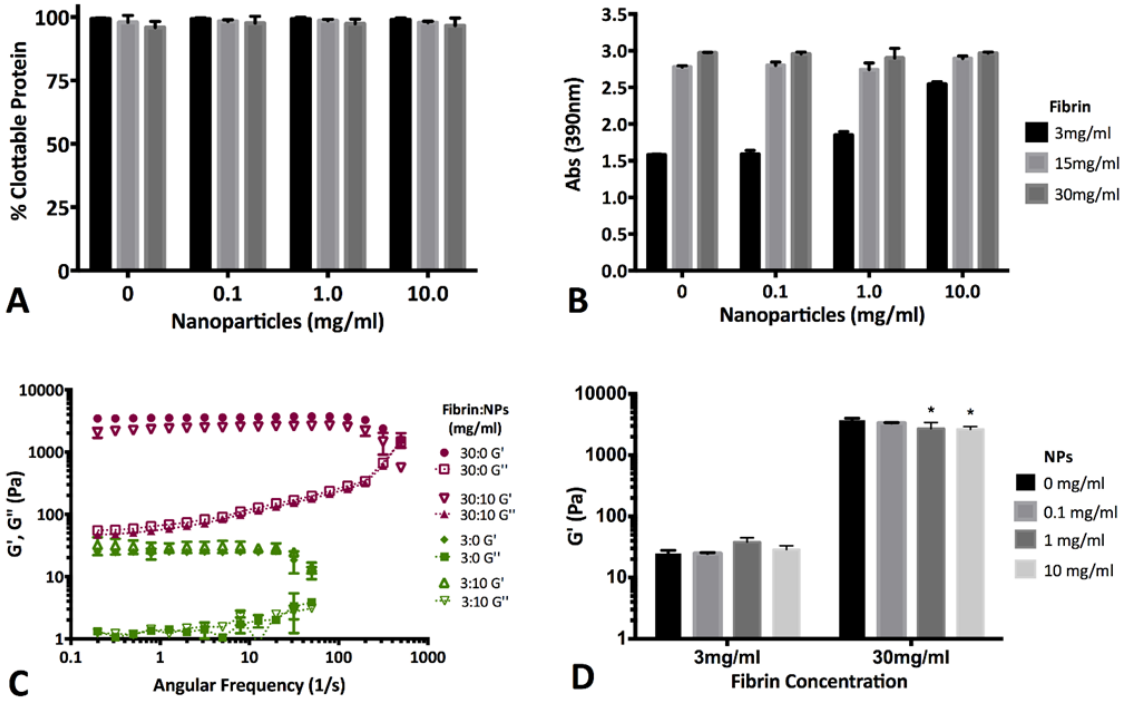

Figure 3.7: NP encapsulation does not significantly affect fibrin clot properties. (A) Percent clottable protein is not a function of NP encapsulation (up to 10mg/mL). Presence of NPs do not affect the ability of fibrinogen to interact with other monomers to form the insoluble fibrin clot. (B) Terminal turbidity of fibrin clots is not affected by NP concentrations up to 10 mg/mL. The increase in turbidity seen in the 3mg/mL

fibrinogen group with 10mg/mL NPs is likely due to the presence of the NPs themselves. (C) Storage (G') and loss (G"; dotted plots) moduli of 3mg/mL (green) and 30mg/mL (red) fibrin clots. Native fibrin (no NPs) and fibrin with 10mg/mL NP illustrate that the presence of NPs cause minimal changes in fibrin mechanical properties. (D) Overall strength of 3mg/mL fibrin gels are not a function of NP content. Although 30mg/mL gels did show significant differences at 1 & 10mg/mL NP groups, two-way ANOVA analysis indicates NPs do not play a statistically significant role in fibrin storage modulus ($p=0.05$). (* represent $p<0.05$ relative to 30mg/mL fibrin with 0mg/mL NPs).

CHAPTER 4

SPATIOTEMPORAL PRESENTATION OF EXOGENOUS SDF-1 MODUATES THE IN-VIVO OF SDF-1/CXCR4 SIGNALING AXIS IN THE RODENT CORTEX

4.1. Introduction

The SDF-1α/CXCR4 signaling axis has gained considerable attention as a therapeutic target in diverse areas of study such as immune-modulation, trafficking of stem cells and cancer metastasis. Among them is the role of SDF-1α in the migration of neural progenitor/stem cells (NPSCs) during pathological conditions of the central nervous system (CNS) [255], [256]. After neural injury (traumatic brain injury, TBI, or stroke), NPSCs in the neurogenic niches, exhibit a remarkable ability for directed migration to reach the injury penumbra [36], [81]. Migrated NPSCs not only maintain neurogenic capacity, but they also secrete neurotropic factors and assist in preserving synaptic connectivity in the injury area [255], [257]. As such, ablation of endogenous NPSC populations before induction of neural injury significantly hampers the endogenous neurogenic potential contribution to increased cognitive impairments [83]. However, this NPSC migratory response is transient, peaking at 3-7 days post injury (in rodent models) and decreases dramatically, although not completely, by two weeks post injury [87]. Mechanisms controlling this endogenous injury response are not yet fully understood, but the SDF-1α/CXCR4 signaling cascade is thought to play an important role due to the following: 1) NPSCs are $CXCR4^{+}$ and respond chemotactically to SDF-1α gradients *in vitro* [4], 2) NPSCs migrate to local sources of SDF-1α *in vivo* after neural injury [36], [81], 3) local administration of the CXCR4 antagonist, AMD3100 attenuates NPSC migration [84], and 4) decreasing local concentrations of SDF-1α coincides with the aforementioned decrease in the number of migrating NPSCs *in vivo* after neural injury [81], [87]. Thus, control over the local bioavailability of SDF-1α serves as a

potential means for amplifying/sustaining the innate NPSC homing response after neural injury. We have previously developed poly(D,L,-lactic-co-glycolic) acid (PLGA) nanoparticles (NPs) that encapsulate and release bioactive SDF-1α over a period of 60 days [258]. PLGA is FDA-approved and PLGA-based NPs have the added benefits of: 1) direct injection into target tissues, 2) biodegradability, 4) metabolizable degradation products and, 5) lowering risks of infections compared to conventional osmotic pumps [222], [258]. Moreover, PLGA matrices maintain prolonged, localized bioavailability and may aid in protecting the encapsulated cargo from degradation, a critical parameter for protein delivery [187], [191], [192].

Growing evidence indicates that the spatio-temporal presentation of bioactive factor(s) alters the overall biochemical cellular response. For example, sustained release of proteins differentially affects stem cell proliferation, migration and differentiation both *in vitro* and *in vivo* when compared to bolus administration [140], [141], [259]. Additional studies demonstrate that sustained release of proteins do not always lead to an improvement in therapeutic efficacy [142], [146]. Instead, differing protein release profiles (bolus, sustained, delayed and pulsed) may activate distinct biochemical cascades that determines overall therapeutic outcome [260]. Additionally, receptor desensitization/downregulation due to overstimulation is another well-known phenomenon that may occur with sustained controlled release devices [144], [145]. Specifically, for SDF-1α/CXCR4, it is unclear how or if autocrine/paracrine signaling affects regulation of SDF-1α/CXCR4 expression. Furthermore, discovery of a second SDF-1α receptor, CXCR7, further complicates our understanding of how the SDF-1α mediated signal transduction propagates. Some *in vitro* evidence points to downregulation of CXCR4 after continuous exposure to SDF-1α in neonatal E14.5 telencephalic neurons, but its relation to native cortical tissues in the mature forebrain

where multiple cell-types express CXCR4 and secrete SDF-1α is not certain [15], [186]. Although a number of studies have focused on endogenous SDF-1α/CXCR4 signaling in the developing brain and after neural injury, none have directly assessed endogenous SDF-1α/CXCR4 signaling in response to different spatiotemporal presentations of exogenous SDF-1α. We believe that this represents a fundamental barrier in the development of efficacious strategies for manipulating the SDF-1α/CXCR4 signaling cascade, a ubiquitous therapeutic target for diverse applications.

The goal of this study was to begin elucidating the SDF-1α/CXCR4 signal propagation in the adult rodent cortex in response to either bolus or sustained release of exogenous SDF-1α. To facilitate a more direct correlation between administration of exogenous SDF-1α and endogenous SDF-1α/CXCR4 signaling, we performed *in vivo* studies in the intact (uninjured) mouse cortex to avoid confounding factors otherwise present in the complex injured microenvironment [255]. Critical tools employed include: 1) transgenic (CXCR4-EGFP) mice that have a intracellular reporter (enhanced green fluorescent protein; EGFP) for CXCR4 expression [186], 2) fluorophore-conjugated SDF-1 (AFSDF-1) that retains bioactivity and, 3) PLGA nanoparticles that encapsulates bioactive AFSDF-1 [258]. Using this toolset, we tracked spatiotemporal localization of endogenous SDF-1 and CXCR4+ cells (1, 3 & 7 day timepoints) in response to intracortical injections of either bolus AFSDF-1 or AFSDF-1-loaded NPs. We hypothesized that endogenous SDF-1/CXCR4 expression will increase acutely after exposure to both bolus and controlled release of exogenous AFSDF-1. However, bolus administration leads to a transient response from the endogenous SDF-1/CXCR4 signaling axis; whereas sustained release of exogenous SDF-1α may lead to downregulation of CXCR4 expression overtime despite bioavailable exogenous SDF-1. The results of these experiments will inform design and testing of future biologically

relevant release devices capable to modulating the SDF-1/CXCR4 signaling axis over extended periods of time.

4.2. Experimental Methods

4.2.1 Materials

Poly(lactic-*co*-glycolic) acid (PLGA; 50:50 ester-terminated; inherent viscosity = 0.55-0.75dL/g) was purchased from Lactel (Birmingham, USA). Recombinant mouse stromal cell-derived factor-1 α (SDF-1α) were acquired from PeproTech (Rocky Hill, USA). Recombinant human-derived SDF-1α conjugated with AlexaFluor-647 at the C-terminus (AFSDF-1) was acquired from Almac (Craigavon, UK). B27 growth supplement, DAPI nuclear stain, and Dulbecco's modified eagle medium were acquired from Life Technologies (Carlsbad, USA). Glucose was obtained from Acros Organics (Geel, Belgium). The organic solvent ethyl acetate was acquired from Alfa Aesar (Ward Hill, USA) and dimethyl sulfoxide (DMSO) from American bioanalytical (Natick, USA). All other materials and chemicals were purchased from Sigma-Aldrich (St. Louis, USA) and used without further modification or purification.

4.2.1 NPSC Harvest and Culture

Murine fetal derived neural progenitor/stem cells (NPSCs) were isolated from the medial and lateral germinal eminences of E14.5 C57BL/6 mice based on previously published protocols and in accordance with approval by the Institutional Animal Care and Use Committee at Arizona State University [235]. The germinal eminences were harvested, mechanically disassociated and cultured in NPSC medium (Dulbecco's modified eagle medium (DMEM:F12) with 2.4mg/mL sodium bicarbonate ($NaHCO_3$), 6 mg/mL glucose, 5mM HEPES, 62.9 ng/mL progesterone, 9.6 μg/mL putrescine, 1.83 μg/mL heparin, 1X B27 growth supplement, 20 ng/mL epidermal growth factor

(EGF), 5 ng/mL FGF, 5 μg/mL insulin, 5 μg/mL transferrin, and 5 ng/mL sodium selenite). NPSCs were cultured as non-adherent neurospheres and used for experimentation between passages 3-6.

4.2.2 Chemotactic NPSC Migration Assay

NPSC chemotaxis in a modified-Boyden chamber assay was used to validate AFSDF-1 bioactivity on mouse-derived NPSCs as previously described [12]. In short, disassociated NPSCs were plated (70,000 cells/cm^2) on laminin-coated transwell inserts with 8μm pore diameter (Millipore, Temecula, CA). Growth factor-free NPSC medium (no EGF or FGF) with 0, 250, or 1000ng/mL SDF-1α was added in the bottom chamber. NPSCs were then allowed to undergo chemotaxis for 24hrs in an incubator (37^{o}C and 5% CO_2). Subsequently, cells on the topside of the transwell membrane were removed using a cotton swab whereas migrated cells that reached the bottom were fixed, underwent a DAPI nuclear stain and imaged. NPSC nuclei have diameters of approximately 20μm [236]. After intensity thresholding, nuclei count was quantified using a particle count algorithm in ImageJ where stained nuclei 10-30μm in diameter were counted as individual cells. Nuclei count was determined by imaging and quantifying whole transwell membranes.

3.2.2. Fabrication of AFSDF-1 Loaded Nanoparticles

AFSDF-1 loaded PLGA nanoparticles were fabricated using a water/oil/water (W/O/W) emulsion technique using a previously published protocol [258]. Briefly, the first emulsion (W/O) was obtained by vortexing the oil phase (100 mg/mL PLGA in ethyl acetate) with PBS buffer solution (pH = 7.4) containing 2.0mg/mL AFSDF-1 (0.2% w/w of PLGA). The above solution was added dropwise to a 3.6x volume excess of an aqueous 5.0% (w/v) d-α tocopheryl polyethylene glycol 1000 succinate (TPGS) and the second

emulsion (W/O/W) was produced by ultrasonicating (Omni Ruptor 4000; Omni International; Kennesaw, USA) the solution for two consecutive 15sec periods in an ice bath. The emulsion was then quickly transferred to a stirring (300RPM) aqueous bath containing 0.5% TPGS + 1.25% (w/v) NaCl (10x volume excess) and left undisturbed for 3hrs for solvent evaporation. The particle suspension was washed three and recovered through lyophilization.

4.2.3 Animal Model

The CXCR4-EGFP transgenic mice were kindly donated to us by Dr. Richard Miller of Northwestern University. All studies were conducted in accordance with approved protocols reviewed by the Institutional Animal Care and Use Committee at Arizona State University. The CXCR4-EGFP mice are well characterized and utilized in studies characterizing the developing and adult rodent CNS [186], [261], [262]. CXCR4–EGFP bacterial artificial chromosome (BAC) transgenic mice was originally developed by the gene expression nervous system atlas (GENSAT; NINDS contract N01Ns02331 to Rockefeller University, NY). Expression of EGFP in these mice is expected to be identical to endogenous gene expression as examined by in situ hybridization (http://www.gensat.org/index.html).

4.2.4 Controlled Cortical Impact (CCI) Model of TBI: Validation of Transgenic Mouse

All studies were conducted in accordance with approved protocols reviewed by the Institutional Animal Care and Use Committee at Arizona State University. CCI was used to produce unilateral cortical contusions in adult, male and female CXCR4-EGFP transgenic mice to validate that the animal model recapitulates known known CXCR4 and SDF-1 patterns after CCI [263]. Briefly, the mice were anesthetized using isoflurane and immobilized in a stereotactic frame (Leica; Wetzlar, Germany). A biopsy punch was

used to produce a 3 mm diameter craniotomy centered on 1.5 mm anterior of bregma and 1.5 mm lateral of midline leaving the dura mater intact. A 2 mm diameter piston was then centered over the craniotomy and was electromagnetically driven 1 mm into the cortical tissue at a velocity of 6 m/s for a duration of 200 ms (ImpactOne, Leica). At specified timepoints post-injury, the mice were anesthetized and sacrificed through pericardial perfusion to extract the brain that was post-fixed in 4% paraformaldehyde for 24 hrs.

4.3.5. Intracortical Injections

Adult, male and female CXCR4-EGFP transgenic mice (n=5 per group/time point) were anesthetized and a 1.5mm craniotomy was performed centered over 1.5mm anterior of bregma and 1.5mm lateral of midline. 3μL injections were performed at a depth of 0.8mm into the cortical tissue using a 26G needle for the following groups: 1) bolus AFSDF-1α, 2) bolus vehicle, 3) AFSDF-1α NPs and, 4) NP vehicle. Separate Hamilton syringes and needles were used for all groups (Hamilton, Reno, NV). The syringe and needle was stereotaxically placed, lowered 0.8 mm into the cortical tissue at a rate of 0.15 mm/min and kept stationary for 1 min. The needle was then retracted back up to 0.5 mm before the injections were initiated at 0.5 μL/min, pausing every 1μl for 30s until 3μl dose was delivered. The needle was subsequently held in place for 1 min before being retracted at 0.15 mm/min. For the particle groups, lyophilized NPs were resuspended at 140mg/ml, subjected to water-bath sonication (on ice) for 2mins immediately before the injection procedure. After the operation, mice were anaesthetized and sacrificed at 1, 3, and 7 days post-injection by pericardial perfusion to extract the brain that was post-fixed in 4% paraformaldehyde for 24 hrs.

4.3.6 Immunohistochemistry and Image Processing

Following fixation, extracted brain tissues were saturated with sucrose by incubation in 30% sucrose for 48hrs. The specimen was then cryo-fixed and serially sectioned at 25μm thickness. Sections were blocked with goat serum, permeabilized and stained for SDF-1α (rabbit anti-SDF-1α, Abcam; AlexaFluor-555 conjugated goat anti-rabbit, Life Technologies). Stained sections were visualized using fluorescence microscopy (DMI6000B, Leica) and 20x tiles scans were used to produce cortical representations. Fluorescence-based semi-quantitative analysis were conducted on the resulting images using ImageJ to determine spatiotemporal localization of CXCR4+ cell bodies as well as, endogenous SDF-1α and exogenous AFSDF-1.

Some differences in tissue and cellular morphology were observed at the needle tract between the bolus and NP implant groups (discussed in the following sections; Figure 4.1). Thus, two different approaches were used to assess the effects of bolus administration (AFSDF-1 vs vehicle) as well as, differences between bolus and sustained release of AFSDF-1. All cortical representations were first divided in four basic zones (Figure 4.1):

1) Needle tract: Region of tissue (100-200 μm across) that was punctured by the needle to administer the injections.

2) Injection site: a 600 μm section centered on the needle tract.

3) Proximal to injection: two 400 μm sections located directly adjacent to the injection site (medially and laterally).

4) Distal to injection: Remaining portions of images that extends past 700 μm from the needle tract in both, medial and lateral directions out to 1700 μm.

Secondly, three regions of interest (ROIs) that make up one or more of the above zones were selected based on the type of comparison (Figure 4.1). The principal

difference was omitting the injection site for any comparisons that include the sustained release groups (Figure 4.1). Thirdly, relative differences in CXCR4+ cell density and SDF-1 localization with respect to the needle tract were determined using an average of 12 cortical representations for every group, at each timepoint. CXCR4+ cells exhibited strong EGFP signal where cell bodies with intermediate or weak EGFP expression was not prevalent (Figure 4.3B). The apparent "on/off" nature of the endogenous CXCR4 expression reporter allowed for thresholding, followed by particle count algorithms to determine total count and spatio-temporal localization of CXCR4 overexpressing cells. SDF-1 immunostains on the other hand, indicated complex, non-uniform patterns of staining, especially in the AFSDF-1-loaded NP groups. Additionally, IHC stains are considered "semi-quantitative" due to a host of variables related to tissue processing before, during and after completion of IHC [264]. Thus we used contralateral-adjusted (to minimize subjectivity) thresholding values to determine the area fraction of SDF-1 overexpression in the desired ROIs. These semi-quantitative measurements are presented to glean overarching patterns in SDF-1 localization between the experimental groups.

4.3.7 Statistical Analysis

Statistical analysis was performed on all quantitative assays. All results are depicted as the mean ± one standard deviation, unless otherwise stated. Statistical analyses (GraphPad Prism, La Jolla, CA) evaluated differences between groups using analysis of variance (ANOVA) followed by Tukey post-hoc tests to determine statistical significance with $p < 0.05$ considered significant. Multiplicity adjusted p-values are reported for Tukey post-hoc comparisons.

4.3. Results

4.3.1. Validation of AFSDF-1 and CXCR4-EGFP Mouse Model

The N-terminus of SDF-1 is critical for binding and activation of CXCR4 [265]. Thus, site-specific modifications at the C-terminus is predicted to better maintain SDF-1 bioactivity [266]–[269]. The only commercially available fluorescently-tagged SDF-1 was human-derived recombinant SDF-1 with AlexaFluor-647 conjugated to the C-terminus (AFSDF-1) from Almac Chemokines (Craigavon, UK). Previous studies have noted cross-reactivity between diverse species, yet we wanted to verify that mouse NPSCs respond to this human AFSDF1. A modified-Boyden chamber migration assay was used with 8μm pore width membranes. NPSCs were plated on the topside of membrane and the nuclei of cells that migrate to reach the bottom in response to SDF-1α were counted after a 24hr incubation period. Since the SDF-1 gene is over 90% homologous between mouse to human species, both types of SDF-1α elicited a similar pattern of migratory behavior from mouse-derived NPSCs (Figure 4.2) [270]. Three different SDF-1α concentrations (0, 250 & 1000ng/ml) were evaluated in the bottom chamber of the Boyden assay. Nuclei count increased in a SDF-1α dose-dependent manner although only the human SDF-1α at 1000ng/ml elicited a statistically significant change in nuclei count. Regardless, similar patterns in NPSC response validated the bioactivity of human-derived SDF-1α on mouse NPSCs.

The CXCR4-EGFP animal model has been characterized in literature extensively to study development in prenatal mice as well as pathology in adult mice [38], [262], [271], [272]. However, we are the first to our knowledge to utilize them in the context of TBI. To demonstrate validity of the CXCR4-EGFP animal as a model for focal injury models of TBI, we performed CCI injuries and probed for SDF-1 (immunohistochemistry; IHC) and CXCR4 (intracellular EGFP) one day-post injury. The CXCR4-EGFP transgenic mice recapitulated known SDF-1 and CXCR4 overexpression in the pericontusional region acutely in response to CCI (Figure 4.3) [36], [81], [87]. The

ipsilateral cortex exhibited high concentrations of EGFP+ cell bodies (indicating CXCR4 overexpression) relative to contralateral. SDF-1 immunostaining also qualitatively revealed relatively strong signal in the ipsilateral cortex.

4.3.2. AFSDF-1 Delivery and Diffusion in the Cortex

Intracortical injections of 420μg of PLGA NPs was expected to release 29.4 ng of AFSDF-1 in the first 24hrs and an additional 9.1 ng through the following 7 days as estimated from previously published release profile of SDF-1α from PLGA NPs fabricated under the same conditions [4]. Previous *in vivo* studies deliver significantly higher doses of SDF-1 (4μg) in the form of bolus injections [168], [218]. We were however constrained by the AFSDF-1 loaded PLGA NPs, specifically its protein loading capacity and the total deliverable dosage of NPs in the cortex. Thus, AFSDF-1 dosage in the bolus group was 30 ng to match the estimated cumulative AFSDF-1 release in the first 24hrs from the NPs. One day post-injection, penetration of bolus AFSDF-1 in the cortex was limited approximately to 100 μm from the needle tract (Figure 4.4A). For the sustained release groups, strong AFSDF-1 signal in the immediate vicinity of the injection tract may indicate both released and encapsulated AFSDF-1 (Figure 4.4B). Whereas more diffuse and significantly weaker signal near the periphery of the injection tract likely indicated diffusion of exogenous AFSDF-1 in the cortical parenchyma (Figure 4.4C). Although fluorescent signal from AFSDF-1 does not necessarily indicate its bioactivity, the short diffusion lengths agree with previous studies that report limited protein diffusion in the brain parenchyma [136], [273], [274].

4.3.3. Bolus AFSDF-1 Induced Transient and Localized Expression of CXCR4

Nuclear staining (4',6-diamidino-2-phenylindole; DAPI) qualitatively indicated some disruption in tissue organization in the immediate vicinity (within 50-100 μm) of

the needle tract after bolus injections (Figure 4.5). Bolus AFSDF-1 induced increased local expression of CXCR4 as indicated by intracellular EGFP signal that colocalized with DAPI nuclear stain (Figure 4.5). Here, the majority of CXCR4+ cells along with AFSDF-1 were localized in close proximity to the needle tract. CXCR4+ cells in and around the needle tract exhibited relatively well compartmentalized EGFP signal suggesting intact plasma membranes (Figure 4.1B). Across the total ROI evaluated (~2.8 mm; Figure 4.1A), the CXCR4+ cell body density (# of cells/mm^2) 1 day post bolus injection of AFSDF-1 significantly increased relative to vehicle. Moreover, this maximal response at 1 day post injection was significantly higher than bolus or vehicle injections at 3 and 7 days post injection (Figure 4.6A). Total CXCR4+ cell density decreased for bolus AFSDF-1 at day 3 & 7, where AFSDF-1 bolus was comparable to vehicle injection (Figure 4.6A). No significant differences were observed in the vehicle groups across the 1, 3, and 7 days post injection (Figure 4.6A). Looking solely at the region proximal to the injection site, bolus AFSDF-1 elicited a modest yet significant increase in CXCR4+ cell density compared to vehicle at day 1 (Figure 4.6B). This significance was not observed at day 3 and 7 and CXCR4 expression returned to levels similar to the vehicle group (Figure 4.6B). Bolus injection of AFSDF-1 had no impact on CXCR4 expression at most distal to the injection site (~700um away; Figure 4.6C), suggesting that the vast majority of the CXCR4+ cell bodies in response to bolus AFSDF-1 were located at the injection site. Results suggest that a 30ng payload of bolus AFSDF-1 has localized and transient effects on CXCR4 expression that then decreases between day 3 and 7 post injection.

4.3.4. Bolus AFSDF-1 Did Not Modulate SDF-1 Expression Outside of the Injection site

IHC trends for total SDF-1 (endogenous and exogenous) suggested an increase in total SDF-1 immunostaining (as measured by % area) at day 1 relative to all vehicle groups, but not the day 3 or 7 AFSDF-1 groups (Figure 4.7A). Total SDF-1

immunostaining continued to trend downwards until day 7 comparable to the vehicle group (Figure 4.7A). AFSDF-1 administration does not affect overall SDF-1 expression at either the proximal or distal ROIs (Figure 4.7B & C). As such, increases in total SDF-1 levels were likely due to changes occurring in the injection site (Figure 4.8). A substantial source of total SDF-1 surrounding the needle tract is exogenous AFSDF-1 signal from which was expected to attenuate over time. A decreasing trend in total SDF-1 immunostaining is also observed at the injection site (Figure 4.8A). However, representative images of AFSDF-1 and SDF-1 immunostains indicated an incomplete overlap between exogenous and total SDF-1 at the needle tract (Figure 4.8B – G). Thus, a transient expression of endogenous SDF-1 due to AFSDF-1 administration may contribute to the overall increase in SDF-1 immunostaining observed at day 1 for the AFSDF-1 bolus group (Figure 4.7A). Furthermore, bolus AFSDF-1 administration did not affect endogenous SDF-1 expression in areas proximal and distal to the injection site (Figure 4.7B-C). It is also important to note that neither SDF-1 immunostaining, nor AFSDF-1 fluorescent signal is a direct measurement of bioactive SDF-1; rather the former is representative of an epitope site that mediates binding with the SDF-1 primary antibody and the latter, AlexaFluor-647 fluorophore stability.

4.3.5. Sustained Release of AFSDF-1 Induced Transient CXCR4 Expression in Cells Located Distally from the Injection site

As mentioned previously, quantifications for the particle groups excluded the injection site and thus, total CXCR4 counts were no provided, instead, only the proximal, distal and “proximal + distal” ROIs were quantified. Sustained release of AFSDF-1 elicited a significant increase in CXCR4+ cell density in the “proximal + distal” ROI (Figure 4.1C) at day 1 compared to both blank NP and AFSDF-1 bolus groups (Figure 4.9A). Subsequently, CXCR4+ cell density decreased at day 3 for the AFSDF-1 NPs

compared to blank NP yet remained significantly higher than the AFSDF-1 bolus group. By day 7, CXCR4+ cell density was comparable between all groups in the proximal + distal ROI (Figure 4.9A). Looking more closely at the region proximal to the injection site, CXCR4+ cell density was significantly higher at days 1 & 3 for the AFSDF-1 NPs compared to their respective bolus AFSDF-1 groups, but not the blank NPs (Figure4.10B). No statistically significant trends were observed at day 7. Most distally to the injection site, CXCR4+ cell density for AFSDF-1 NP was increased significantly at day 1 compared to all other groups in the study (Figure 4.9C). However, the number CXCR4+ cells decreased at day 3, eventually approaching the control groups by day 7. It is also important to note that some replicates for the blank NPs exhibited relatively high CXCR4+ cell density outside of the injection site. A significant difference between the blank NPs and bolus vehicle group was noted at day 1 ($p=0.023$) for the proximal ROI, however no other time-matched comparisons were statistically significant between the two control groups (Figure 4.12). Furthermore, no statistically significant time-matched comparisons were found between the Blank NP and Bolus AFSDF-1 group (Figure 4.12).

4.3.6. Sustained Release of AFSDF-1 Affected SDF-1 Immunostaining Beyond the Injection Site

SDF-1 immunostaining, especially for the AFSDF-1 NPs resulted in highly complex and non-homogenous distribution of positive staining with relatively high variability between replicates (Figure 4.10). Additionally, averaging the medial and lateral percent area of positive immunostaining (for the proximal and distal ROIs) did not account for the non-uniformity of SDF-1 signal distribution. Regardless, the overall trends suggest that SDF-1 levels were relatively higher for the AFSDF-1 NP group compared all blank NP and bolus AFSDF-1 groups outside of the injection site ("proximal + distal" ROI; Figure 4.11A). Focusing on solely the region adjacent to the

injection site (proximal ROI), SDF-1 immunostaining was significantly increased with AFSDF-1 NPs as compared to blank NPs only at one day post injection (Figure 4.11B). However, no statistical difference was revealed in regions most distal to the injection site (Figure 4.11C).

4.4. Discussion

The SDF-1/CXCR4 signaling axis is implicated in a host of pathological conditions, is thus investigated as a therapeutic target in diverse applications such as cancer metastases and tissue engineering after injury [11], [255]. Thus elucidating mechanisms that efficiently modulate the SDF-1/CXCR4 signaling axis is of great value. Bolus delivery is the most common method used to study the effects of exogenous SDF-1 thus far in the CNS [168], [218]. Although, bolus injections have inherent advantages such as local delivery in the target tissue and control over dosage, it negates temporal control over concentration or payload degradation leading to only transient therapeutic benefits. Bioengineered approaches for sustained SDF-1 bioavailability include a number of hydrogel-based devices for various applications with diffusion-limited release periods of 7-14 days [170], [171], [173], [178]. Others have proposed polyester-based systems to prolong release over period of weeks to months [180], [185]. We have previously developed and characterized PLGA nanoparticles (NPs) that sustains release of bioactive SDF-1α over 60 days [258]. However, given the complexity and possible auto-regulatory processes that modulate SDF-1α signal transduction, it is unclear whether slow, and sustained release of SDF-1α locally is the most efficacious means of modulating the SDF-1/CXCR4 signaling axis in the long-term. Indeed recent reports suggest downregulation of CXCR4 when continuously stimulated with SDF-1 [15]. Others are shedding light on a new receptor, CXCR7 that modulates sensitivity to extracellular SDF-1 [20]. There is a lack of studies devoted to understanding how the SDF-1/CXCR4 signaling axis responds

to various spatiotemporal presentations of exogenous SDF-1 *in vivo*. We thus used the CXCR4-EGFP transgenic mouse model to study the effects of bolus and controlled release of exogenous AFSDF-1 on the endogenous spatiotemporal localization of SDF-1 and CXCR4-expressing cells over a period of 7 days.

AFSDF-1 penetration in the cortical tissues was limited, detectable AFSDF-1 bolus payload was confined to within 100μm from the needle tract (Figure 4.4). Once in the interstitial space, protein diffusion, rather than convection is the main mechanism of transport in the brain extracellular space (ECS). Diffusion over short distances (<0.1mm) is relatively efficient, however the densely packed architecture of the ECS means diffusion in the order of millimeters is unlikely to occur in therapeutically-relevant time scales [131]. In addition to a small void fraction, cortical extracellular matrix (ECM) is composed of negatively charged components such as hyaluronic acid, heparan sulfate and chondroitin sulfate proteoglycans among others. Thus, diffusion of highly basic proteins such as SDF-1 (isoelectric point ~9.6 for the SDF-1α isoform) is expected to be hindered and/or be fully immobilized due to electrostatic interactions. Since encapsulated and released AFSDF-1 could not be differentiated near the needle tract for the NP implant groups, comparisons for AFSDF-1 tissue penetration between the bolus and sustained release were not presented (Figure 4.4). However, previous studies indicate that protein penetration in the brain interstitial space is enhanced through sustained release devices (protein release from hydrogels) or continuous infusions (i.e. convection enhanced delivery via osmotic pumps) [140], [275]. Enhanced diffusion is these cases is partly mediated by a maintenance of a concentration gradient for a longer period of time relative to a bolus administration.

SDF-1α PLGA NPs were adapted to achieve sustained release of exogenous AFSDF-1 [4]. EGFP signal was observed within, and at the edges of the NP implants

(Figure 4.10). Previous reports demonstrate PLGA microparticles implants in the striatum stimulate localized activation of microglia/macrophage as early as one day post-injection [276]. Since activated microglia and infiltrating systemic macrophages employ the SDF-1/CXCR4 signaling cascade, the EGFP signal from the NP implants is a possible indicator of a host response [33], [277]. Further cell phenotype characterizations are required to determine if/how immune cell-types contribute to CXCR4+ cell density observed near the NP implants. However, the measured outcomes of the study (CXCR4+ cell density and SDF-1 immunostains) from blank NP implant groups suggest that the NP implants did not induce a widespread foreign body immune response (material response; Figure 4.12). Increased CXCR4+ cell density was limited primarily to the injection site and increased SDF-1 immunostaining was not observed for any of the blank NP groups regardless of timepoint (Figure 4.10 & 4.12). Thus the localized effects of NP implants at the injection site were omitted and quantitative analyses comparing the effects of bolus and sustained release of AFSDF-1 included the proximal, distal, and "proximal + distal" ROIs.

We report statistically significant differences in CXCR4+ cellular activity in response to a bolus dosage of 30ng of AFSDF-1 [218]. At day 1, 193.1 ± 136 cell bodies/mm^2 expressed CXCR4 at the injection site, which decreased 12-fold at day 3, eventually reaching comparable levels to controls by day 7. This trend may be attributed to a decrease in bioactivity/bioavailability of AFSDF-1 over time, especially at the 3 and 7 day time points. Densely populated EGFP+ cell bodies were closely associated with the needle tract at day 1 post bolus injection suggesting that exogenous AFSDF-1 induced CXCR4 expression, agreeing with *in vitro* and *in vivo* trends reported in literature (Figure 4.5) [15], [218], [278]. A wide range of cell types, are expected to contribute to the overall CXCR4+ cell densities reported. CNS resident cell types such as, mature

neurons, oligodendrocytes, astrocytes, endothelial cells are not only CXCR4+, but they also regulate CXCR4 expression when exposed to SDF-1 [14], [15], [277], [279], [280]. Furthermore, NPSCs are CXCR4+ and are known to migrate towards SDF-1 gradients *in vitro* and *in vivo* [4], [36], [81]. Hematopoietic [281] and mesenchymal stem cells [282] from the systemic circulation also home towards local sources of SDF-1. As a result, stem/progenitor cells associated with repair and regeneration likely comprised the CXCR4+ cell counts in addition to neuronal, glial and immunomodulatory cells. Further phenotypic characterization is required to probe which cell types respond to exogenous SDF-1.

Sustained release of AFSDF-1 induced significantly higher total populations of CXCR4+ cells compared to bolus AFSDF-1. More importantly, large fractions of these CXCR4+ cells were located well beyond the injection site (>300μm from the needle tract). For example, the AFSDF-1 sustained release at day 1 was the only group that elicited a significant increase in CXCR4+ cell density in the distal ROI (>700um away from the needle tract; Figure 4.9C). This observation raises the question of how exogenous SDF-1 with minimal direct diffusion into the brain interstitial space (Figure 4.4) affected cellular activation at such large distances. Previous studies with pretreatment of mesenchymal stem cells (MSCs) with SDF-1, upregulated SDF-1 mRNA [278]. Thus, the relatively slow release of AFSDF-1 in the sustained release groups (even in the first 24hrs) may have induced upregulation of endogenous SDF-1, propagating the signal much further than AFSDF-1 can physically diffuse. Additionally, in contrast to bolus injection where the entire delivered dose is bioavailable immediately and subject to proteolytic degradation, the sustained release group is expected to release AFSDF-1 in a more controlled fashion even in the first 24hrs. This slower rate of protein release from the NPs may have provided insulation of released AFSDF-1 from environmental factors.

Thus, increased CXCR4+ cell density may also be a product of improved AFSDF-1 half-life and bioavailability [187].

Aside from a strict feed-forward autocrine/paracrine signaling loop for SDF-1, we cannot rule out the involvement of other propagating signal mediators. Several soluble factors (i.e., vascular endothelial growth factor, VEGF; basic fibroblast growth factor, FGF; immune modulators) are known to cross-talk with SDF-1/CXCR4 signaling axis [278], [283]. The VEGF interaction with the SDF-1/CXCR4 signaling is of particular interest since SDF-1 treatment of MSCs stimulate increased VEGF secretion *in vitro* [278], while other studies indicate that VEGF upregulates expression of both SDF-1 and CXCR4 [284]. VEGF and SDF-1 also contain significant overlap in their gene regulation (i.e. through hypoxia inducible factor-1), as such endothelial progenitor cells are found to express both simultaneously under hypoxia [285], [286]. FGF is another signaling mediator that may be involved in transducing AFSDF-1 signal distally. CXCR4 and SDF-1 expression increases significantly in CXCR4+ endothelial cells after exposure to FGF [287], [288]. More interestingly, VEGF and FGF both appear to increase only CXCR4 expression and do not modulate expression of other CXC or CC chemokine receptors [289]. This result suggests that SDF-1, VEGF and FGF take part in a positive feedback loop to directly and indirectly propagate SDF-1/CXCR4 signaling [289]. Immune modulators such as, tumor necrosis factor-α (TNF-α) and interleukin 1-β (IL-1β) also affect the SDF-1/CXCR4 signaling axis indirectly by inducing release of VEGF and/or FGF [288], [290]. TNF-α also has a reported biphasic effect on CXCR4 expression where, CXCR4 expression is downregulated initially (within in 3 hrs), and upregulated subsequently (after 24 hrs) [288], [290]. In this case, TNF-α-mediated expression of VEGF and FGF does not fully account for the delayed CXCR4 upregulation, suggesting TNF-α plays a more indirect role in modulating the SDF-1/CXCR4 signaling axis [289].

The same biphasic response on CXCR4 expression is observed for interleukin 1-β [290]. Other cytokines such as, interferon-γ (IFN-γ) and granulocyte colony-stimulating factor (GCSF) are inhibitors of the SDF-1/CXCR4 signaling axis by downregulating SDF-1 and/or CXCR4 expression [288], [290], [292], [293]. Thus, secondary signaling mediators may play an important role in propagating SDF-1/CXCR4 signaling to the distal areas of the cortex. Another mechanism for activation of distal cells may be due to exogenous SDF-1 bypassing diffusion through the brain interstitium by entering the brain vasculature that may be transiently leaky (i.e. after neural injury, invasive surgical procedure to implant NPs). Although it is not empirically apparent that intracortical injections lead to breakage of the BBB, neural injuries such as focal TBI are well known to cause BBB dysfunction [65]. In the study presented here, escape of AFSDF-1 into the systemic circulation through leaky vasculature may allow for alternate means of transport and interaction with endothelial cells of the BBB in distal regions of the brain. Endothelial cells strongly express both SDF-1 and CXCR4 and as mentioned before, may relay signals that directly or indirectly affect endogenous SDF-1 expression in distal portions of the brain [287]–[291].

Although, controlled release of AFSDF-1 showed significantly more diffuse effects spatially, these effects were transient, where total CXCR4+ cell density attenuates to reach levels comparable to controls by day 7, similar to the bolus injection groups (Figure 4.9A). In the distal ROI, the decrease in CXCR4+ cell density occurs by day 3 (Figure 4.9C). The estimated drop in AFSDF-1 release rate from NPs past the first 24hrs may contribute to the eventual return of CXCR4+ cell density to that of control groups by day 7. Another potential mechanism may be autoregulation of the SDF-1/CXCR4 signaling axis. CXCR4 receptor downregulation as well as, CXCR7-mediated SDF-1 scavenging are known to be a part of the SDF-1/CXCR4 signaling axis [15], [24].

Specifically, when overstimulated with SDF-1, migrating interneurons in the rostral migratory stream downregulate CXCR4 and CXCR7 functions as a means of preserving adequate CXCR4 concentrations in the plasma membranes [15]. In fact the majority of migrating interneurons express both CXCR4 and CXCR7, and selectively interrupting the function of either receptor leads to morphological defects *in vivo* [19]. Figure 4.10E depicts a replicate for the day 7 AFSDF-1 NP group where cortical representations suggested robust SDF-1 immunostains both lateral and medial to the injection tract. However, little to no CXCR4 overexpressing cells were colocalized within the regions of positive stains. In comparison, day 1 after bolus injection of AFSDF-1, CXCR4+ cells were observed in large numbers colocalized with AFSDF-1 at the needle tract. Similarly, sustained release of AFSDF-1 initially elicited increased expression of both SDF-1 (% area immunostain) and CXCR4 (cell density). However, CXCR4+ cell numbers attenuated by day 7, even for replicates that exhibited strong SDF-1 staining through the cortical tissue (Figure 4.10E). This result may indicate CXCR4 downregulation, or CXCR-7-mediated SDF-1 desensitization at the later timepoints. Further *in vitro* studies will help determine how SDF-1, CXCR4 & CXCR7 expression relates to sustained exposure to SDF-1. Additionally, if desensitization of SDF-1 plays an important role due to a sustained release, it remains to be seen whether other release profiles (delayed or pulsed) is a better fit for modulating the SDF-1/CXCR4 signaling axis in the week-long period tested here, and beyond.

5.5. Conclusion

Bolus administration of exogenous SDF-1 (AFSDF-1) in the intact mouse cortex led to localized and transient expression of CXCR4 at day 1, which attenuated completely at some point between days 3 and 7 days post injection. SDF-1 immunostain denoting total SDF-1 (exogenous + endogenous) increased significantly locally at the injection site.

However, we did not tease out the levels of endogenously expressed SDF-1 to specifically correlate increased bolus injection of exogenous SDF-1 with increased endogenous expression/secretion of SDF-1. Our data conclusively suggested that AFSDF-1 bolus injections did not stimulate endogenous SDF-1 expression at the proximal and distal ROIs. Sustained release of AFSDF-1 led to significant increases in CXCR4+ cell densities locally, and in regions far more distal to the injection site compared to the bolus group. However, CXCR4 expression decreased significantly by day 3, and was comparable to control groups by day 7. AFSDF-1 sustained release elicited complex patterns of widespread SDF-1 immunostains that persisted through day 7 post injections. However, high levels of SDF-1 immunostains did not translate to increased CXCR4 expression in those areas at the later timepoints. It is not clear whether or not autoregulation of the SDF-1/CXCR4 signaling axis played a role in attenuating the effects of AFSDF-1 sustained release. Further studies are required determine the role of CXCR7 as well as how more complex release profiles may be better apt at modulating the SDF-1/CXCR4 signaling axis over extended periods of time.

5.6. Figures

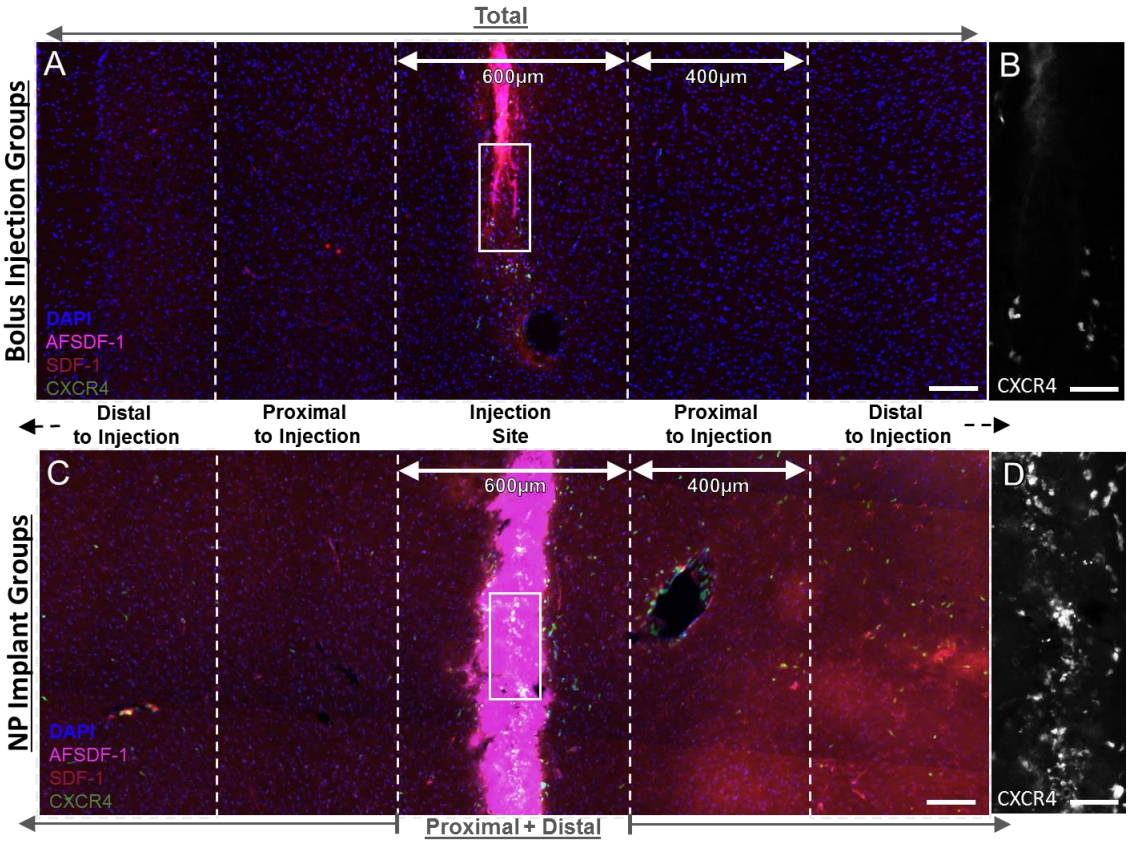

Figure 4.1: Representative fluorescent images of cortical tissue sections and the regions of interest (ROIs) used to quantify fluorescent signals. (A) Cortical reconstruction centered at the injection tract after a bolus injection of AFSDF-1 and (B) AFSDF-1 loaded PLGA NPs. All tissue sections were immunostained for SDF-1 (red channel) and nuclear material (DAPI; blue channel). AFSDF-1 is represented in magenta, whereas the endogenous CXCR4 expression marker is depicted in the green channel. SDF-1 and AFSDF-1 signal exhibited a diffuse pattern, whereas signal from the CXCR4 expression marker was confined intracellularly. All cortical reconstructions (2.8mmx1mm) were divided into a 600µm injection site, two 400µm sections proximal to injection site, and two more 700µm sections distal to the injections site. The figure depicts truncated regions of the distal ROI for illustration purposes and extend further medially and

laterally as represented by the dashed arrows. Data gathered from the medial and lateral sections were averaged before being reported for the proximal and distal ROIs, respectively. (B) & (D) are magnified representations of the needle tract outlined in white for bolus and NP implant groups, respectively. A high concentration of CXCR4+ cell bodies were found inside the needle tract of NP groups compared to the bolus groups. Scale bars = 100μm for A & C; scale bar = 50um for B & D.

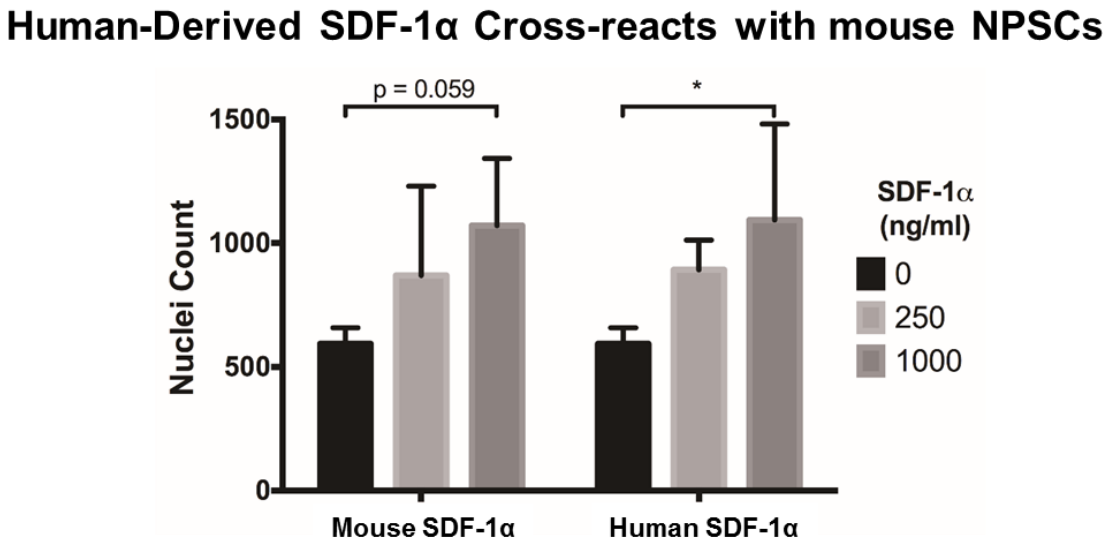

Figure 4.2: Boyden chamber migration assay verified bioactivity of human-derived SDF-1α on mouse NPSCs. Human SDF-1α was compared to mouse SDF-1α at 0, 250 and 1000ng/ml. Only the human SDF-1α at 1000ng/ml was statistically different compared to control. However, both human and mouse SDF-1α exhibited similar trends in eliciting a migratory response from mouse NPSCs. (* represents $p < 0.05$)

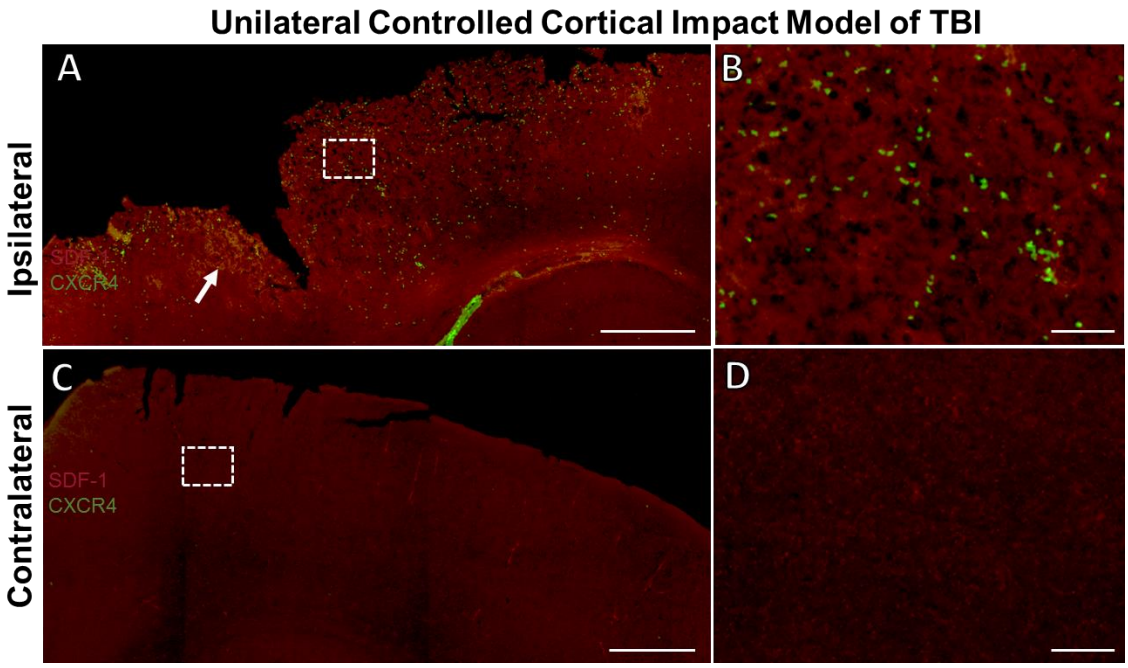

Figure 4.3: CXCR4-EGFP transgenic mouse model overexpresses SDF-1 and CXCR4 after 1 day post injury in a CCI model of TBI. The ipsilateral cortex (A) and a magnified region outlined by while dashed line (B) indicates a high density of CXCR4 expressing cells (green channel) localized at the cortex. The contralateral cortex (C) and a magnified region outlined by while dashed line (D) had little to no cell EGFP+ cell bodies. SDF-1 immunostaining (red channel) suggests stronger SDF-1 signal in the injured cortex (white arrow) relative to a weaker overall signal for the contralateral side. Scale bars = 500μm for B & C; scale bar = 100um for D & E.

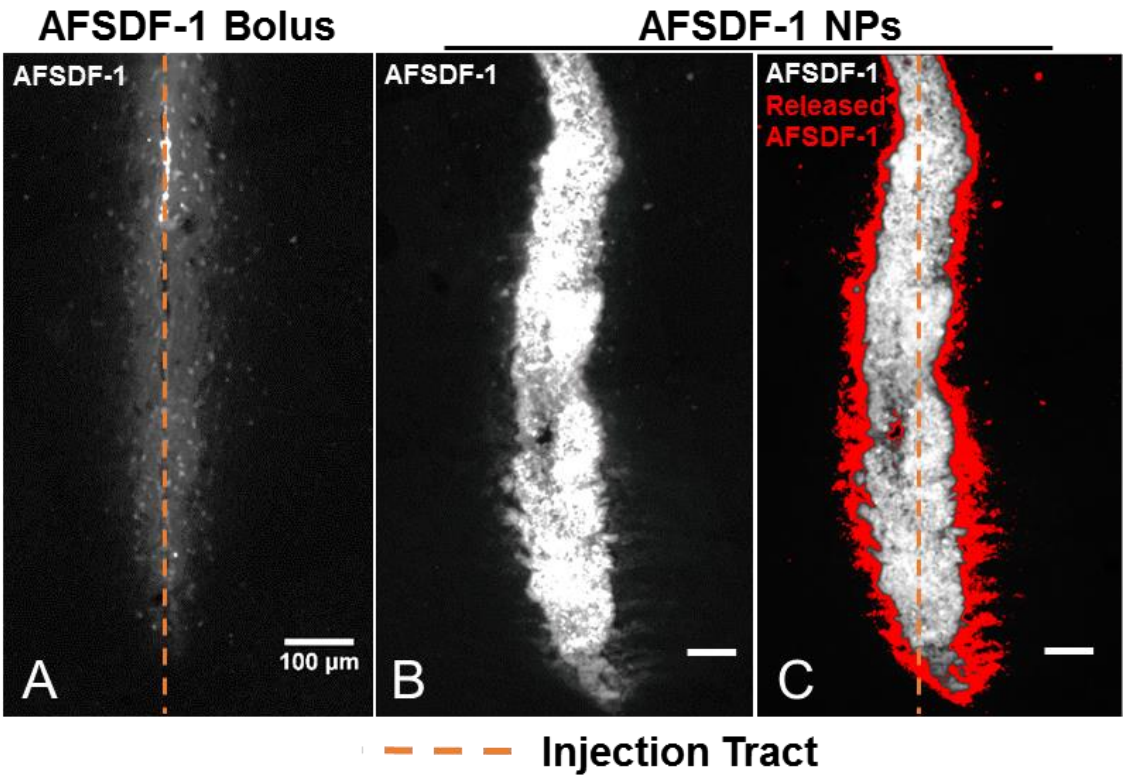

Figure 4.4: Localization of AFSDF-1 signal for all groups is limited to the injection site. (A) Distribution of AFSDF-1 one day after bolus injection suggests <100 µm diffusion into cortical tissues relative to injection tract. (B) Distribution of AFSDF-1 one day after NP implantation. Strong signal within the NP implants indicated encapsulated AFSDF-1. (C) Diffuse signal at the edges of the implant indicated AFSDF-1 release and diffusion the cortical parenchyma. Evidence of AFSDF-1 penetration into the cortical tissue was highlighted (red channel) by thresholding for the highest intensity signals from within the implant, as well as the lowest intensity signals to remove background. Scale bars = 100µm.

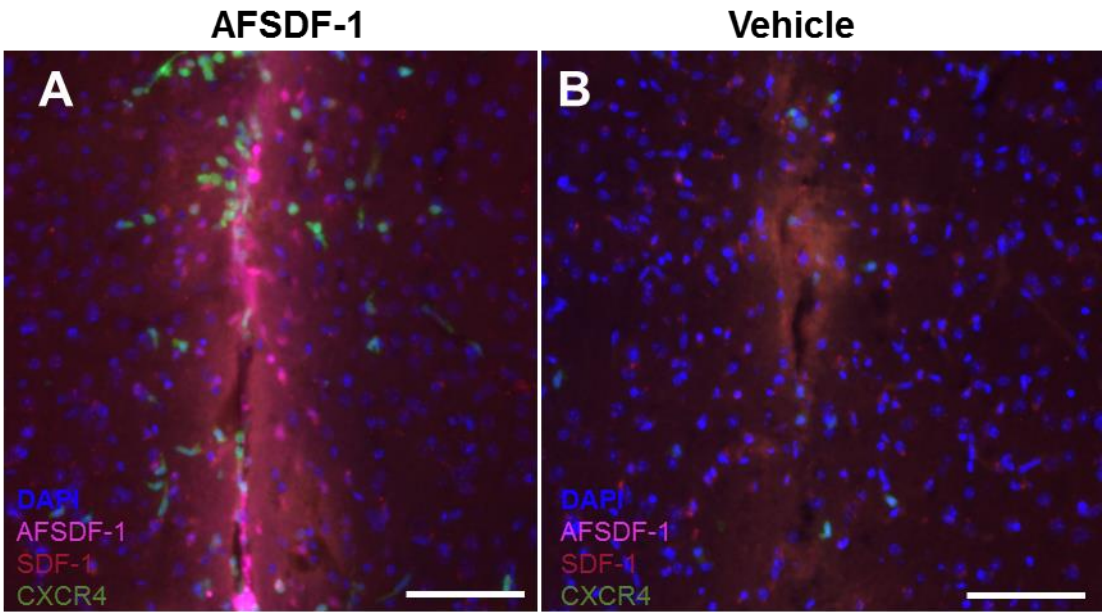

Figure 4.5: CXCR4 expressing cells colocalize with AFSDF-1 one day after bolus administration. (A) Representative fluorescent image centered on the needle tract indicating CXCR+ cell density correlates with AFSDF-1 signal. (B) Vehicle injections qualitatively a lower number of have CXCR4+ cells around the needle tract. Scale bars represent 100μm. Blue = DAPI; magenta = AFSDF-1; red = SDF-1 immunostain; and green = CXCR4+ cells.

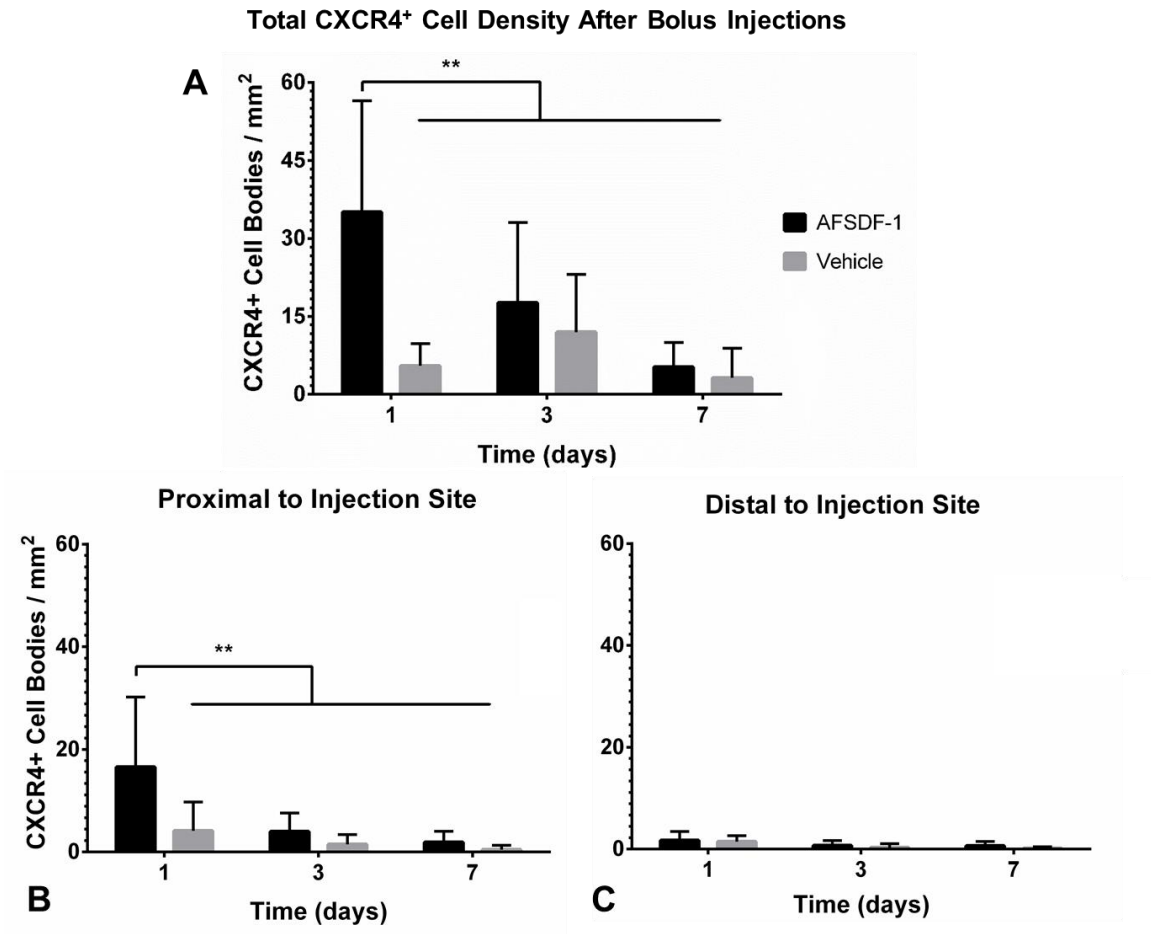

Figure 4.6: Bolus administration of AFSDF-1 has localized and transient effects on CXCR4 expression. (A) Total (injection site + proximal + distal) CXCR4+ cell density increases significantly at day 1 in response to AFSDF-1, which decreases significantly at day 3 and further attenuates becoming comparable to vehicle control by day 7. (B) looking only at the proximal ROI, a statistical significance was observed at the day 1 timepoint, however groups in the day 3 & 7 timepoints were not significantly different. (C) No statistical significance was found in the distal ROI. (** represents $p < 0.001$ compared to AFSDF-1 at day 1)

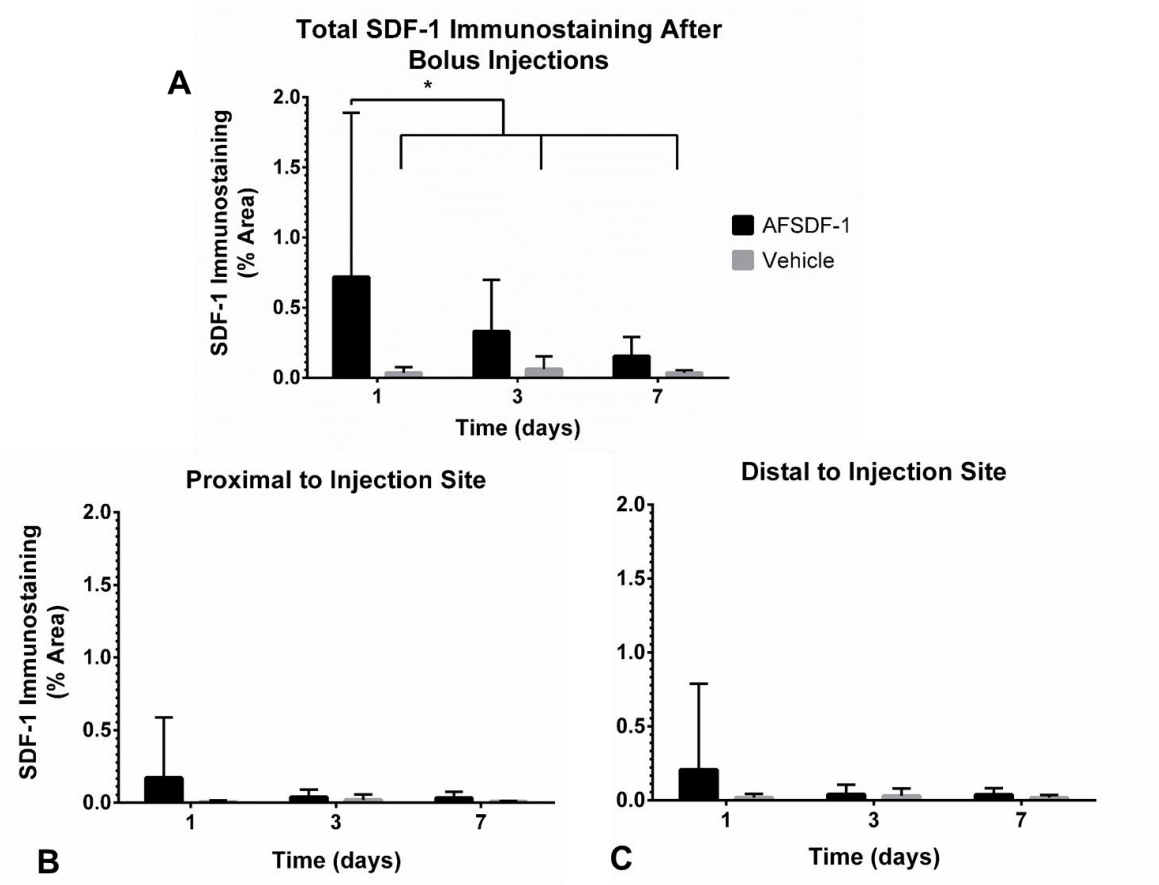

Figure 4.7: Bolus AFSDF-1 did not modulate ADF-1 expression outside of the needle tract. (A) A significant difference in total (injection site + proximal + distal) SDF-1 immunostaining (% area; normalized to the area of the ROI) was observed for the bolus injection group compared to vehicle at day 1 post injection. No other statistically significant comparisons were observed for days 3 & 7. (B - C) No statistically significant trends were existed for the proximal or distal ROIs. (* represents $p < 0.05$ compared to AFSDF-1)

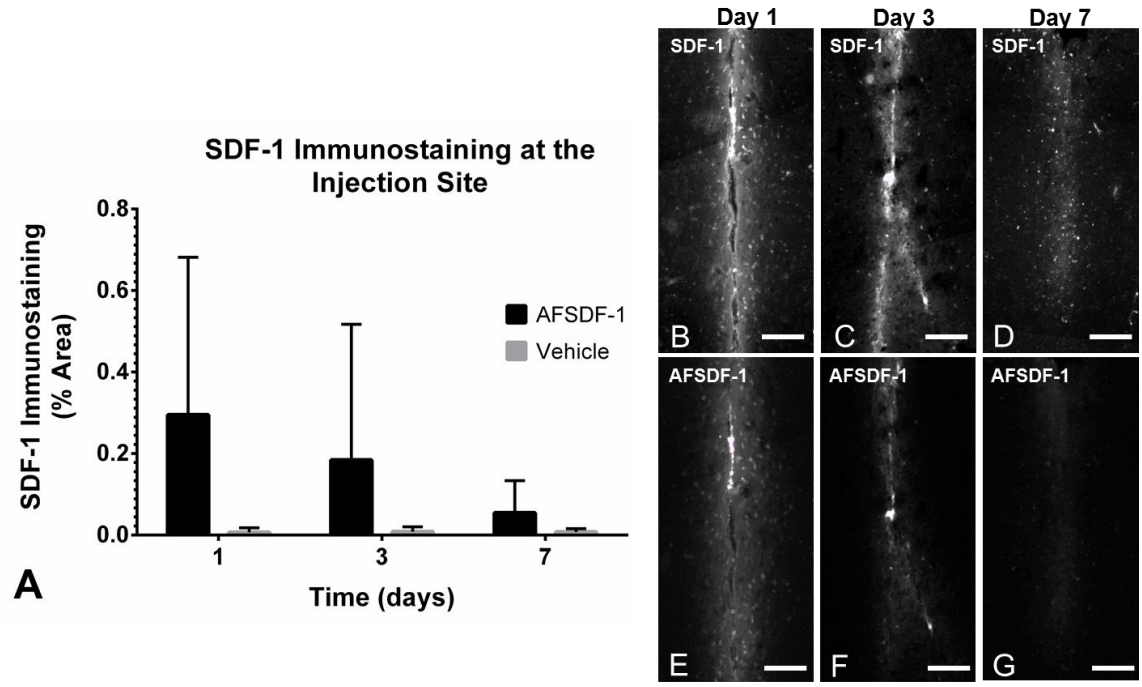

Figure 4.8: Lack of complete overlap between AFSDF-1 signal and SDF-1 immunostain may indicate presence of endogenous SDF-1 at the needle tract. (A) Total (endogenous + exogenous) SDF-1 at the injection site decreased steadily until day 7 when SDF-1 immunostaining was comparable with vehicle groups. Representative images of SDF-1 immunostains (B-D) and AFSDF-1 signal (E-F) at the needle tract indicate lack of complete colocalization between the two. Scale bars represent 100 μm.

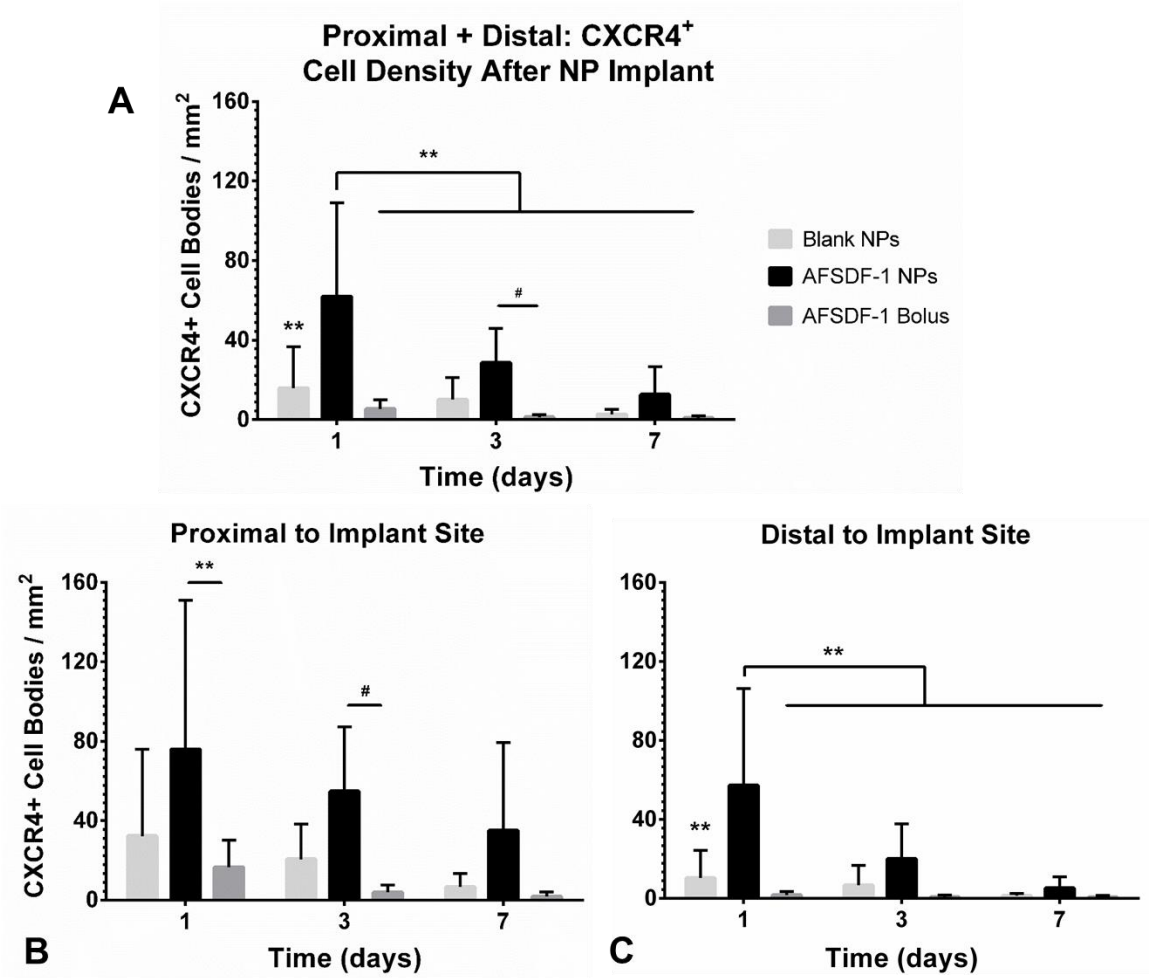

Figure 4.9: Sustained release of AFSDF-1 induced transient CXCR4 overexpression in cells located distally from the injection site. (A) CXCR4+ cell density in the proximal + distal ROI indicated a significant increase for the AFSDF-1 NP group at day 1 (against blank NPs and bolus AFSDF-1) as well as, at day 3 (against only bolus AFSDF-1). (B) Focusing only on the proximal ROI, significant differences were found at day 1 & 3 between the AFSDF-1 NP and bolus AFSDF-1 groups. (C) At the distal ROI, a significant difference was seen at day 1 between both, blank NP and bolus AFSDF-1 groups. (** represents $p < 0.001$ compared to AFSDF NPs at day 1; # represents $p < 0.05$ compared to AFSDF NPs at day 3)

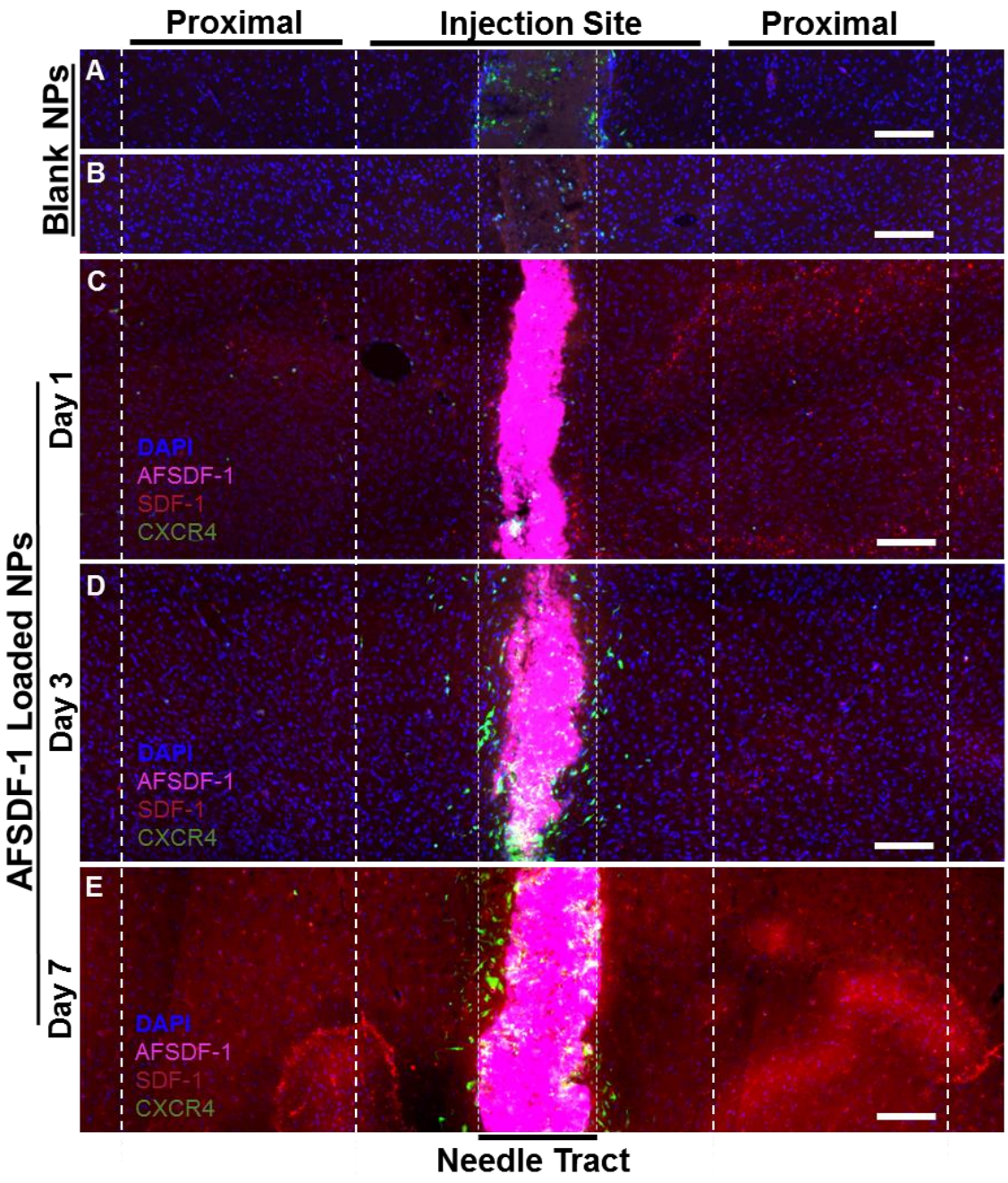

Figure 4.10: SDF-1 immunostaining for the AFSDF-1 NPs resulted in highly complex and non-homogenous distribution of positive staining. (A-B) Cortical representations centered around the blank NP implants. As expected, the blank implants do not have any AFSDF-1. Moreover, there was not a significant increase in SDF-1 immunostaining

regardless of location. Cortical representations of cortices implanted with AFSDF-1 NPs at day 1 (C), day 3 (D) and at day 7 (E) with significantly altered SDF-1 immunostaining compared to blank NPs. Additionally, some replicates had extensive, non-uniform SDF-1 staining but did not correlate with the presence of CXCR4+ cells (E). Scale bars represent 100 μm. Blue = DAPI; magenta = AFSDF-1; red = SDF-1 immunostain; and green = CXCR4+ cells.

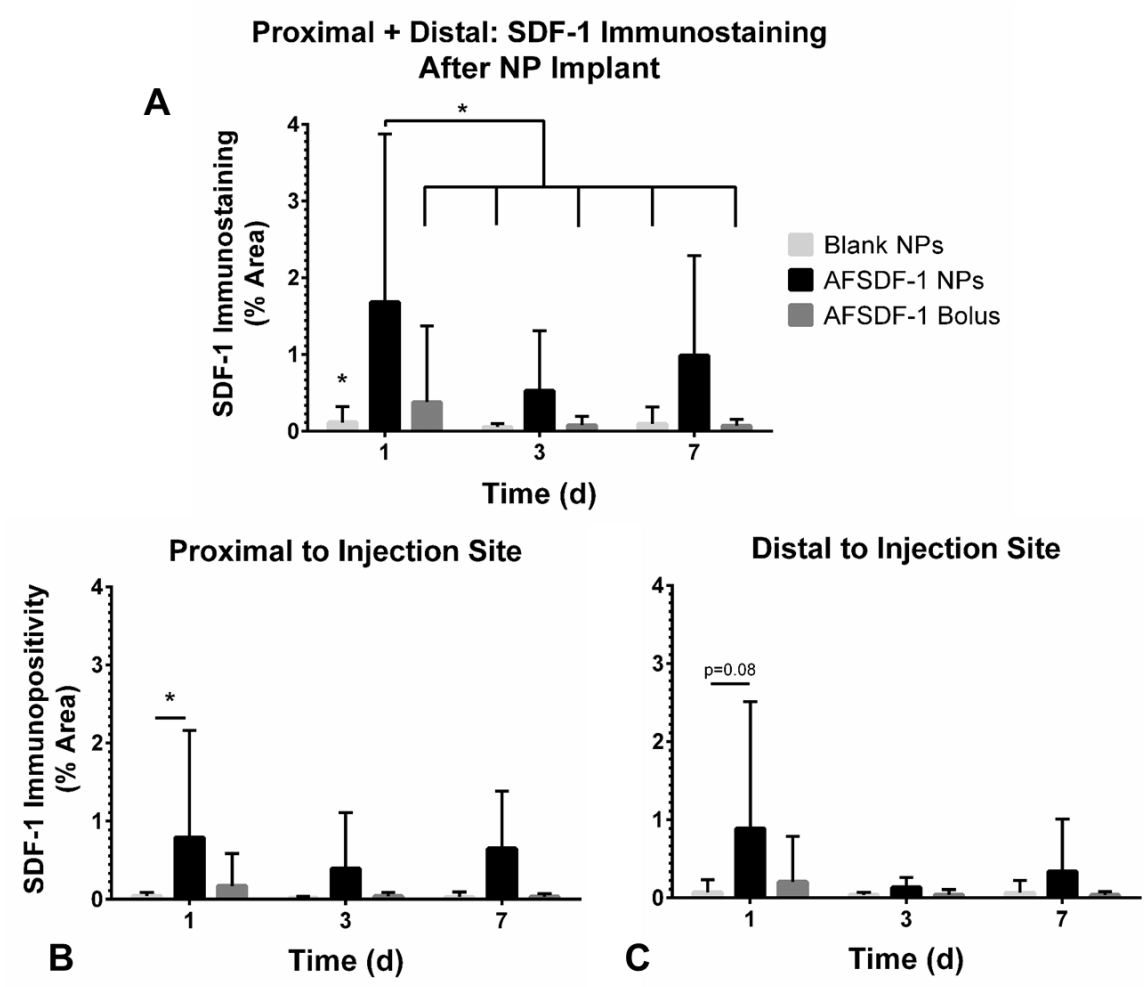

Figure 4.11: Sustained release of AFSDF-1 affected SDF-1 immunostaining beyond the injection site. (A) SDF-1 staining (% area) in the proximal + distal ROI increased significantly at day one for the AFSDF-1 NP group compared to both the blank NPs and

bolus AFSDF-1. Although statistical significance against the Blank NPs and AFSDF-1 bolus did not extend out to days 3 & 7, SDF-1 immunostaining also did not decrease significantly over time for the AFSDF-1 NPs. (B) Looking at only the proximal ROI, a statistical difference was observed between the AFSDF-1 NP and blank NPs at day 1. No other comparisons were significant. (C) No statistical differences were found at the distal ROI. (* represents $p < 0.05$ compared to AFSDF NPs at day 1)

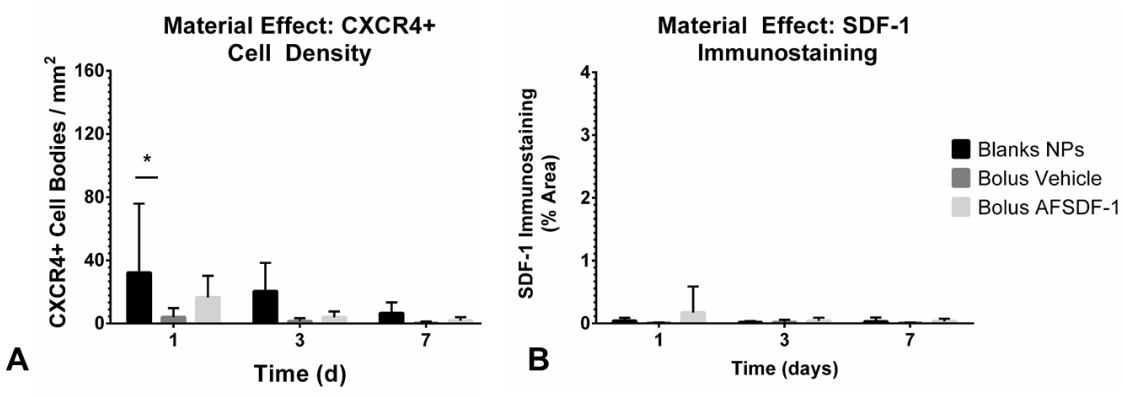

Figure 4.12: Injection of blank or AFSDF-1 NPs did not induce a prolonged and widespread material effect. (A) The implantation of blank NPs caused a transient increase in CXCr4+ cell density at the proximal ROI relative to bolus vehicle at day 1, which decreased by day 7. (B) Implantation of blank NPs had no effect on SDF-1 immunostaining at the proximal (shown) or any other ROI. (* represents $p < 0.05$ compared to Blank NPs at day 1)

CHAPTER 5

SUMMARY AND FUTURE WORK

5.1. Summary of Findings

5.1.1. Aim 1: Validate platform for controlled release of proteins with tunable release profiles.

Due to number and complexity of parameters that affect poly(lactic-co-glycolic) acid (PLGA) particle release properties, changing fabrication procedures to achieve a desired release profile is both time and labor intensive. We have determined that critical release characteristics such as encapsulation efficiency, magnitude of burst release, protein release rate and protein release period is correlated to the average diameter of the protein-loaded PLGA nanoparticles (NPs) particle populations. Additionally, we described how simple centrifugal fractioning parameters may be employed to fractionate particles by size, and therefore tune release profiles without having to change the particle fabrication parameters, potentially compromising desirable particle attributes.

5.1.2. Aim 2: *Explore composite release systems to modulate sustained release of bioactive SDF-1α.*

PLGA NPs from before to was adapted to encapsulate SDF-1α, which exhibited sustained release over a period of 60 days in its bioactive form. The NPs however exhibited a high burst release of 23% in the first 24hrs and we explored composite systems (NPs in hydrogel) that was hypothesized to potentially sequester burst release. We found that SDF-1α has specific binding affinity for fibrin(ogen) and the burst release from PLGA NPs can be sequestered in fibrin gels, in a fibrin concentration-dependent fashion. Additionally, embedding PLGA NPs in fibrin does not affect fibrin matrix properties. These results are significant in potentially obtaining tunable, local and

sustained release of SDF-1α in a variety of applications to modulate the SDF-1/CXCR4 signaling cascade.

5.1.3. Aim 3: *Determine spatiotemporal expression of endogenous SDF-1α/CXCR4 after administration of exogenous SDF-1α in the intact mouse cortex.*

We contrasted the effects of bolus and sustained release of SDF-1 to determine how the endogenous SDF-1/CXCR4 signaling axis responds to spatiotemporal presentations of exogenous SDF-1. Bolus administration of SDF-1 leads to localized and transient effects of CXCR4 expression and hold a limited capacity to modulate endogenous SDF-1 expression. Sustained release of SDF-1 on the other hand, produced robust increases in CXCR4 expression even in regions distal to the injection site. SDF-1 expression was also elevated across the ipsilateral cortex. However, CXCr4 expression decreased significantly past day 3. Although the effect of SDF-1 sustained release was much more spatially diffuse, it was nearly as transient as bolus injections.

5.2. Discussion

In summary, our overarching goal was to develop platforms to achieve tunable, controlled release of SDF-1. FDA-approved polyesters such as PLGA is very common in the field of drug delivery due to a number of reasons: 1) they can encapsulate a wide range of hydrophobic and hydrophilic molecules, 2) their release profiles can be tuned, 3) PLGA devices can be injected directly into target tissues, and 4) they have easily metabolizable degradation products [258]. Moreover, PLGA matrices maintain prolonged, localized bioavailability relative to hydrogels that have relatively short, diffusion-limited release kinetics. Once encapsulated, PLGA particles aid in protecting the cargo from degradation, a critical parameter for protein delivery (albeit the encapsulation process can initially reduce its bioactivity) [187], [191], [192]. However, due to the number of interactions involved in determining release profiles from PLGA

particle, changing formulation parameters to tune release characteristics can often be time and labor intensive. We described a simple centrifugal fractioning method and demonstrated a direct relationship between release properties and the particle population size characteristics (distribution and average diameter). Encapsulation efficiency and several parameters of the release curve (burst release, protein release rate and protein release period) were correlated to the average diameter of the particle population.

Subsequently, we demonstrated successful encapsulation of SDF-1α within PLGA NPs and achieve controlled release of bioactive protein over 60days. Functional bioactivity of encapsulated and released SDF-1α was demonstrated through *in vitro* NPSC chemotactic migration assays. We also determined that soluble SDF-1α was sequestered in fibrin clots and that NPs embedded in different concentrations of fibrin was a means for controlling the magnitude of the burst release. These results are significant in potentially obtaining tunable sustained release of SDF-1α in a variety of injury models, such as after TBI to amplify and/or sustain NPSC-mediated endogenous repair response.

Thirdly, we contrasted the effects of bolus and sustained release of SDF-1 in the intact mouse brain to elucidate underlying mechanisms that would better enable long-term modulation of the endogenous SDF-1/CXCR4 signaling axis. Bolus administration of exogenous SDF-1 (AFSDF-1) in the intact mouse cortex led to localized and transient expression of CXCR4 at day 1, which returned back levels comparable to controls around 3 days post injection. Upregulation of CXCR4 in response to SDF-1 has been reported in literature both *in vitro* and *in vivo* by multiple cell types [15], [218], [278]. Since cell phenotype were not assessed in this study, it is unclear whether higher density of CXCR4+ cells were local neurons and/or astrocyte rather than microglia or systemic

immune cells that may have chemotactically migrated to local high concentrations of AFSDF-1. Moreover, due to the limited diffusivity and short half-life expected from AFSDF-1, the increase in CXCR4+ cell density was transient and localized only in the injection site. Effect of bolus AFSDF-1 on endogenous SDF-1 expression was inconclusive. However, comparisons between SDF-1 immunostains and AFSDF-1 signal at the injection site qualitatively supports trends in previous studies that show exposure to SDF-1 may directly and indirectly lead to upregulation of SDF-1 [15], [284], [289], [290]. No alterations were observed in SDF-1 immunostains in areas proximal and distal to the injection site likely due to the limited diffusivity and short-lived effects of bolus AFSDF-1.

Sustained release of AFSDF-1 led to significant increases in CXCR4-overexpression locally compared to bolus AFSDF-1 and blank NPs. More interestingly, sustained release of AFSDF-1 was the only group to significantly increase CXCR4 expression in cells located distally (>700μm away from the needle tract). This was despite the fact that AFSDF-1 was not detected via IHC more the ~200μm away from the needle tract. This discrepancy in limited tissue penetration and widespread induction of CXCR4+ cells is a strong indicator for secondary and tertiary signaling mediators that transduce SDF-1/CXCR4 signaling. VEGF and FGF are both directly involved with the SDF-1/CXCR4 signaling axis and are strong candidates for transducing SDF-1-mediated signaling beyond the diffusive range of AFSDF-1 in the cortex through autocrine/paracrine signaling [289]. In addition, other factors such as TNF-α act indirectly to modulate the SDF-1/CXCR4 signaling axis may also have been involved in AFSDF-1 mediated signal propagation especially near the NP implants where relatively high concentration of activated microglia was expected to be present [276], [291]. There is also an outside possibility of NP implants inducing a leaky blood-brain-barrier (BBB)

causing AFSDF-1 to reach the systemic circulation undergoing transport through convection to reach distal areas of the brain, rather than simple diffusion. AFSDF-1 interaction with endothelial cells of the BBB may be one direct/indirect mechanism for CXCR4+ cells observed far beyond the injection site [287]–[291].

Similar to the bolus administration, however, CXCR4-expression for sustained release groups decreased significantly by day 3, and was comparable to controls by day 7. Thus the effects of sustained release, although much more spatially diffuse, remained transient similar to the bolus injection groups. One possible reason for the transient response is a significant decrease in the expected rate of AFSDF-1 protein release from the NP implants after the first 24hrs. Other potential mechanisms involve auto-regulatory processes built-in to the SDF-1/CXCR4 signaling axis, namely CXCR7-mediated AFSDF-1 scavenging/desensitization [15], [24]. In addition to signaling mediators that aid in directly and indirectly propagating the SDF-1/CXCR4 signaling axis (i.e. vascular endothelial growth factor, VEGF; basic fibroblast growth factor, FGF; tumor necrosis factor-α, TNF-α; and interleukin 1-β, IL-1β;) other cytokines such as interferon-γ (IFN-γ) act as an inhibitor. IFN-γ treated endothelial cells exhibit a significant decrease in CXCR4 expression, and thus sensitivity to SDF-1 [288], [290]. Granulocyte colony-stimulating factor (GCSF) is another such factor that has multiple effects on the SDF-1/CXCR4 signaling axis. On one hand, GCSF enhances CXCR4 expression, while on the other, it also induces expression of proteases that rapidly degrade SDF-1 [292], [293]. In the bone marrow, GCSF is an important modulator of stem cell mobilization through the SDF-1/CXCR4 signaling axis [289]. AFSDF-1 sustained release also elicited non-uniform and non-symmetric patterns of strong SDF-1 immunostains that persists through day 7 post injections in some replicates. However, higher amounts of SDF-1 at the later timepoints were not correlated to increased

CXCR4+ cell density, which was in contrast with the bolus injection group where immunostaining for SDF-1 colocalized with CXCR4+ cell bodies near the injection tract at day 1. It is not clear whether autoregulation of the SDF-1/CXCR4 signaling axis played a role in the apparent decrease in the CXCR4+ cell body count even in the presence of SDF-1.

The injury microenvironment after TBI is significantly more complicated than the intact cortex model used in chapter 4. The injury area consists of a diverse profile of cells that include resident CNS, as well as systemic stem and immune cell types that actively participate in the SDF-1/CXCR4 signaling axis either directly and/or indirectly through secondary (e.g. VEGF, FGF etc.) and tertiary mediators (e.g. TNF-α). Moreover, the cell phenotypic profile, as well as the resulting signaling milieu is dynamic both spatially and temporally making it more difficult to predict how spatiotemporal presentation of exogenous SDF-1 may affect the endogenous SDF-1/CXCR4 signaling axis. Although, improved bioavailability of exogenous SDF-1 for prolonged periods locally after injury is expected to sustain/amplify NPSC-mediated regeneration after neural injury, our goal was to control for the complexity of the injury microenvironment to study specifically how endogenous SDF-1/CXCR4 signaling axis responds to exogenous AFSDF-1. The cumulative data suggests that sustained release of AFSDF-1 may not be the ideal release profile for modulation of the SDF-1/CXCR4 signaling axis over a 7 day period in the intact rodent cortex. More complex release profiles, such as delayed and/or pulsed release needs to be evaluated to determine if significant increases seen on the first day in the AFSDF-1 sustained release group injections can be repeated at various time intervals over an extended period of time.

5.3. Future Work

To more conclusively substantiate whether sustained release is effective at long-term modulation of the SDF-1/CXCR4 signaling axis, further studies are required to uncover the biochemical basis for the trends observed in the final *in vivo* study. Specifically, future studies will require a wider focus on secondary/tertiary signaling mediators that interact with the SDF-1/CXCR4 signaling axis. As mentioned above, VEGF and FGF are principal factors that are known to be intimately involved with the SDF-1-mediated signaling. Their spatiotemporal localization in addition to SDF-1 will provide valuable insights about the underlying biochemical processes that dictate the patterns observed. Additionally, tissue sections already acquired from the Chapter 4 *in vivo* study can also be immunostained for CXCR7 where CXCR4+ cells call be compared with CXCR7+ cells to gain insights on observed trends. For example, how sustained release of AFSDF-1 from NPs resulted in such a significantly different spatiotemporal localization of CXCR4+ cell bodies after bolus administration.

Studying autoregulation of the SDF-1/CXCR4 signaling cascade is another important aspect and can be verified using supporting *in vitro* assays to quantify SDF-1, CXCR4 and CXCR7 mRNA expression in response to extended exposure to SDF-1. If SDF-1/CXCR4 signaling cascade is desensitized in response to sustained bioavailability of SDF-1 in *in vitro* assays, an interesting question is whether a delayed release profile is capable of repeating the trends seen in SDF-1/CXCR4 expression day 1 in the presented *in vivo* study, at later timepoints. If true, a pulsed release profile of SDF-1 is a better candidate for long-term modulation of SDF-1/CXCR4 signaling cascade. Better understanding of the signaling cascade will lead to development of more biologically relevant release devices. To that end, we have already characterized core-shell microparticles (MPs) made of both PLGA and poly(L-lactic acid) (PLLA) [294]–[300]. Here, a layered structure facilitates delayed release profiles based on cargo localization

within the particle [301]. We have developed straightforward protocols that use water/oil/oil/water (W/O/O/W) emulsions for encapsulating the model protein, bovine serum albumin (BSA) in layered, MPs with PLGA-rich cores and a PLLA-rich shells. We also found that ethanol, a polar protic solvent miscible in the water and oil phases of the W/O/O/W emulsion, modulated protein localization and particle porosity in layered MPs. Moreover, alterations in particle morphology results in distinct release profiles where the delay period and subsequent protein release rate is EtOH-dependent. A future *in vivo* study could involve layered MPs encapsulating AFSDF-1 in order to contrast the effects of sustained and delayed release. Moreover, combining MPs with different delay periods may be means for achieving a pulsed release profiles of SDF-1.

The injured microenvironment after focal TBI for example, is exceedingly complex and dynamic spatially and temporally. In addition to activating the endogenous repair response, TBI causes disruptions in CNS (metabolic/ionic) homeostasis, breakdown of the BBB, prolonged cell death (necrosis/apoptosis) as well as, neuroinflammation. Thus a more nuanced understanding of the mechanisms behind SDF-1/CXCR4 signal propagation will better help transition towards evaluating how bolus, sustained and delayed/pulsed release of SDF-1 *in vivo* translates to mobilization of endogenous NPSCs in the injured brain.

REFERENCES

[1] D. J. Overstreet, D. Dutta, S. E. Stabenfeldt, and B. L. Vernon, "Injectable hydrogels," *J. Polym. Sci. Part B Polym. Phys.*, vol. 50, no. 13, pp. 881–903, Jul. 2012.

[2] Stabenfeldt, C. Addington, D. Dutta, and A. Roussas, "Endogenous Repair Signaling after Brain Injury and Complementary Bioengineering Approaches to Enhance Neural Regeneration," *Biomark. Insights*, p. 43, May 2015.

[3] D. Dutta, M. Salifu, R. W. Sirianni, and S. E. Stabenfeldt, "Tailoring Sub-Micron PLGA Particle Release Profiles via Centrifugal Fractioning," *J. Biomed. Mater. Res. A*, Oct. 2015.

[4] D. Dutta, C. Fauer, H. L. Mulleneux, and S. E. Stabenfeldt, "Tunable controlled release of bioactive SDF-1α via specific protein interactions within fibrin/nanoparticle composites," *J. Mater. Chem. B*, vol. 3, no. 40, pp. 7963–7973, Oct. 2015.

[5] P. Bianco, P. G. Robey, and P. J. Simmons, "Mesenchymal Stem Cells: Revisiting History, Concepts, and Assays," *Cell Stem Cell*, vol. 2, no. 4, pp. 313–319, Apr. 2008.

[6] M. Z. Ratajczak, E. Zuba-Surma, M. Kucia, R. Reca, W. Wojakowski, and J. Ratajczak, "The pleiotropic effects of the SDF-1–CXCR4 axis in organogenesis, regeneration and tumorigenesis," *Leukemia*, vol. 20, no. 11, pp. 1915–1924, 2006.

[7] J. M. Busillo and J. L. Benovic, "Regulation of CXCR4 Signaling," *Biochim. Biophys. Acta*, vol. 1768, no. 4, pp. 952–963, Apr. 2007.

[8] L. Yu, J. Cecil, S.-B. Peng, J. Schrementi, S. Kovacevic, D. Paul, E. W. Su, and J. Wang, "Identification and expression of novel isoforms of human stromal cell-derived factor 1," *Gene*, vol. 374, pp. 174–179, Jun. 2006.

[9] B. Kirkpatrick, L. Nguyen, G. Kondrikova, S. Herberg, and W. D. Hill, "Stability of Human Stromal-Derived Factor-1α (CXCL12α) After Blood Sampling," *Ann. Clin. Lab. Sci.*, vol. 40, no. 3, pp. 257–260, Jun. 2010.

[10] D. A. Davis, K. E. Singer, M. D. L. L. Sierra, M. Narazaki, F. Yang, H. M. Fales, R. Yarchoan, and G. Tosato, "Identification of carboxypeptidase N as an enzyme responsible for C-terminal cleavage of stromal cell-derived factor-1α in the circulation," *Blood*, vol. 105, no. 12, pp. 4561–4568, Jun. 2005.

[11] D. G. Duda, S. V. Kozin, N. D. Kirkpatrick, L. Xu, D. Fukumura, and R. K. Jain, "CXCL12 (SDF1α)-CXCR4/CXCR7 Pathway Inhibition: An Emerging Sensitizer for Anticancer Therapies?," *Clin. Cancer Res.*, vol. 17, no. 8, pp. 2074–2080, Apr. 2011.

[12] C. P. Addington, C. M. Pauken, M. R. Caplan, and S. E. Stabenfeldt, "The role of SDF-1α–ECM crosstalk in determining neural stem cell fate," *Biomaterials*, vol. 35, no. 10, pp. 3263–3272, Mar. 2014.

[13] B. A. Teicher and S. P. Fricker, "CXCL12 (SDF-1)/CXCR4 Pathway in Cancer," *Clin. Cancer Res.*, vol. 16, no. 11, pp. 2927–2931, Jun. 2010.

[14] R. Würth, A. Bajetto, J. K. Harrison, F. Barbieri, and T. Florio, "CXCL12 modulation of CXCR4 and CXCR7 activity in human glioblastoma stem-like cells and regulation of the tumor microenvironment," *Front. Cell. Neurosci.*, vol. 8, May 2014.

[15] P. Abe, W. Mueller, D. Schutz, F. MacKay, M. Thelen, P. Zhang, and R. Stumm, "CXCR7 prevents excessive CXCL12-mediated downregulation of CXCR4 in migrating cortical interneurons," *Development*, vol. 141, no. 9, pp. 1857–1863, May 2014.

[16] G. J. Graham, M. Locati, A. Mantovani, A. Rot, and M. Thelen, "The biochemistry and biology of the atypical chemokine receptors," *Immunol. Lett.*, vol. 145, no. 1–2, pp. 30–38, Jul. 2012.

[17] J. M. Burns, B. C. Summers, Y. Wang, A. Melikian, R. Berahovich, Z. Miao, M. E. T. Penfold, M. J. Sunshine, D. R. Littman, C. J. Kuo, K. Wei, B. E. McMaster, K. Wright, M. C. Howard, and T. J. Schall, "A novel chemokine receptor for SDF-1 and I-TAC involved in cell survival, cell adhesion, and tumor development," *J. Exp. Med.*, vol. 203, no. 9, pp. 2201–2213, Sep. 2006.

[18] T. N. Hartmann, V. Grabovsky, R. Pasvolsky, Z. Shulman, E. C. Buss, A. Spiegel, A. Nagler, T. Lapidot, M. Thelen, and R. Alon, "A crosstalk between intracellular CXCR7 and CXCR4 involved in rapid CXCL12-triggered integrin activation but not in chemokine-triggered motility of human T lymphocytes and CD34+ cells," *J. Leukoc. Biol.*, vol. 84, no. 4, pp. 1130–1140, Oct. 2008.

[19] Y. Wang, G. Li, A. Stanco, J. E. Long, D. Crawford, G. B. Potter, S. J. Pleasure, T. Behrens, and J. L. R. Rubenstein, "CXCR4 and CXCR7 have distinct functions in regulating interneuron migration," *Neuron*, vol. 69, no. 1, pp. 61–76, Jan. 2011.

[20] A. K. Singh, R. K. Arya, A. K. Trivedi, S. Sanyal, R. Baral, O. Dormond, D. M. Briscoe, and D. Datta, "Chemokine receptor trio: CXCR3, CXCR4 and CXCR7

crosstalk via CXCL11 and CXCL12," *Cytokine Growth Factor Rev.*, vol. 24, no. 1, pp. 41–49, Feb. 2013.

[21] T. T. Lau and D.-A. Wang, "Stromal cell-derived factor-1 (SDF-1): homing factor for engineered regenerative medicine," *Expert Opin. Biol. Ther.*, vol. 11, no. 2, pp. 189–197, Feb. 2011.

[22] M. Kucia, R. Reca, K. Miekus, J. Wanzeck, W. Wojakowski, A. Janowska-Wieczorek, J. Ratajczak, and M. Z. Ratajczak, "Trafficking of normal stem cells and metastasis of cancer stem cells involve similar mechanisms: pivotal role of the SDF-1-CXCR4 axis," *Stem Cells Dayt. Ohio*, vol. 23, no. 7, pp. 879–894, Aug. 2005.

[23] R. J. Miller, G. Banisadr, and B. J. Bhattacharyya, "CXCR4 signaling in the regulation of stem cell migration and development," *J. Neuroimmunol.*, vol. 198, no. 0, pp. 31–38, Jul. 2008.

[24] Y. Takabatake, T. Sugiyama, H. Kohara, T. Matsusaka, H. Kurihara, P. A. Koni, Y. Nagasawa, T. Hamano, I. Matsui, N. Kawada, E. Imai, T. Nagasawa, H. Rakugi, and Y. Isaka, "The CXCL12 (SDF-1)/CXCR4 Axis Is Essential for the Development of Renal Vasculature," *J. Am. Soc. Nephrol. JASN*, vol. 20, no. 8, pp. 1714–1723, Aug. 2009.

[25] M. Kucia, K. Jankowski, R. Reca, M. Wysoczynski, L. Bandura, D. J. Allendorf, J. Zhang, J. Ratajczak, and M. Z. Ratajczak, "CXCR4-SDF-1 signalling, locomotion, chemotaxis and adhesion," *J. Mol. Histol.*, vol. 35, no. 3, pp. 233–245, Mar. 2004.

[26] G. C. Bellenchi, F. Volpicelli, V. Piscopo, C. Perrone-Capano, and U. di Porzio, "Adult neural stem cells: an endogenous tool to repair brain injury?," *J. Neurochem.*, vol. 124, no. 2, pp. 159–167, Jan. 2013.

[27] S. Avasthi, R. N. Srivastava, A. Singh, and M. Srivastava, "Stem cell: past, present and future–a review article," *Internet J. Med. Update*, vol. 3, no. 1, pp. 22–31, 2008.

[28] H. Geminder, O. Sagi-Assif, L. Goldberg, T. Meshel, G. Rechavi, I. P. Witz, and A. Ben-Baruch, "A possible role for CXCR4 and its ligand, the CXC chemokine stromal cell-derived factor-1, in the development of bone marrow metastases in neuroblastoma," *J. Immunol. Baltim. Md 1950*, vol. 167, no. 8, pp. 4747–4757, Oct. 2001.

[29] J. M. Hall and K. S. Korach, "Stromal cell-derived factor 1, a novel target of estrogen receptor action, mediates the mitogenic effects of estradiol in ovarian and breast cancer cells," *Mol. Endocrinol. Baltim. Md*, vol. 17, no. 5, pp. 792–803, May 2003.

[30] C. F. B. Kim, E. L. Jackson, A. E. Woolfenden, S. Lawrence, I. Babar, S. Vogel, D. Crowley, R. T. Bronson, and T. Jacks, "Identification of bronchioalveolar stem cells in normal lung and lung cancer," *Cell*, vol. 121, no. 6, pp. 823–835, Jun. 2005.

[31] A. T. Collins, P. A. Berry, C. Hyde, M. J. Stower, and N. J. Maitland, "Prospective identification of tumorigenic prostate cancer stem cells," *Cancer Res.*, vol. 65, no. 23, pp. 10946–10951, Dec. 2005.

[32] Y.-X. Sun, J. Wang, C. E. Shelburne, D. E. Lopatin, A. M. Chinnaiyan, M. A. Rubin, K. J. Pienta, and R. S. Taichman, "Expression of CXCR4 and CXCL12 (SDF-1) in human prostate cancers (PCa) in vivo," *J. Cell. Biochem.*, vol. 89, no. 3, pp. 462–473, Jun. 2003.

[33] C. D. Sharp, J. D. Glawe, M. Huang, S. C. Barlow, and C. G. Kevil, "Chemokine repulsion of autoimmune T cell adhesion," *FASEB J.*, vol. 20, no. 4, pp. A202–A202, Mar. 2006.

[34] N. Karin, "The multiple faces of CXCL12 (SDF-1α) in the regulation of immunity during health and disease," *J. Leukoc. Biol.*, vol. 88, no. 3, pp. 463–473, Sep. 2010.

[35] C. C. Carter, L. A. McNamara, A. Onafuwa-Nuga, M. Shackleton, J. Riddell, D. Bixby, M. R. Savona, S. J. Morrison, and K. L. Collins, "HIV-1 utilizes the CXCR4 chemokine receptor to infect multipotent hematopoietic stem and progenitor cells," *Cell Host Microbe*, vol. 9, no. 3, pp. 223–234, Mar. 2011.

[36] J. Imitola, K. Raddassi, K. I. Park, F.-J. Mueller, M. Nieto, Y. D. Teng, D. Frenkel, J. Li, R. L. Sidman, C. A. Walsh, E. Y. Snyder, and S. J. Khoury, "Directed migration of neural stem cells to sites of CNS injury by the stromal cell-derived factor 1/CXC chemokine receptor 4 pathway," *Proc. Natl. Acad. Sci. U. S. A.*, vol. 101, no. 52, pp. 18117–18122, Dec. 2004.

[37] A. Toksoy, V. Müller, R. Gillitzer, and M. Goebeler, "Biphasic expression of stromal cell-derived factor-1 during human wound healing," *Br. J. Dermatol.*, vol. 157, no. 6, pp. 1148–1154, Dec. 2007.

[38] M. Cheng, K. Huang, J. Zhou, D. Yan, Y.-L. Tang, T. C. Zhao, R. J. Miller, R. Kishore, D. W. Losordo, and G. Qin, "A critical role of Src family kinase in SDF-1/CXCR4-mediated bone-marrow progenitor cell recruitment to the ischemic heart," *J. Mol. Cell. Cardiol.*, vol. 81, pp. 49–53, Apr. 2015.

[39] O. Kollet, S. Shivtiel, Y.-Q. Chen, J. Suriawinata, S. N. Thung, M. D. Dabeva, J. Kahn, A. Spiegel, A. Dar, S. Samira, P. Goichberg, A. Kalinkovich, F. Arenzana-Seisdedos, A. Nagler, I. Hardan, M. Revel, D. A. Shafritz, and T. Lapidot, "HGF, SDF-1, and MMP-9 are involved in stress-induced human CD34+ stem cell recruitment to the liver," *J. Clin. Invest.*, vol. 112, no. 2, pp. 160–169, Jul. 2003.

[40] H. Iwaguro, J. Yamaguchi, C. Kalka, S. Murasawa, H. Masuda, S. Hayashi, M. Silver, T. Li, J. M. Isner, and T. Asahara, "Endothelial progenitor cell vascular endothelial growth factor gene transfer for vascular regeneration," *Circulation*, vol. 105, no. 6, pp. 732–738, Feb. 2002.

[41] T. Ponomaryov, A. Peled, I. Petit, R. S. Taichman, L. Habler, J. Sandbank, F. Arenzana-Seisdedos, A. Magerus, A. Caruz, N. Fujii, A. Nagler, M. Lahav, M. Szyper-Kravitz, D. Zipori, and T. Lapidot, "Induction of the chemokine stromal-derived factor-1 following DNA damage improves human stem cell function," *J. Clin. Invest.*, vol. 106, no. 11, pp. 1331–1339, Dec. 2000.

[42] A. Peled, O. Kollet, T. Ponomaryov, I. Petit, S. Franitza, V. Grabovsky, M. M. Slav, A. Nagler, O. Lider, R. Alon, D. Zipori, and T. Lapidot, "The chemokine SDF-1 activates the integrins LFA-1, VLA-4, and VLA-5 on immature human CD34(+) cells: role in transendothelial/stromal migration and engraftment of NOD/SCID mice," *Blood*, vol. 95, no. 11, pp. 3289–3296, Jun. 2000.

[43] L. Liu, M. A. Eckert, H. Riazifar, D.-K. Kang, D. Agalliu, W. Zhao, L. Liu, M. A. Eckert, H. Riazifar, D.-K. Kang, D. Agalliu, and W. Zhao, "From Blood to the Brain: Can Systemically Transplanted Mesenchymal Stem Cells Cross the Blood-Brain Barrier?, From Blood to the Brain: Can Systemically Transplanted Mesenchymal Stem Cells Cross the Blood-Brain Barrier?," *Stem Cells Int. Stem Cells Int.*, vol. 2013, 2013, p. e435093, Aug. 2013.

[44] D. Thurman and J. Guerrero, "Trends in hospitalization associated with traumatic brain injury," *JAMA*, vol. 282, no. 10, pp. 954–957, Sep. 1999.

[45] V. G. Coronado, L. C. McGuire, K. Sarmiento, J. Bell, M. R. Lionbarger, C. D. Jones, A. I. Geller, N. Khoury, and L. Xu, "Trends in Traumatic Brain Injury in the U.S. and the public health response: 1995-2009," *J. Safety Res.*, vol. 43, no. 4, pp. 299–307, Sep. 2012.

[46] A. W. Selassie, M. L. McCarthy, P. L. Ferguson, J. Tian, and J. A. Langlois, "Risk of posthospitalization mortality among persons with traumatic brain injury, South Carolina 1999-2001," *J. Head Trauma Rehabil.*, vol. 20, no. 3, pp. 257–269, Jun. 2005.

[47] A. F. Ramlackhansingh, D. J. Brooks, R. J. Greenwood, S. K. Bose, F. E. Turkheimer, K. M. Kinnunen, S. Gentleman, R. A. Heckemann, K. Gunanayagam,

G. Gelosa, and D. J. Sharp, “Inflammation after trauma: microglial activation and traumatic brain injury,” *Ann. Neurol.*, vol. 70, no. 3, pp. 374–383, Sep. 2011.

[48] T. W. McAllister, “Neurobiological consequences of traumatic brain injury,” *Dialogues Clin. Neurosci.*, vol. 13, no. 3, pp. 287–300, 2011.

[49] K. Blennow, J. Hardy, and H. Zetterberg, “The Neuropathology and Neurobiology of Traumatic Brain Injury,” *Neuron*, vol. 76, no. 5, pp. 886–899, Dec. 2012.

[50] A. C. McKee, R. C. Cantu, C. J. Nowinski, E. T. Hedley-Whyte, B. E. Gavett, A. E. Budson, V. E. Santini, H.-S. Lee, C. A. Kubilus, and R. A. Stern, “Chronic Traumatic Encephalopathy in Athletes: Progressive Tauopathy After Repetitive Head Injury,” *J. Neuropathol. Exp. Neurol.*, vol. 68, no. 7, pp. 709–735, Jul. 2009.

[51] C. Werner and K. Engelhard, “Pathophysiology of traumatic brain injury,” *Br. J. Anaesth.*, vol. 99, no. 1, pp. 4–9, Jul. 2007.

[52] M. C. Morganti-Kossmann, L. Satgunaseelan, N. Bye, and T. Kossmann, “Modulation of immune response by head injury,” *Injury*, vol. 38, no. 12, pp. 1392–1400, Dec. 2007.

[53] S.-F. Chen, H. K. Richards, P. Smielewski, P. Johnström, R. Salvador, J. D. Pickard, and N. G. Harris, “Relationship between flow-metabolism uncoupling and evolving axonal injury after experimental traumatic brain injury,” *J. Cereb. Blood Flow Metab. Off. J. Int. Soc. Cereb. Blood Flow Metab.*, vol. 24, no. 9, pp. 1025–1036, Sep. 2004.

[54] M. Bergsneider, D. A. Hovda, E. Shalmon, D. F. Kelly, P. M. Vespa, N. A. Martin, M. E. Phelps, D. L. McArthur, M. J. Caron, J. F. Kraus, and D. P. Becker, “Cerebral hyperglycolysis following severe traumatic brain injury in humans: a positron emission tomography study,” *J. Neurosurg.*, vol. 86, no. 2, pp. 241–251, Feb. 1997.

[55] Yoichi Katayama, Donald P. Becker, Toru Tamura, and David A. Hovda, “Massive increases in extracellular potassium and the indiscriminate release of glutamate following concussive brain injury,” *http://dx.doi.org/10.3171/jns.1990.73.6.0889*, 13-May-2009.

[56] T. P. Obrenovitch and J. Urenjak, “Is high extracellular glutamate the key to excitotoxicity in traumatic brain injury?,” *J. Neurotrauma*, vol. 14, no. 10, pp. 677–698, Oct. 1997.

[57] Y. Dong and E. N. Benveniste, “Immune function of astrocytes,” *Glia*, vol. 36, no. 2, pp. 180–190, Nov. 2001.

[58] M. Keel and O. Trentz, “Pathophysiology of polytrauma,” *Injury*, vol. 36, no. 6, pp. 691–709, Jun. 2005.

[59] R. S. Clark, J. K. Schiding, S. L. Kaczorowski, D. W. Marion, and P. M. Kochanek, “Neutrophil accumulation after traumatic brain injury in rats: comparison of weight drop and controlled cortical impact models,” *J. Neurotrauma*, vol. 11, no. 5, pp. 499–506, Oct. 1994.

[60] V. Parpura and P. G. Haydon, “Physiological astrocytic calcium levels stimulate glutamate release to modulate adjacent neurons,” *Proc. Natl. Acad. Sci. U. S. A.*, vol. 97, no. 15, pp. 8629–8634, Jul. 2000.

[61] R. L. Hayes, L. W. Jenkins, and B. G. Lyeth, “Neurotransmitter-mediated mechanisms of traumatic brain injury: acetylcholine and excitatory amino acids,” *J. Neurotrauma*, vol. 9 Suppl 1, pp. S173-187, Mar. 1992.

[62] J. E. Burda, A. M. Bernstein, and M. V. Sofroniew, “Astrocyte roles in traumatic brain injury,” *Exp. Neurol.*, vol. 275, Part 3, pp. 305–315, Jan. 2016.

[63] S. M. Schwarzmaier, S.-W. Kim, R. Trabold, and N. Plesnila, “Temporal profile of thrombogenesis in the cerebral microcirculation after traumatic brain injury in mice,” *J. Neurotrauma*, vol. 27, no. 1, pp. 121–130, Jan. 2010.

[64] D. Shlosberg, M. Benifla, D. Kaufer, and A. Friedman, “Blood–brain barrier breakdown as a therapeutic target in traumatic brain injury,” *Nat. Rev. Neurol.*, vol. 6, pp. 393–403, Jun. 2010.

[65] A. Chodobski, B. J. Zink, and J. Szmydynger-Chodobska, “Blood-brain barrier pathophysiology in traumatic brain injury,” *Transl. Stroke Res.*, vol. 2, no. 4, pp. 492–516, Dec. 2011.

[66] I. Y. Chung and E. N. Benveniste, “Tumor necrosis factor-alpha production by astrocytes. Induction by lipopolysaccharide, IFN-gamma, and IL-1 beta,” *J. Immunol. Baltim. Md 1950*, vol. 144, no. 8, pp. 2999–3007, Apr. 1990.

[67] K.-T. Lu, Y.-W. Wang, J.-T. Yang, Y.-L. Yang, and H.-I. Chen, “Effect of interleukin-1 on traumatic brain injury-induced damage to hippocampal neurons,” *J. Neurotrauma*, vol. 22, no. 8, pp. 885–895, Aug. 2005.

[68] S. T. DeKosky, S. D. Styren, M. E. O’Malley, J. R. Goss, P. Kochanek, D. Marion, C. H. Evans, and P. D. Robbins, “Interleukin-1 receptor antagonist suppresses neurotrophin response in injured rat brain,” *Ann. Neurol.*, vol. 39, no. 1, pp. 123–127, Jan. 1996.

[69] M. Romano, M. Sironi, C. Toniatti, N. Polentarutti, P. Fruscella, P. Ghezzi, R. Faggioni, W. Luini, V. van Hinsbergh, S. Sozzani, F. Bussolino, V. Poli, G. Ciliberto, and A. Mantovani, "Role of IL-6 and its soluble receptor in induction of chemokines and leukocyte recruitment," *Immunity*, vol. 6, no. 3, pp. 315–325, Mar. 1997.

[70] T. Kossmann, V. Hans, H. G. Imhof, O. Trentz, and M. C. Morganti-Kossmann, "Interleukin-6 released in human cerebrospinal fluid following traumatic brain injury may trigger nerve growth factor production in astrocytes," *Brain Res.*, vol. 713, no. 1–2, pp. 143–152, Mar. 1996.

[71] A. Jaerve, F. Bosse, and H. W. Müller, "SDF-1/CXCL12: Its role in spinal cord injury," *Int. J. Biochem. Cell Biol.*, vol. 44, no. 3, pp. 452–456, Mar. 2012.

[72] J. W. Fawcett and R. A. Asher, "The glial scar and central nervous system repair," *Brain Res. Bull.*, vol. 49, no. 6, pp. 377–391, Aug. 1999.

[73] S. Elkabes, E. M. DiCicco-Bloom, and I. B. Black, "Brain microglia/macrophages express neurotrophins that selectively regulate microglial proliferation and function," *J. Neurosci. Off. J. Soc. Neurosci.*, vol. 16, no. 8, pp. 2508–2521, Apr. 1996.

[74] D. P. Schafer, E. K. Lehrman, A. G. Kautzman, R. Koyama, A. R. Mardinly, R. Yamasaki, R. M. Ransohoff, M. E. Greenberg, B. A. Barres, and B. Stevens, "Microglia Sculpt Postnatal Neural Circuits in an Activity and Complement-Dependent Manner," *Neuron*, vol. 74, no. 4, pp. 691–705, May 2012.

[75] A. I. Maas, B. Roozenbeek, and G. T. Manley, "Clinical trials in traumatic brain injury: past experience and current developments," *Neurotherapeutics*, vol. 7, no. 1, pp. 115–126, 2010.

[76] "National Guideline Clearinghouse | Traumatic brain injury medical treatment guidelines." [Online]. Available: https://www.guideline.gov/content.aspx?id=43752.

[77] M. S. Kaplan and J. W. Hinds, "Neurogenesis in the adult rat: electron microscopic analysis of light radioautographs," *Science*, vol. 197, no. 4308, pp. 1092–1094, Sep. 1977.

[78] J. Altman, "Are new neurons formed in the brains of adult mammals?," *Science*, vol. 135, no. 3509, pp. 1127–1128, Mar. 1962.

[79] L. Oboti, R. Schellino, C. Giachino, P. Chamero, M. Pyrski, T. Leinders-Zufall, F. Zufall, A. Fasolo, and P. Peretto, "Newborn Interneurons in the Accessory

Olfactory Bulb Promote Mate Recognition in Female Mice," *Front. Neurosci.*, vol. 5, Sep. 2011.

[80] G. M. Thomsen, J. E. Le Belle, J. A. Harnisch, W. S. Mc Donald, D. A. Hovda, M. V. Sofroniew, H. I. Kornblum, and N. G. Harris, "Traumatic brain injury reveals novel cell lineage relationships within the subventricular zone," *Stem Cell Res.*, vol. 13, no. 1, pp. 48–60, Jul. 2014.

[81] T. Itoh, T. Satou, H. Ishida, S. Nishida, M. Tsubaki, S. Hashimoto, and H. Ito, "The relationship between SDF-1alpha/CXCR4 and neural stem cells appearing in damaged area after traumatic brain injury in rats," *Neurol. Res.*, vol. 31, no. 1, pp. 90–102, 2009.

[82] K. Park and T. Biederer, "Neuronal adhesion and synapse organization in recovery after brain injury," *Future Neurol.*, vol. 8, no. 5, pp. 555–567, Sep. 2013.

[83] C. Sun, H. Sun, S. Wu, C. C. Lee, Y. Akamatsu, R. K. Wang, S. G. Kernie, and J. Liu, "Conditional Ablation of Neuroprogenitor Cells in Adult Mice Impedes Recovery of Poststroke Cognitive Function and Reduces Synaptic Connectivity in the Perforant Pathway," *J. Neurosci.*, vol. 33, no. 44, pp. 17314–17325, Oct. 2013.

[84] P. Thored, A. Arvidsson, E. Cacci, H. Ahlenius, T. Kallur, V. Darsalia, C. T. Ekdahl, Z. Kokaia, and O. Lindvall, "Persistent production of neurons from adult brain stem cells during recovery after stroke," *Stem Cells Dayt. Ohio*, vol. 24, no. 3, pp. 739–747, Mar. 2006.

[85] Q. Xu, S. Wang, X. Jiang, Y. Zhao, M. Gao, Y. Zhang, X. Wang, K. Tano, M. Kanehara, W. Zhang, and T. Ishida, "Hypoxia-induced astrocytes promote the migration of neural progenitor cells via vascular endothelial factor, stem cell factor, stromal-derived factor-1alpha and monocyte chemoattractant protein-1 upregulation in vitro," *Clin. Exp. Pharmacol. Physiol.*, vol. 34, no. 7, pp. 624–631, Jul. 2007.

[86] W. D. Hill, D. C. Hess, A. Martin-Studdard, J. J. Carothers, J. Zheng, D. Hale, M. Maeda, S. C. Fagan, J. E. Carroll, and S. J. Conway, "SDF-1 (CXCL12) Is Upregulated in the Ischemic Penumbra Following Stroke: Association with Bone Marrow Cell Homing to Injury," *J. Neuropathol. Exp. Neurol.*, vol. 63, no. 1, pp. 84–96, 2004.

[87] X. Yi, G. Jin, X. Zhang, W. Mao, H. Li, J. Qin, J. Shi, K. Dai, and F. Zhang, "Cortical Endogenic Neural Regeneration of Adult Rat after Traumatic Brain Injury," *PLoS ONE*, vol. 8, no. 7, p. e70306, Jul. 2013.

[88] A. Oyagi, N. Morimoto, J. Hamanaka, M. Ishiguro, K. Tsuruma, M. Shimazawa, and H. Hara, "Forebrain specific heparin-binding epidermal growth factor-like

growth factor knockout mice show exacerbated ischemia and reperfusion injury," *Neuroscience*, vol. 185, pp. 116–124, Jun. 2011.

[89] S. Ahmed, B. A. Reynolds, and S. Weiss, "BDNF enhances the differentiation but not the survival of CNS stem cell-derived neuronal precursors," *J. Neurosci. Off. J. Soc. Neurosci.*, vol. 15, no. 8, pp. 5765–5778, Aug. 1995.

[90] A. M. Choo, W. J. Miller, Y.-C. Chen, P. Nibley, T. P. Patel, C. Goletiani, B. Morrison, M. K. Kutzing, B. L. Firestein, J.-Y. Sul, P. G. Haydon, and D. F. Meaney, "Antagonism of purinergic signalling improves recovery from traumatic brain injury," *Brain*, Jan. 2013.

[91] C. A. Reynolds, S. Schafer, R. Pirooz, A. Marinica, A. Chbib, C. Bedford, M. Fronczak, J. A. Rafols, D. Kuhn, and C. W. Kreipke, "Differential effects of endothelin receptor A and B antagonism on behavioral outcome following traumatic brain injury," *Neurol. Res.*, vol. 33, no. 2, pp. 197–200, Mar. 2011.

[92] D. R. Namjoshi, G. Martin, J. Donkin, A. Wilkinson, S. Stukas, J. Fan, M. Carr, S. Tabarestani, K. Wuerth, R. E. W. Hancock, and C. L. Wellington, "The Liver X Receptor Agonist GW3965 Improves Recovery from Mild Repetitive Traumatic Brain Injury in Mice Partly through Apolipoprotein E," *PLoS ONE*, vol. 8, no. 1, p. e53529, Jan. 2013.

[93] I. Paterniti, A. Melani, S. Cipriani, F. Corti, T. Mello, E. Mazzon, E. Esposito, P. Bramanti, S. Cuzzocrea, and F. Pedata, "Selective adenosine A2A receptor agonists and antagonists protect against spinal cord injury through peripheral and central effects," *J. Neuroinflammation*, vol. 8, no. 1, p. 31, Apr. 2011.

[94] W. M. Tian, C. L. Zhang, S. P. Hou, X. Yu, F. Z. Cui, Q. Y. Xu, S. L. Sheng, H. Cui, and H. D. Li, "Hyaluronic acid hydrogel as Nogo-66 receptor antibody delivery system for the repairing of injured rat brain: in vitro," *J. Controlled Release*, vol. 102, no. 1, pp. 13–22, Jan. 2005.

[95] V. Ramaglia, R. Wolterman, M. de Kok, M. A. Vigar, I. Wagenaar-Bos, R. H. M. King, B. P. Morgan, and F. Baas, "Soluble Complement Receptor 1 Protects the Peripheral Nerve from Early Axon Loss after Injury," *Am. J. Pathol.*, vol. 172, no. 4, pp. 1043–1052, Apr. 2008.

[96] O. Y. Bang, J. S. Lee, P. H. Lee, and G. Lee, "Autologous mesenchymal stem cell transplantation in stroke patients," *Ann. Neurol.*, vol. 57, no. 6, pp. 874–882, 2005.

[97] J. E. Carroll and R. W. Mays, "Update on stem cell therapy for cerebral palsy," *Expert Opin. Biol. Ther.*, vol. 11, no. 4, pp. 463–471, Apr. 2011.

[98] V. Johann, J. Schiefer, C. Sass, J. Mey, G. Brook, A. Krüttgen, C. Schlangen, C. Bernreuther, M. Schachner, M. Dihné, and C. M. Kosinski, "Time of transplantation and cell preparation determine neural stem cell survival in a mouse model of Huntington's disease," *Exp. Brain Res. Exp. Hirnforsch. Expérimentation Cérébrale*, vol. 177, no. 4, pp. 458–470, Mar. 2007.

[99] D. Galimberti and E. Scarpini, "Disease-modifying treatments for Alzheimer's disease," *Ther. Adv. Neurol. Disord.*, vol. 4, no. 4, pp. 203–216, Jul. 2011.

[100] C. T. J. van Velthoven, R. A. Sheldon, A. Kavelaars, N. Derugin, Z. S. Vexler, H. L. D. M. Willemen, M. Maas, C. J. Heijnen, and D. M. Ferriero, "Mesenchymal Stem Cell Transplantation Attenuates Brain Injury After Neonatal Stroke," *Stroke*, vol. 44, no. 5, pp. 1426–1432, May 2013.

[101] M. T. Harting, L. E. Sloan, F. Jimenez, J. Baumgartner, and C. S. Cox Jr, "Subacute Neural Stem Cell Therapy for Traumatic Brain Injury," *J. Surg. Res.*, vol. 153, no. 2, pp. 188–194, May 2009.

[102] H. Inoue, "Neurodegenerative disease-specific induced pluripotent stem cell research," *Exp. Cell Res.*, vol. 316, no. 16, pp. 2560–2564, Oct. 2010.

[103] B. Chen, X.-Q. Gao, C.-X. Yang, S.-K. Tan, Z.-L. Sun, N.-H. Yan, Y.-G. Pang, M. Yuan, G.-J. Chen, G.-T. Xu, K. Zhang, and Q. L. Yuan, "Neuroprotective effect of grafting GDNF gene-modified neural stem cells on cerebral ischemia in rats," *Brain Res.*, vol. 1284, pp. 1–11, Aug. 2009.

[104] C. P. Addington, J. M. Heffernan, C. S. Millar-Haskell, E. W. Tucker, R. W. Sirianni, and S. E. Stabenfeldt, "Enhancing neural stem cell response to SDF-1α gradients through hyaluronic acid-laminin hydrogels," *Biomaterials*, vol. 72, pp. 11–19, Dec. 2015.

[105] S. Pluchino, A. Quattrini, E. Brambilla, A. Gritti, G. Salani, G. Dina, R. Galli, U. Del Carro, S. Amadio, A. Bergami, R. Furlan, G. Comi, A. L. Vescovi, and G. Martino, "Injection of adult neurospheres induces recovery in a chronic model of multiple sclerosis," *Nature*, vol. 422, no. 6933, pp. 688–694, Apr. 2003.

[106] M. Janowski, C. Engels, M. Gorelik, A. Lyczek, S. Bernard, J. Bulte W., and P. Walczak, "Survival of Neural Progenitors Allografted into the CNS of Immunocompetent Recipients is Highly Dependent on Transplantation Site," *Cell Transplant.*, 2012.

[107] Y. Jiang, J. Zhu, G. Xu, and X. Liu, "Intranasal delivery of stem cells to the brain," *Expert Opin. Drug Deliv.*, vol. 8, no. 5, pp. 623–632, May 2011.

[108] S. Jozwiak, A. Habich, K. Kotulska, A. Sarnowska, T. Kropiwnicki, M. Janowski, E. Jurkiewicz, B. Lukomska, T. Kmiec, J. Walecki, M. Roszkowski, M. Litwin, T. Oldak, D. Boruczkowski, and K. Domanska-Janik, "Intracerebroventricular Transplantation of Cord Blood-Derived Neural Progenitors in a Child With Severe Global Brain Ischemic Injury," *Cell Med.*, vol. 1, no. 2, pp. 71–80, 2010.

[109] H. Okano, T. Yoshizaki, T. Shimazaki, and K. Sawamoto, "Isolation and transplantation of dopaminergic neurons and neural stem cells," *Parkinsonism Relat. Disord.*, vol. 9, no. 1, pp. 23–28, Oct. 2002.

[110] S. I. Savitz, V. Misra, M. Kasam, H. Juneja, C. S. Cox Jr, S. Alderman, I. Aisiku, S. Kar, A. Gee, and J. C. Grotta, "Intravenous autologous bone marrow mononuclear cells for ischemic stroke," *Ann. Neurol.*, vol. 70, no. 1, pp. 59–69, Jul. 2011.

[111] M. R. Hoane, G. D. Becerra, J. E. Shank, L. Tatko, E. S. Pak, M. Smith, and A. K. Murashov, "Transplantation of neuronal and glial precursors dramatically improves sensorimotor function but not cognitive function in the traumatically injured brain," *J. Neurotrauma*, vol. 21, no. 2, pp. 163–174, Feb. 2004.

[112] P. Riess, M. Molcanyi, K. Bentz, M. Maegele, C. Simanski, C. Carlitscheck, A. Schneider, J. Hescheler, B. Bouillon, U. Schäfer, and E. Neugebauer, "Embryonic stem cell transplantation after experimental traumatic brain injury dramatically improves neurological outcome, but may cause tumors," *J. Neurotrauma*, vol. 24, no. 1, pp. 216–225, Jan. 2007.

[113] M. Korhonen and J. Jolkkonen, "Intravascular cell therapy in stroke patients: where the cells go and what they do," *Regen. Med.*, vol. 8, no. 2, pp. 93–95, Mar. 2013.

[114] C. Sun, H. Zhang, J. Li, H. Huang, H. Cheng, Y. Wang, P. Li, and Y. An, "Modulation of the major histocompatibility complex by neural stem cell-derived neurotrophic factors used for regenerative therapy in a rat model of stroke," *J. Transl. Med.*, vol. 8, p. 77, 2010.

[115] M. Bacigaluppi, S. Pluchino, L. Peruzzotti-Jametti, L. P. Jametti, E. Kilic, U. Kilic, G. Salani, E. Brambilla, M. J. West, G. Comi, G. Martino, and D. M. Hermann, "Delayed post-ischaemic neuroprotection following systemic neural stem cell transplantation involves multiple mechanisms," *Brain J. Neurol.*, vol. 132, no. Pt 8, pp. 2239–2251, Aug. 2009.

[116] C. Capone, S. Frigerio, S. Fumagalli, M. Gelati, M.-C. Principato, C. Storini, M. Montinaro, R. Kraftsik, M. D. Curtis, E. Parati, and M.-G. D. Simoni, "Neurosphere-Derived Cells Exert a Neuroprotective Action by Changing the Ischemic Microenvironment," *PLoS ONE*, vol. 2, no. 4, p. e373, Apr. 2007.

[117] F.-M. Chen, L.-A. Wu, M. Zhang, R. Zhang, and H.-H. Sun, “Homing of endogenous stem/progenitor cells for in situ tissue regeneration: Promises, strategies, and translational perspectives,” *Biomaterials*, vol. 32, no. 12, pp. 3189–3209, Apr. 2011.

[118] B. Baykara, I. Aksu, E. Buyuk, M. Kiray, A. Sisman, B. Baykara, A. Dayi, A. Tas, D. Ozdemir, M. Arda, and N. Uysal, “Progesterone treatment decreases traumatic brain injury induced anxiety and is correlated with increased serum IGF-1 levels; prefrontal cortex, amygdala, hippocampus neuron density; and reduced serum corticosterone levels in immature rats,” *Biotech. Histochem.*, pp. 1–8, Mar. 2013.

[119] F. Wang, M. Kameda, T. Yasuhara, N. Tajiri, Y. Kikuchi, H. B. Liang, J. T. Tayra, A. Shinko, T. Wakamori, T. Agari, and I. Date, “GDNF-pretreatment enhances the survival of neural stem cells following transplantation in a rat model of Parkinson’s disease,” *Neurosci. Res.*, vol. 71, no. 1, pp. 92–98, Sep. 2011.

[120] S. R. Alcalá-Barraza, M. S. Lee, L. R. Hanson, A. A. McDonald, W. H. Frey, and L. K. McLoon, “Intranasal delivery of neurotrophic factors BDNF, CNTF, EPO, and NT-4 to the CNS,” *J. Drug Target.*, vol. 18, no. 3, pp. 179–190, Apr. 2010.

[121] M. Molné, L. Studer, V. Tabar, Y. T. Ting, M. V. Eiden, and R. D. McKay, “Early cortical precursors do not undergo LIF-mediated astrocytic differentiation,” *J. Neurosci. Res.*, vol. 59, no. 3, pp. 301–311, Feb. 2000.

[122] A. Benraiss, E. Chmielnicki, K. Lerner, D. Roh, and S. A. Goldman, “Adenoviral brain-derived neurotrophic factor induces both neostriatal and olfactory neuronal recruitment from endogenous progenitor cells in the adult forebrain,” *J. Neurosci. Off. J. Soc. Neurosci.*, vol. 21, no. 17, pp. 6718–6731, Sep. 2001.

[123] K. Jin, X. O. Mao, Y. Sun, L. Xie, L. Jin, E. Nishi, M. Klagsbrun, and D. A. Greenberg, “Heparin-binding epidermal growth factor-like growth factor: hypoxia-inducible expression in vitro and stimulation of neurogenesis in vitro and in vivo,” *J. Neurosci. Off. J. Soc. Neurosci.*, vol. 22, no. 13, pp. 5365–5373, Jul. 2002.

[124] P. Taupin, J. Ray, W. H. Fischer, S. T. Suhr, K. Hakansson, A. Grubb, and F. H. Gage, “FGF-2-responsive neural stem cell proliferation requires CCg, a novel autocrine/paracrine cofactor,” *Neuron*, vol. 28, no. 2, pp. 385–397, Nov. 2000.

[125] P. Johnson, A. Tatara, A. Shiu, and S. E. Sakiyama-Elbert, “Controlled release of neurotrophin-3 and platelet-derived growth factor from fibrin scaffolds containing neural progenitor cells enhances survival and differentiation into neurons in a subacute model of SCI,” *Cell Transpl.*, vol. 19, no. 1, pp. 89–101, 2010.

[126] T. W. Weiss, A. L. Samson, B. Niego, P. B. Daniel, and R. L. Medcalf, “Oncostatin M is a neuroprotective cytokine that inhibits excitotoxic injury in vitro and in vivo,” *FASEB J.*, vol. 20, no. 13, pp. 2369–2371, Nov. 2006.

[127] K. Nakaguchi, H. Jinnou, N. Kaneko, M. Sawada, T. Hikita, S. Saitoh, Y. Tabata, and K. Sawamoto, “Growth Factors Released from Gelatin Hydrogel Microspheres Increase New Neurons in the Adult Mouse Brain,” *Stem Cells Int.*, vol. 2012, Oct. 2012.

[128] B. S. Zolnik and D. J. Burgess, “Evaluation of in vivo–in vitro release of dexamethasone from PLGA microspheres,” *J. Controlled Release*, vol. 127, no. 2, pp. 137–145, Apr. 2008.

[129] J. Panyam, M. M. Dali, S. K. Sahoo, W. Ma, S. S. Chakravarthi, G. L. Amidon, R. J. Levy, and V. Labhasetwar, “Polymer degradation and in vitro release of a model protein from poly(d,l-lactide-co-glycolide) nano- and microparticles,” *J. Controlled Release*, vol. 92, no. 1–2, pp. 173–187, Sep. 2003.

[130] N. J. Abbott, L. Rönnbäck, and E. Hansson, “Astrocyte–endothelial interactions at the blood–brain barrier,” *Nat. Rev. Neurosci.*, vol. 7, no. 1, pp. 41–53, Jan. 2006.

[131] X. Yi, D. S. Manickam, A. Brynskikh, and A. V. Kabanov, “Agile delivery of protein therapeutics to CNS,” *J. Controlled Release*, vol. 190, pp. 637–663, Sep. 2014.

[132] D. Wu, B.-W. Song, H. V. Vinters, and W. M. Pardridge, “Pharmacokinetics and Brain Uptake of Biotinylated Basic Fibroblast Growth Factor Conjugated to a Blood-Brain Barrier Drug Delivery System,” *J. Drug Target.*, vol. 10, no. 3, pp. 239–245, Jan. 2002.

[133] W. M. Pardridge, “Drug and gene targeting to the brain via blood–brain barrier receptor-mediated transport systems,” *Int. Congr. Ser.*, vol. 1277, pp. 49–62, Apr. 2005.

[134] J. A. Falcone, T. S. Salameh, X. Yi, B. J. Cordy, W. G. Mortell, A. V. Kabanov, and W. A. Banks, “Intranasal Administration as a Route for Drug Delivery to the Brain: Evidence for a Unique Pathway for Albumin,” *J. Pharmacol. Exp. Ther.*, vol. 351, no. 1, pp. 54–60, Oct. 2014.

[135] S. Pathan, Z. Iqbal, S. Zaidi, S. Talegaonkar, D. Vohra, G. Jain, A. Azeem, N. Jain, J. Lalani, R. Khar, and F. Ahmad, “CNS Drug Delivery Systems: Novel Approaches,” *Recent Pat. Drug Deliv. Formul.*, vol. 3, no. 1, pp. 71–89, Jan. 2009.

[136] V. Pencea, K. D. Bingaman, S. J. Wiegand, and M. B. Luskin, “Infusion of Brain-Derived Neurotrophic Factor into the Lateral Ventricle of the Adult Rat Leads to

New Neurons in the Parenchyma of the Striatum, Septum, Thalamus, and Hypothalamus," *J. Neurosci.*, vol. 21, no. 17, pp. 6706–6717, Sep. 2001.

[137] K. Choudhuri and M. L. Dustin, "Signaling microdomains in T cells," *FEBS Lett.*, vol. 584, no. 24, pp. 4823–4831, Dec. 2010.

[138] B. G. Fuller, "Self-organization of intracellular gradients during mitosis," *Cell Div.*, vol. 5, p. 5, 2010.

[139] D. Sun, M. R. Bullock, N. Altememi, Z. Zhou, S. Hagood, A. Rolfe, M. J. McGinn, R. Hamm, and R. J. Colello, "The effect of epidermal growth factor in the injured brain after trauma in rats," *J. Neurotrauma*, vol. 27, no. 5, pp. 923–938, May 2010.

[140] M. J. Cooke, Y. Wang, C. M. Morshead, and M. S. Shoichet, "Controlled epicortical delivery of epidermal growth factor for the stimulation of endogenous neural stem cell proliferation in stroke-injured brain," *Biomaterials*, vol. 32, no. 568, p. 8e5697, 2011.

[141] F. Huang, Z. Yin, D. Wu, and J. Hao, "Effects of controlled release of brain-derived neurotrophic factor from collagen gel on rat neural stem cells:," *NeuroReport*, vol. 24, no. 3, pp. 101–107, Feb. 2013.

[142] Y. Cai, M. Xu, M. Yuan, Z. Liu, and W. Yuan, "Developments in human growth hormone preparations: sustained-release, prolonged half-life, novel injection devices, and alternative delivery routes," *Int. J. Nanomedicine*, vol. 9, pp. 3527–3538, Jul. 2014.

[143] R. W. Sirianni, P. Olausson, A. S. Chiu, J. R. Taylor, and W. M. Saltzman, "The behavioral and biochemical effects of BDNF containing polymers implanted in the hippocampus of rats," *Brain Res.*, vol. 1321, pp. 40–50, Mar. 2010.

[144] A. R. Finch, C. J. Caunt, S. P. Armstrong, and C. A. McArdle, "Agonist-induced internalization and downregulation of gonadotropin-releasing hormone receptors," *Am. J. Physiol. - Cell Physiol.*, vol. 297, no. 3, pp. C591–C600, Sep. 2009.

[145] C. W. Olanow and J. A. Obeso, "Preventing levodopa-induced dyskinesias," *Ann. Neurol.*, vol. 47, no. 4 Suppl 1, pp. S167-176-178, Apr. 2000.

[146] P. J. Lefèbvre, G. Paolisso, A. J. Scheen, and J. C. Henquin, "Pulsatility of insulin and glucagon release: physiological significance and pharmacological implications," *Diabetologia*, vol. 30, no. 7, pp. 443–452, Jul. 1987.

[147] D. J. Martens, R. M. Seaberg, and D. van der Kooy, “In vivo infusions of exogenous growth factors into the fourth ventricle of the adult mouse brain increase the proliferation of neural progenitors around the fourth ventricle and the central canal of the spinal cord,” *Eur. J. Neurosci.*, vol. 16, no. 6, pp. 1045–1057, Sep. 2002.

[148] M. C. Jimenez Hamann, C. H. Tator, and M. S. Shoichet, “Injectable intrathecal delivery system for localized administration of EGF and FGF-2 to the injured rat spinal cord,” *Exp. Neurol.*, vol. 194, no. 1, pp. 106–119, Jul. 2005.

[149] Y. Wang, M. J. Cooke, N. Sachewsky, C. M. Morshead, and M. S. Shoichet, “Bioengineered sequential growth factor delivery stimulates brain tissue regeneration after stroke,” *J. Controlled Release*, vol. 172, no. 1, pp. 1–11, Nov. 2013.

[150] Y. Wang, Y. T. Wei, Z. H. Zu, R. K. Ju, M. Y. Guo, X. M. Wang, Q. Y. Xu, and F. Z. Cui, “Combination of hyaluronic acid hydrogel scaffold and PLGA microspheres for supporting survival of neural stem cells,” *Pharm. Res.*, vol. 28, no. 6, pp. 1406–1414, Jun. 2011.

[151] H. Chu and Y. Wang, “Therapeutic angiogenesis: controlled delivery of angiogenic factors,” *Ther. Deliv.*, vol. 3, no. 6, pp. 693–714, Jun. 2012.

[152] C.-C. Lin and A. T. Metters, “Hydrogels in controlled release formulations: Network design and mathematical modeling,” *Adv. Drug Deliv. Rev.*, vol. 58, no. 12–13, pp. 1379–1408, Nov. 2006.

[153] M. M. Martino, P. S. Briquez, A. Ranga, M. P. Lutolf, and J. A. Hubbell, “Heparin-binding domain of fibrin(ogen) binds growth factors and promotes tissue repair when incorporated within a synthetic matrix,” *Proc. Natl. Acad. Sci.*, vol. 110, no. 12, pp. 4563–4568, Mar. 2013.

[154] D. F. Emerich, E. Silva, O. Ali, D. Mooney, W. Bell, S. J. Yu, Y. Kaneko, and C. Borlongan, “Injectable VEGF Hydrogels Produce Near Complete Neurological and Anatomical Protection Following Cerebral Ischemia in Rats,” *Cell Transplant.*, vol. 19, no. 9, pp. 1063–1071, Sep. 2010.

[155] U. Galderisi, G. Peluso, G. Di Bernardo, A. Calarco, M. D’Apolito, O. Petillo, M. Cipollaro, F. R. Fusco, and M. A. B. Melone, “Efficient cultivation of neural stem cells with controlled delivery of FGF-2,” *Stem Cell Res.*, vol. 10, no. 1, pp. 85–94, Jan. 2013.

[156] Y.-B. Lee, S. Polio, W. Lee, G. Dai, L. Menon, R. S. Carroll, and S.-S. Yoo, “Bio-printing of collagen and VEGF-releasing fibrin gel scaffolds for neural stem cell culture,” *Exp. Neurol.*, vol. 223, no. 2, pp. 645–652, Jun. 2010.

[157] D. F. Emerich, D. J. Mooney, H. Storrie, R. S. Babu, and J. H. Kordower, "Injectable hydrogels providing sustained delivery of vascular endothelial growth factor are neuroprotective in a rat model of Huntington's disease," *Neurotox. Res.*, vol. 17, no. 1, pp. 66–74, Jan. 2010.

[158] O. Jeon, S.-W. Kang, H.-W. Lim, J. Hyung Chung, and B.-S. Kim, "Long-term and zero-order release of basic fibroblast growth factor from heparin-conjugated poly(l-lactide-co-glycolide) nanospheres and fibrin gel," *Biomaterials*, vol. 27, no. 8, pp. 1598–1607, Mar. 2006.

[159] M. K. Horne, D. R. Nisbet, J. S. Forsythe, and C. L. Parish, "Three-dimensional nanofibrous scaffolds incorporating immobilized BDNF promote proliferation and differentiation of cortical neural stem cells," *Stem Cells Dev.*, vol. 19, no. 6, pp. 843–852, Jun. 2010.

[160] L. Conova, P. Kubinski, Y. Jin, J. Vernengo, B. Neuhuber, I. Fischer, B. Neuhuber, and A. Lowman, "Injectable multifunctional scaffold for spinal cord repair," in *Proceedings of the 2010 IEEE 36th Annual Northeast Bioengineering Conference (NEBEC)*, 2010, pp. 1–2.

[161] A. Jain, Y.-T. Kim, R. J. McKeon, and R. V. Bellamkonda, "In situ gelling hydrogels for conformal repair of spinal cord defects, and local delivery of BDNF after spinal cord injury," *Biomaterials*, vol. 27, no. 3, pp. 497–504, Jan. 2006.

[162] R. P. Batycky, J. Hanes, R. Langer, and D. A. Edwards, "A theoretical model of erosion and macromolecular drug release from biodegrading microspheres," *J. Pharm. Sci.*, vol. 86, no. 12, pp. 1464–1477, 1997.

[163] H. K. Makadia and S. J. Siegel, "Poly Lactic-co-Glycolic Acid (PLGA) as Biodegradable Controlled Drug Delivery Carrier," *Polymers*, vol. 3, no. 3, pp. 1377–1397, Sep. 2011.

[164] D. Fon, K. Zhou, F. Ercole, F. Fehr, S. Marchesan, M. R. Minter, P. J. Crack, D. I. Finkelstein, and J. S. Forsythe, "Nanofibrous scaffolds releasing a small molecule BDNF-mimetic for the re-direction of endogenous neuroblast migration in the brain," *Biomaterials*, vol. 35, no. 9, pp. 2692–2712, Mar. 2014.

[165] J. P. Bertram, M. F. Rauch, K. Chang, and E. B. Lavik, "Using Polymer Chemistry to Modulate the Delivery of Neurotrophic Factors from Degradable Microspheres: Delivery of BDNF," *Pharm. Res.*, vol. 27, no. 1, pp. 82–91, Jan. 2010.

[166] M. D. Baumann, C. E. Kang, J. C. Stanwick, Y. Wang, H. Kim, Y. Lapitsky, and M. S. Shoichet, "An injectable drug delivery platform for sustained combination

therapy," *J. Control. Release Off. J. Control. Release Soc.*, vol. 138, no. 3, pp. 205–213, Sep. 2009.

[167] S. Li, M. Wei, Z. Zhou, B. Wang, X. Zhao, and J. Zhang, "SDF-1α induces angiogenesis after traumatic brain injury," *Brain Res.*, vol. 1444, pp. 76–86, Mar. 2012.

[168] W. Sun, J. Liu, Y. Huan, and C. Zhang, "Intracranial injection of recombinant stromal-derived factor-1 alpha (SDF-1α) attenuates traumatic brain injury in rats," *Inflamm. Res.*, vol. 63, no. 4, pp. 287–297, Apr. 2014.

[169] J. Opatz, P. Küry, N. Schiwy, A. Järve, V. Estrada, N. Brazda, F. Bosse, and H. W. Müller, "SDF-1 stimulates neurite growth on inhibitory CNS myelin," *Mol. Cell. Neurosci.*, vol. 40, no. 2, pp. 293–300, Feb. 2009.

[170] P. W. Henderson, S. P. Singh, D. D. Krijgh, M. Yamamoto, D. C. Rafii, J. J. Sung, S. Rafii, S. Y. Rabbany, and J. A. Spector, "Stromal-derived factor-1 delivered via hydrogel drug-delivery vehicle accelerates wound healing in vivo: Hydrogel drug delivery vehicle," *Wound Repair Regen.*, vol. 19, no. 3, pp. 420–425, May 2011.

[171] S. Y. Rabbany, J. Pastore, M. Yamamoto, T. Miller, S. Rafii, R. Aras, and M. Penn, "Continuous Delivery of Stromal Cell-Derived Factor-1 From Alginate Scaffolds Accelerates Wound Healing," *Cell Transplant.*, vol. 19, no. 4, pp. 399–408, Apr. 2010.

[172] P. T. Thevenot, A. M. Nair, J. Shen, P. Lotfi, C.-Y. Ko, and L. Tang, "The effect of incorporation of SDF-1α into PLGA scaffolds on stem cell recruitment and the inflammatory response," *Biomaterials*, vol. 31, no. 14, pp. 3997–4008, May 2010.

[173] M. Fujio, A. Yamamoto, Y. Ando, R. Shohara, K. Kinoshita, T. Kaneko, H. Hibi, and M. Ueda, "Stromal cell-derived factor-1 enhances distraction osteogenesis-mediated skeletal tissue regeneration through the recruitment of endothelial precursors," *Bone*, vol. 49, no. 4, pp. 693–700, Oct. 2011.

[174] K. Higashino, M. Viggeswarapu, M. Bargouti, H. Liu, L. Titus, and S. D. Boden, "Stromal Cell-Derived Factor-1 Potentiates Bone Morphogenetic Protein-2 Induced Bone Formation," *Tissue Eng. Part A*, vol. 17, no. 3–4, pp. 523–530, Feb. 2011.

[175] V. F. M. Segers, T. Tokunou, L. J. Higgins, C. MacGillivray, J. Gannon, and R. T. Lee, "Local Delivery of Protease-Resistant Stromal Cell Derived Factor-1 for Stem Cell Recruitment After Myocardial Infarction," *Circulation*, vol. 116, pp. 1683–1692, Oct. 2007.

[176] G. Zhang, Y. Nakamura, X. Wang, Q. Hu, L. J. Suggs, and J. Zhang, "Controlled Release of Stromal Cell–Derived Factor-1alpha *In Situ* Increases C-kit $^{+}$ Cell Homing to the Infarcted Heart," *Tissue Eng.*, vol. 13, no. 8, pp. 2063–2071, Aug. 2007.

[177] B. P. Purcell, J. A. Elser, A. Mu, K. B. Margulies, and J. A. Burdick, "Synergistic effects of SDF-1α chemokine and hyaluronic acid release from degradable hydrogels on directing bone marrow derived cell homing to the myocardium," *Biomaterials*, vol. 33, no. 31, pp. 7849–7857, Nov. 2012.

[178] S. Prokoph, E. Chavakis, K. R. Levental, A. Zieris, U. Freudenberg, S. Dimmeler, and C. Werner, "Sustained delivery of SDF-1α from heparin-based hydrogels to attract circulating pro-angiogenic cells," *Biomaterials*, vol. 33, no. 19, pp. 4792–4800, Jun. 2012.

[179] L. Baumann, S. Prokoph, C. Gabriel, U. Freudenberg, C. Werner, and A. G. Beck-Sickinger, "A novel, biased-like SDF-1 derivative acts synergistically with starPEG-based heparin hydrogels and improves eEPC migration in vitro," *J. Controlled Release*, vol. 162, no. 1, pp. 68–75, Aug. 2012.

[180] D. P. Cross and C. Wang, "Stromal-Derived Factor-1 Alpha-Loaded PLGA Microspheres for Stem Cell Recruitment," *Pharm. Res.*, vol. 28, no. 10, pp. 2477–2489, May 2011.

[181] Y.-C. Huang and T.-J. Liu, "Mobilization of mesenchymal stem cells by stromal cell-derived factor-1 released from chitosan/tripolyphosphate/fucoidan nanoparticles," *Acta Biomater.*, vol. 8, no. 3, pp. 1048–1056, Mar. 2012.

[182] X. He, J. Ma, and E. Jabbari, "Migration of marrow stromal cells in response to sustained release of stromal-derived factor-1α from poly(lactide ethylene oxide fumarate) hydrogels," *Int. J. Pharm.*, vol. 390, no. 2, pp. 107–116, May 2010.

[183] F.-M. Chen, H. Lu, L.-A. Wu, L.-N. Gao, Y. An, and J. Zhang, "Surface-engineering of glycidyl methacrylated dextran/gelatin microcapsules with thermo-responsive poly(N-isopropylacrylamide) gates for controlled delivery of stromal cell-derived factor-1α," *Biomaterials*, vol. 34, no. 27, pp. 6515–6527, Sep. 2013.

[184] Z.-W. Li, R.-H. Tang, J.-P. Zhang, Z.-P. Tang, W.-S. Qu, W.-H. Zhu, J.-J. Li, M.-J. Xie, D.-S. Tian, and W. Wang, "Inhibiting epidermal growth factor receptor attenuates reactive astrogliosis and improves functional outcome after spinal cord injury in rats," *Neurochem. Int.*, vol. 58, no. 7, pp. 812–819, Jun. 2011.

185] M. Zamani, M. P. Prabhakaran, E. S. Thian, and S. Ramakrishna, "Controlled delivery of stromal derived factor-1α from poly lactic-co-glycolic acid core–shell

particles to recruit mesenchymal stem cells for cardiac regeneration," *J. Colloid Interface Sci.*, vol. 451, pp. 144–152, Aug. 2015.

[186] P. B. Tran, G. Banisadr, D. Ren, A. Chenn, and R. J. Miller, "Chemokine receptor expression by neural progenitor cells in neurogenic regions of mouse brain," *J. Comp. Neurol.*, vol. 500, no. 6, pp. 1007–1034, Feb. 2007.

[187] F. Danhier, E. Ansorena, J. M. Silva, R. Coco, A. Le Breton, and V. Préat, "PLGA-based nanoparticles: An overview of biomedical applications," *J. Controlled Release*, vol. 161, no. 2, pp. 505–522, Jul. 2012.

[188] S. Fredenberg, M. Wahlgren, M. Reslow, and A. Axelsson, "The mechanisms of drug release in poly(lactic-co-glycolic acid)-based drug delivery systems—A review," *Int. J. Pharm.*, vol. 415, no. 1–2, pp. 34–52, Aug. 2011.

[189] J. Panyam and V. Labhasetwar, "Biodegradable nanoparticles for drug and gene delivery to cells and tissue," *Adv. Drug Deliv. Rev.*, vol. 55, no. 3, pp. 329–347, 2003.

[190] M. Azizi, F. Farahmandghavi, M. Joghataei, M. Zandi, M. Imani, M. Bakhtiary, F. A. Dorkoosh, and F. Ghazizadeh, "Fabrication of protein-loaded PLGA nanoparticles: effect of selected formulation variables on particle size and release profile," *J. Polym. Res.*, vol. 20, no. 4, Mar. 2013.

[191] G. Zhu, S. R. Mallery, and S. P. Schwendeman, "Stabilization of proteins encapsulated in injectable poly (lactide-co-glycolide)," *Nat. Biotechnol.*, vol. 18, no. 1, pp. 52–57, 2000.

[192] S. M. Moghimi, A. C. Hunter, and J. C. Murray, "Long-circulating and target-specific nanoparticles: theory to practice," *Pharmacol. Rev.*, vol. 53, no. 2, pp. 283–318, Jun. 2001.

[193] M. S. Cartiera, K. M. Johnson, V. Rajendran, M. J. Caplan, and W. M. Saltzman, "The Uptake and Intracellular Fate of PLGA Nanoparticles in Epithelial Cells," *Biomaterials*, vol. 30, no. 14, pp. 2790–2798, May 2009.

[194] K. T. Householder, D. M. DiPerna, E. P. Chung, G. M. Wohlleb, H. D. Dhruv, M. E. Berens, and R. W. Sirianni, "Intravenous delivery of camptothecin-loaded PLGA nanoparticles for the treatment of intracranial glioma," *Int. J. Pharm.*, vol. 479, no. 2, pp. 374–380, Feb. 2015.

[195] J. Zhou, T. R. Patel, R. W. Sirianni, G. Strohbehn, M.-Q. Zheng, N. Duong, T. Schafbauer, A. J. Huttner, Y. Huang, R. E. Carson, Y. Zhang, D. J. Sullivan, J. M. Piepmeier, and W. M. Saltzman, "Highly penetrative, drug-loaded nanocarriers

improve treatment of glioblastoma," *Proc. Natl. Acad. Sci. U. S. A.*, vol. 110, no. 29, pp. 11751–11756, Jul. 2013.

[196] T. Feczkó, J. Tóth, G. Dósa, and J. Gyenis, "Optimization of protein encapsulation in PLGA nanoparticles," *Chem. Eng. Process. Process Intensif.*, vol. 50, no. 8, pp. 757–765, Aug. 2011.

[197] C. E. Astete and C. M. Sabliov, "Synthesis and characterization of PLGA nanoparticles," *J. Biomater. Sci. Polym. Ed.*, vol. 17, no. 3, pp. 247–289, 2006.

[198] A. N. Ford Versypt, D. W. Pack, and R. D. Braatz, "Mathematical modeling of drug delivery from autocatalytically degradable PLGA microspheres — A review," *J. Controlled Release*, vol. 165, no. 1, pp. 29–37, Jan. 2013.

[199] Y. Fu and W. J. Kao, "Drug Release Kinetics and Transport Mechanisms of Non-degradable and Degradable Polymeric Delivery Systems," *Expert Opin. Drug Deliv.*, vol. 7, no. 4, pp. 429–444, Apr. 2010.

[200] Y. Yeo and K. Park, "Control of encapsulation efficiency and initial burst in polymeric microparticle systems," *Arch. Pharm. Res.*, vol. 27, no. 1, pp. 1–12, 2004.

[201] R. C. Mehta, B. C. Thanoo, and P. P. Deluca, "Peptide containing microspheres from low molecular weight and hydrophilic poly(d,l-lactide-co-glycolide)," *J. Controlled Release*, vol. 41, no. 3, pp. 249–257, Sep. 1996.

[202] H.-Y. Kwon, J.-Y. Lee, S.-W. Choi, Y. Jang, and J.-H. Kim, "Preparation of PLGA nanoparticles containing estrogen by emulsification–diffusion method," *Colloids Surf. Physicochem. Eng. Asp.*, vol. 182, no. 1–3, pp. 123–130, Jun. 2001.

[203] Y.-Y. Yang, T.-S. Chung, and N. Ping Ng, "Morphology, drug distribution, and in vitro release profiles of biodegradable polymeric microspheres containing protein fabricated by double-emulsion solvent extraction/evaporation method," *Biomaterials*, vol. 22, no. 3, pp. 231–241, Feb. 2001.

[204] R. L. McCall and R. W. Sirianni, "PLGA Nanoparticles Formed by Single- or Double-emulsion with Vitamin E-TPGS," *J. Vis. Exp.*, no. 82, Dec. 2013.

[205] A. Kumari, S. K. Yadav, and S. C. Yadav, "Biodegradable polymeric nanoparticles based drug delivery systems," *Colloids Surf. B Biointerfaces*, vol. 75, no. 1, pp. 1–18, Jan. 2010.

[206] A. Lamprecht, N. Ubrich, M. Hombreiro Pérez, C.-M. Lehr, M. Hoffman, and P. Maincent, "Biodegradable monodispersed nanoparticles prepared by pressure homogenization-emulsification," *Int. J. Pharm.*, vol. 184, no. 1, pp. 97–105, Jul. 1999.

[207] M. . Blanco and M. . Alonso, "Development and characterization of protein-loaded poly(lactide-co-glycolide) nanospheres," *Eur. J. Pharm. Biopharm.*, vol. 43, no. 3, pp. 287–294, Jun. 1997.

[208] T. Feczkó, J. Tóth, and J. Gyenis, "Comparison of the preparation of PLGA–BSA nano- and microparticles by PVA, poloxamer and PVP," *Colloids Surf. Physicochem. Eng. Asp.*, vol. 319, no. 1–3, pp. 188–195, Apr. 2008.

[209] C. Berkland, M. King, A. Cox, K. (Kevin) Kim, and D. W. Pack, "Precise control of PLG microsphere size provides enhanced control of drug release rate," *J. Controlled Release*, vol. 82, no. 1, pp. 137–147, Jul. 2002.

[210] B. Mukherjee, K. Santra, G. Pattnaik, and S. Ghosh, "Preparation, characterization and in-vitro evaluation of sustained release protein-loaded nanoparticles based on biodegradable polymers," *Int. J. Nanomedicine*, vol. 3, no. 4, pp. 487–496, 2008.

[211] G. T. S. Kirby, L. J. White, C. V. Rahman, H. C. Cox, O. Qutachi, F. R. A. J. Rose, D. W. Hutmacher, K. M. Shakesheff, and M. A. Woodruff, "PLGA-Based Microparticles for the Sustained Release of BMP-2," *Polymers*, vol. 3, no. 1, pp. 571–586, Mar. 2011.

[212] H. Sah, R. Toddywala, and Y. W. Chien, "Continuous release of proteins from biodegradable microcapsules and in vivo evaluation of their potential as a vaccine adjuvant," *J. Controlled Release*, vol. 35, no. 2–3, pp. 137–144, Aug. 1995.

[213] C. Wischke and S. P. Schwendeman, "Principles of encapsulating hydrophobic drugs in PLA/PLGA microparticles," *Int. J. Pharm.*, vol. 364, no. 2, pp. 298–327, Dec. 2008.

[214] S. Cohen, T. Yoshioka, M. Lucarelli, L. H. Hwang, and R. Langer, "Controlled Delivery Systems for Proteins Based on Poly(Lactic/Glycolic Acid) Microspheres," *Pharm. Res.*, vol. 8, no. 6, pp. 713–720, Jun. 1991.

[215] J. Siepmann, K. Elkharraz, F. Siepmann, and D. Klose, "How autocatalysis accelerates drug release from PLGA-based microparticles: a quantitative treatment," *Biomacromolecules*, vol. 6, no. 4, pp. 2312–2319, Aug. 2005.

[216] J. L. Chen, M. K. Yeh, and C. H. Chiang, "The mechanism of surface-indented protein-loaded PLGA microparticle formation: the effects of salt (NaCl) on the solidification process," *J. Microencapsul.*, vol. 21, no. 8, pp. 877–888, Dec. 2004.

[217] M. Faul, M. M. Wald, W. Rutland-Brown, E. E. Sullivent, and R. W. Sattin, “Using a Cost-Benefit Analysis to Estimate Outcomes of a Clinical Treatment Guideline: Testing the Brain Trauma Foundation Guidelines for the Treatment of Severe Traumatic Brain Injury:,” *J. Trauma Inj. Infect. Crit. Care*, vol. 63, no. 6, pp. 1271–1278, Dec. 2007.

[218] S. Li, M. Wei, Z. Zhou, B. Wang, X. Zhao, and J. Zhang, “SDF-1α induces angiogenesis after traumatic brain injury,” *Brain Res.*, vol. 1444, pp. 76–86, Mar. 2012.

[219] N. L. Sundholm-Peters, H. K. C. Yang, G. E. Goings, A. S. Walker, and F. G. Szele, “Subventricular zone neuroblasts emigrate toward cortical lesions,” *J. Neuropathol. Exp. Neurol.*, vol. 64, no. 12, pp. 1089–1100, Dec. 2005.

[220] S. Chen, J. D. Pickard, and N. G. Harris, “Time course of cellular pathology after controlled cortical impact injury,” *Exp. Neurol.*, vol. 182, no. 1, pp. 87–102, Jul. 2003.

[221] C. Moon, M. Ahn, S. Kim, J.-K. Jin, K.-B. Sim, H.-M. Kim, M.-Y. Lee, and T. Shin, “Temporal patterns of the embryonic intermediate filaments nestin and vimentin expression in the cerebral cortex of adult rats after cryoinjury,” *Brain Res.*, vol. 1028, no. 2, pp. 238–242, Dec. 2004.

[222] D. Aprili, O. Bandschapp, C. Rochlitz, A. Urwyler, and W. Ruppen, “Serious complications associated with external intrathecal catheters used in cancer pain patients: a systematic review and meta-analysis.,” *Anesthesiology*, vol. 111, no. 6, pp. 1346–1355, 2009.

[223] T. C. Lim, S. Rokkappanavar, W. S. Toh, L.-S. Wang, M. Kurisawa, and M. Spector, “Chemotactic recruitment of adult neural progenitor cells into multifunctional hydrogels providing sustained SDF-1 release and compatible structural support,” *FASEB J.*, vol. 27, no. 3, pp. 1023–1033, Mar. 2013.

[224] R. W. Sirianni, M.-Q. Zheng, T. R. Patel, T. Shafbauer, J. Zhou, W. M. Saltzman, R. E. Carson, and Y. Huang, “Radiolabeling of poly(lactic-co-glycolic acid) (PLGA) nanoparticles with biotinylated F-18 prosthetic groups and imaging of their delivery to the brain with positron emission tomography,” *Bioconjug. Chem.*, vol. 25, no. 12, pp. 2157–2165, Dec. 2014.

[225] J. Zhang and M. Saltzman, “Engineering biodegradable nanoparticles for drug and gene delivery,” *Chem. Eng. Prog.*, vol. 109, no. 3, pp. 25–30, Mar. 2013.

[226] P. Misra, D. Lebeche, H. Ly, M. Schwarzkopf, G. Diaz, R. J. Hajjar, A. D. Schecter, and J. V. Frangioni, “Quantitation of CXCR4 Expression in Myocardial Infarction

Using 99mTc-Labeled SDF-1," *J. Nucl. Med.*, vol. 49, no. 6, pp. 963–969, May 2008.

[227] A. S. Pandit, D. J. Wilson, and D. S. Feldman, "Fibrin scaffold as an effective vehicle for the delivery of acidic fibroblast growth factor (FGF-1)," *J. Biomater. Appl.*, vol. 14, no. 3, pp. 229–242, Jan. 2000.

[228] P. P. Spicer and A. G. Mikos, "Fibrin Glue as a Drug Delivery System," *J. Control. Release Off. J. Control. Release Soc.*, vol. 148, no. 1, pp. 49–55, Nov. 2010.

[229] M. D. Wood, G. H. Borschel, and S. E. Sakiyama-Elbert, "Controlled release of glial-derived neurotrophic factor from fibrin matrices containing an affinity-based delivery system," *J. Biomed. Mater. Res. A*, vol. 89A, no. 4, pp. 909–918, 2009.

[230] S. E. Sakiyama-Elbert and J. A. Hubbell, "Controlled release of nerve growth factor from a heparin-containing fibrin-based cell ingrowth matrix," *J. Controlled Release*, vol. 69, no. 1, pp. 149–158, Oct. 2000.

[231] K. Vulic and M. S. Shoichet, "Affinity-Based Drug Delivery Systems for Tissue Repair and Regeneration," *Biomacromolecules*, vol. 15, no. 11, pp. 3867–3880, Nov. 2014.

[232] A. Breen, T. O'Brien, and A. Pandit, "Fibrin as a delivery system for therapeutic drugs and biomolecules," *Tissue Eng. Part B Rev.*, vol. 15, no. 2, pp. 201–214, 2009.

[233] G. S. Schultz and A. Wysocki, "Interactions between extracellular matrix and growth factors in wound healing," *Wound Repair Regen. Off. Publ. Wound Heal. Soc. Eur. Tissue Repair Soc.*, vol. 17, no. 2, pp. 153–162, Apr. 2009.

[234] C. Wong, E. Inman, R. Spaethe, and S. Helgerson, "Fibrin-based biomaterials to deliver human growth factors," *Thromb. Haemost.*, vol. 89, no. 3, pp. 573–582, Mar. 2003.

[235] H. Azari, S. Sharififar, M. Rahman, S. Ansari, and B. A. Reynolds, "Establishing Embryonic Mouse Neural Stem Cell Culture Using the Neurosphere Assay," *J. Vis. Exp. JoVE*, no. 47, Jan. 2011.

[236] T. Aoto, N. Saitoh, T. Ichimura, H. Niwa, and M. Nakao, "Nuclear and chromatin reorganization in the MHC-Oct3/4 locus at developmental phases of embryonic stem cell differentiation," *Dev. Biol.*, vol. 298, no. 2, pp. 354–367, Oct. 2006.

[237] T. Riedel, E. Brynda, J. E. Dyr, and M. Houska, “Controlled preparation of thin fibrin films immobilized at solid surfaces,” *J. Biomed. Mater. Res. A*, vol. 88A, no. 2, pp. 437–447, Feb. 2009.

[238] S. E. Stabenfeldt, M. Gourley, L. Krishnan, J. B. Hoying, and T. H. Barker, “Engineering fibrin polymers through engagement of alternative polymerization mechanisms,” *Biomaterials*, vol. 33, no. 2, pp. 535–544, Jan. 2012.

[239] W. Asghar, M. Islam, A. S. Wadajkar, Y. Wan, A. Ilyas, K. T. Nguyen, and S. M. Iqbal, “PLGA Micro- and Nanoparticles Loaded Into Gelatin Scaffold for Controlled Drug Release,” *IEEE Trans. Nanotechnol.*, vol. 11, no. 3, pp. 546–553, May 2012.

[240] D. J. Hines and D. L. Kaplan, “Poly (lactic-co-glycolic acid) controlled release systems: experimental and modeling insights,” *Crit. Rev. Ther. Drug Carrier Syst.*, vol. 30, no. 3, pp. 257–276, 2013.

[241] A. M. Robin, Z. G. Zhang, L. Wang, R. L. Zhang, M. Katakowski, L. Zhang, Y. Wang, C. Zhang, and M. Chopp, “Stromal cell-derived factor 1alpha mediates neural progenitor cell motility after focal cerebral ischemia,” *J. Cereb. Blood Flow Metab. Off. J. Int. Soc. Cereb. Blood Flow Metab.*, vol. 26, no. 1, pp. 125–134, Jan. 2006.

[242] S. Bhakta, P. Hong, and O. Koc, “The surface adhesion molecule CXCR4 stimulates mesenchymal stem cell migration to stromal cell-derived factor-1 in vitro but does not decrease apoptosis under serum deprivation,” *Cardiovasc. Revasc. Med.*, vol. 7, no. 1, pp. 19–24, Jan. 2006.

[243] R. S. Klein, J. B. Rubin, H. D. Gibson, E. N. DeHaan, X. Alvarez-Hernandez, R. A. Segal, and A. D. Luster, “SDF-1α induces chemotaxis and enhances Sonic hedgehog-induced proliferation of cerebellar granule cells,” *Development*, vol. 128, no. 11, pp. 1971–1981, Jun. 2001.

[244] N. Signoret, J. Oldridge, A. Pelchen-Matthews, P. J. Klasse, T. Tran, L. F. Brass, M. M. Rosenkilde, T. W. Schwartz, W. Holmes, W. Dallas, M. A. Luther, T. N. C. Wells, J. A. Hoxie, and M. Marsh, “Phorbol Esters and SDF-1 Induce Rapid Endocytosis and Down Modulation of the Chemokine Receptor CXCR4,” *J. Cell Biol.*, vol. 139, no. 3, pp. 651–664, Nov. 1997.

[245] A. Giteau, M. C. Venier-Julienne, A. Aubert-Pouëssel, and J. P. Benoit, “How to achieve sustained and complete protein release from PLGA-based microparticles?,” *Int. J. Pharm.*, vol. 350, no. 1–2, pp. 14–26, Feb. 2008.

[246] N. S. P. Edith J. A.M Schlicher, “Preparation and characterisation of poly(D,L-lactic-co-glycolic acid) microspheres containing desferrioxamine,” *Int. J. Pharm.*, vol. 153, no. 2, pp. 235–245, 1997.

[247] J. C. Stanwick, M. D. Baumann, and M. S. Shoichet, “Enhanced neurotrophin-3 bioactivity and release from a nanoparticle-loaded composite hydrogel,” *J. Controlled Release*, vol. 160, no. 3, pp. 666–675, Jun. 2012.

[248] D.-H. Kim and D. C. Martin, “Sustained release of dexamethasone from hydrophilic matrices using PLGA nanoparticles for neural drug delivery,” *Biomaterials*, vol. 27, no. 15, pp. 3031–3037, May 2006.

[249] P. G. Campbell, S. K. Durham, J. D. Hayes, A. Suwanichkul, and D. R. Powell, “Insulin-like Growth Factor-binding Protein-3 Binds Fibrinogen and Fibrin,” *J. Biol. Chem.*, vol. 274, no. 42, pp. 30215–30221, Oct. 1999.

[250] M. W. Mosesson, “Fibrinogen and fibrin structure and functions,” *J. Thromb. Haemost. JTH*, vol. 3, no. 8, pp. 1894–1904, Aug. 2005.

[251] I. Catelas, J. F. Dwyer, and S. Helgerson, “Controlled Release of Bioactive Transforming Growth Factor Beta-1 from Fibrin Gels In Vitro,” *Tissue Eng. Part C Methods*, vol. 14, no. 2, pp. 119–128, Jun. 2008.

[252] J. M. Zuidema, C. J. Rivet, R. J. Gilbert, and F. A. Morrison, “A protocol for rheological characterization of hydrogels for tissue engineering strategies,” *J. Biomed. Mater. Res. B Appl. Biomater.*, vol. 102, no. 5, pp. 1063–1073, Jul. 2014.

[253] J. Wedgwood, A. J. Freemont, and N. Tirelli, “Rheological and Turbidity Study of Fibrin Hydrogels,” *Macromol. Symp.*, vol. 334, no. 1, pp. 117–125, Dec. 2013.

[254] E. A. Ryan, L. F. Mockros, J. W. Weisel, and L. Lorand, “Structural Origins of Fibrin Clot Rheology,” *Biophys. J.*, vol. 77, no. 5, pp. 2813–2826, Nov. 1999.

[255] Stabenfeldt, C. Addington, D. Dutta, and A. Roussas, “Endogenous Repair Signaling after Brain Injury and Complementary Bioengineering Approaches to Enhance Neural Regeneration,” *Biomark. Insights*, p. 43, May 2015.

[256] K. Christie and A. Turnley, “Regulation of endogenous neural stem/progenitor cells for neural repair—factors that promote neurogenesis and gliogenesis in the normal and damaged brain,” *Front. Cell. Neurosci.*, vol. 6, p. 70, 2013.

[257] K. J. Dixon, M. H. Theus, C. M. Nelersa, J. Mier, L. G. Travieso, T.-S. Yu, S. G. Kernie, and D. J. Liebl, “Endogenous Neural Stem/Progenitor Cells Stabilize the

Cortical Microenvironment after Traumatic Brain Injury," *J. Neurotrauma*, vol. 32, no. 11, pp. 753–764, Jun. 2015.

[258] D. Dutta, C. Fauer, H. L. Mullenaux, and S. E. Stabenfeldt, "Tunable Controlled Release of Bioactive SDF-1α via Protein Specific Interactions within Fibrin/Nanoparticle Composites," *J. Mater. Chem. B*, Aug. 2015.

[259] D. Sun, M. R. Bullock, N. Altememi, Z. Zhou, S. Hagood, A. Rolfe, M. J. McGinn, R. Hamm, and R. J. Colello, "The Effect of Epidermal Growth Factor in the Injured Brain after Trauma in Rats," *J. Neurotrauma*, vol. 27, no. 5, pp. 923–938, May 2010.

[260] T. Laursen, "Clinical pharmacological aspects of growth hormone administration," *Growth Horm. IGF Res.*, vol. 14, no. 1, pp. 16–44, Feb. 2004.

[261] B. J. Bhattacharyya, G. Banisadr, H. Jung, D. Ren, D. G. Cronshaw, Y. Zou, and R. J. Miller, "The Chemokine Stromal Cell-Derived Factor-1 Regulates GABAergic Inputs to Neural Progenitors in the Postnatal Dentate Gyrus," *J. Neurosci.*, vol. 28, no. 26, pp. 6720–6730, Jun. 2008.

[262] A. Belmadani, H. Jung, D. Ren, and R. J. Miller, "The chemokine SDF-1/CXCL12 regulates the migration of melanocyte progenitors in mouse hair follicles," *Differ. Res. Biol. Divers.*, vol. 77, no. 4, pp. 395–411, Apr. 2009.

[263] C. E. Dixon, G. L. Clifton, J. W. Lighthall, A. A. Yaghmai, and R. L. Hayes, "A controlled cortical impact model of traumatic brain injury in the rat," *J. Neurosci. Methods*, vol. 39, no. 3, pp. 253–262, Oct. 1991.

[264] C. R. Taylor and R. M. Levenson, "Quantification of immunohistochemistry? Issues concerning methods, utility and semiquantitative assessment II," *Histopathology*, vol. 49, no. 4, pp. 411–424, Oct. 2006.

[265] L. Xu, Y. Li, H. Sun, D. Li, and T. Hou, "Structural basis of the interactions between CXCR4 and CXCL12/SDF-1 revealed by theoretical approaches," *Mol. Biosyst.*, vol. 9, no. 8, pp. 2107–2117, Jul. 2013.

[266] M.-L. Humpert, M. Tzouros, S. Thelen, A. Bignon, A. Levoye, F. Arenzana-Seisdedos, K. Balabanian, F. Bachelerie, H. Langen, and M. Thelen, "Complementary methods provide evidence for the expression of CXCR7 on human B cells," *Proteomics*, vol. 12, no. 12, pp. 1938–1948, Jun. 2012.

[267] K. Luker, M. Gupta, and G. Luker, "Bioluminescent CXCL12 fusion protein for cellular studies of CXCR4 and CXCR7," *BioTechniques*, vol. 47, no. 1, pp. 625–632, Jul. 2009.

[268] B. Boldajipour, H. Mahabaleshwar, E. Kardash, M. Reichman-Fried, H. Blaser, S. Minina, D. Wilson, Q. Xu, and E. Raz, "Control of chemokine-guided cell migration by ligand sequestration," *Cell*, vol. 132, no. 3, pp. 463–473, Feb. 2008.

[269] T. Kawamura, B. Stephens, L. Qin, X. Yin, M. R. Dores, T. H. Smith, N. Grimsey, R. Abagyan, J. Trejo, I. Kufareva, M. M. Fuster, C. L. Salanga, and T. M. Handel, "A General Method for Site Specific Fluorescent Labeling of Recombinant Chemokines," *PLoS ONE*, vol. 9, no. 1, Jan. 2014.

[270] M. Shirozu, T. Nakano, J. Inazawa, K. Tashiro, H. Tada, T. Shinohara, and T. Honjo, "Structure and chromosomal localization of the human stromal cell-derived factor 1 (SDF1) gene," *Genomics*, vol. 28, no. 3, pp. 495–500, Aug. 1995.

[271] A. A. Ardelt, B. J. Bhattacharyya, A. Belmadani, D. Ren, and R. J. Miller, "Stromal derived growth factor-1 (CXCL12) modulates synaptic transmission to immature neurons during post-ischemic cerebral repair," *Exp. Neurol.*, vol. 248, pp. 246–253, Oct. 2013.

[272] G. Banisadr, P. Fontanges, F. Haour, P. Kitabgi, W. Rostène, and S. Mélik Parsadaniantz, "Neuroanatomical distribution of CXCR4 in adult rat brain and its localization in cholinergic and dopaminergic neurons," *Eur. J. Neurosci.*, vol. 16, no. 9, pp. 1661–1671, Nov. 2002.

[273] D. J. Wolak and R. G. Thorne, "Diffusion of Macromolecules in the Brain: Implications for Drug Delivery," *Mol. Pharm.*, vol. 10, no. 5, pp. 1492–1504, May 2013.

[274] E. J. Mufson, J. S. Kroin, Y.-T. Liu, T. Sobreviela, R. D. Penn, J. A. Miller, and J. H. Kordower, "Intrastriatal and intraventricular infusion of brain-derived neurotrophic factor in the cynomologous monkey: Distribution, retrograde transport and co-localization with substantia nigra dopamine-containing neurons," *Neuroscience*, vol. 71, no. 1, pp. 179–191, Mar. 1996.

[275] D. P. Ankeny, D. M. McTigue, Z. Guan, Q. Yan, O. Kinstler, B. T. Stokes, and L. B. Jakeman, "Pegylated brain-derived neurotrophic factor shows improved distribution into the spinal cord and stimulates locomotor activity and morphological changes after injury," *Exp. Neurol.*, vol. 170, no. 1, pp. 85–100, Jul. 2001.

[276] P. Menei, V. Daniel, C. Montero-Menei, M. Brouillard, A. Pouplard-Barthelaix, and J. P. Benoit, "Biodegradation and brain tissue reaction to poly(D,L-lactide-co-glycolide) microspheres," *Biomaterials*, vol. 14, no. 6, pp. 470–478, May 1993.

[277] R. K. Stumm, J. Rummel, V. Junker, C. Culmsee, M. Pfeiffer, J. Krieglstein, V. Höllt, and S. Schulz, "A Dual Role for the SDF-1/CXCR4 Chemokine Receptor System in Adult Brain: Isoform-Selective Regulation of SDF-1 Expression Modulates CXCR4-Dependent Neuronal Plasticity and Cerebral Leukocyte Recruitment after Focal Ischemia," *J. Neurosci.*, vol. 22, no. 14, pp. 5865–5878, Jul. 2002.

[278] X. Liu, B. Duan, Z. Cheng, X. Jia, L. Mao, H. Fu, Y. Che, L. Ou, L. Liu, and D. Kong, "SDF-1/CXCR4 axis modulates bone marrow mesenchymal stem cell apoptosis, migration and cytokine secretion," *Protein Cell*, vol. 2, no. 10, pp. 845–854, Oct. 2011.

[279] R. Bonavia, A. Bajetto, S. Barbero, P. Pirani, T. Florio, and G. Schettini, "Chemokines and their receptors in the CNS: expression of CXCL12/SDF-1 and CXCR4 and their role in astrocyte proliferation," *Toxicol. Lett.*, vol. 139, no. 2–3, pp. 181–189, Apr. 2003.

[280] J. F. Ji, B. P. He, S. T. Dheen, and S. S. W. Tay, "Expression of chemokine receptors CXCR4, CCR2, CCR5 and CX3CR1 in neural progenitor cells isolated from the subventricular zone of the adult rat brain," *Neurosci. Lett.*, vol. 355, no. 3, pp. 236–240, Jan. 2004.

[281] A. Dunac, C. Frelin, M. Popolo-Blondeau, M. Chatel, M. H. Mahagne, and P. J.-M. Philip, "Neurological and functional recovery in human stroke are associated with peripheral blood CD34+ cell mobilization," *J. Neurol.*, vol. 254, no. 3, pp. 327–332, Mar. 2007.

[282] D. J. Ceradini and G. C. Gurtner, "Homing to hypoxia: HIF-1 as a mediator of progenitor cell recruitment to injured tissue," *Trends Cardiovasc. Med.*, vol. 15, no. 2, pp. 57–63, Feb. 2005.

[283] E. E. McCandless, M. Budde, J. R. Lees, D. Dorsey, E. Lyng, and R. S. Klein, "IL-1R signaling within the CNS regulates CXCL12 expression at the blood-brain barrier and disease severity during experimental autoimmune encephalomyelitis," *J. Immunol. Baltim. Md 1950*, vol. 183, no. 1, pp. 613–620, Jul. 2009.

[284] Z. Liang, J. Brooks, M. Willard, K. Liang, Y. Yoon, S. Kang, and H. Shim, "CXCR4/CXCL12 axis promotes VEGF-mediated tumor angiogenesis through Akt signaling pathway," *Biochem. Biophys. Res. Commun.*, vol. 359, no. 3, pp. 716–722, Aug. 2007.

[285] W. X. Hong, M. S. Hu, M. Esquivel, G. Y. Liang, R. C. Rennert, A. McArdle, K. J. Paik, D. Duscher, G. C. Gurtner, H. P. Lorenz, and M. T. Longaker, "The Role of Hypoxia-Inducible Factor in Wound Healing," *Adv. Wound Care*, vol. 3, no. 5, pp. 390–399, May 2014.

[286] C. Hitchon, K. Wong, G. Ma, J. Reed, D. Lyttle, and H. El-Gabalawy, "Hypoxia-induced production of stromal cell–derived factor 1 (CXCL12) and vascular endothelial growth factor by synovial fibroblasts," *Arthritis Rheum.*, vol. 46, no. 10, pp. 2587–2597, Oct. 2002.

[287] O. Salvucci, L. Yao, S. Villalba, A. Sajewicz, S. Pittaluga, and G. Tosato, "Regulation of endothelial cell branching morphogenesis by endogenous chemokine stromal-derived factor-1," *Blood*, vol. 99, no. 8, pp. 2703–11, May 2002.

[288] R. Salcedo, K. Wasserman, H. A. Young, M. C. Grimm, O. M. Z. Howard, M. R. Anver, H. K. Kleinman, W. J. Murphy, and J. J. Oppenheim, "Vascular endothelial growth factor and basic fibroblast growth factor induce expression of CXCR4 on human endothelial cells: In vivo neovascularization induced by stromal-derived factor-1alpha," *Am. J. Pathol.*, vol. 154, no. 4, pp. 1125–35, May 1999.

[289] R. Salcedo and J. J. Oppenheim, "Role of Chemokines in Angiogenesis: CXCL12/SDF-1 and CXCR4 Interaction, a Key Regulator of Endothelial Cell Responses," *Microcirculation*, vol. 10, no. 3–4, pp. 359–370, Jan. 2010.

[290] S. K. Gupta, P. G. Lysko, K. Pillarisetti, E. Ohlstein, and J. M. Stadel, "Chemokine receptors in human endothelial cells. Functional expression of CXCR4 and its transcriptional regulation by inflammatory cytokines," *J. Biol. Chem.*, vol. 273, no. 7, pp. 4282–4287, Feb. 1998.

[291] K. K. Y. Liu and K. Dorovini-Zis, "Regulation of CXCL12 and CXCR4 expression by human brain endothelial cells and their role in CD4+ and CD8+ T cell adhesion and transendothelial migration," *J. Neuroimmunol.*, vol. 215, no. 1–2, pp. 49–64, Oct. 2009.

[292] I. Petit, M. Szyper-Kravitz, A. Nagler, M. Lahav, A. Peled, L. Habler, T. Ponomaryov, R. S. Taichman, F. Arenzana-Seisdedos, N. Fujii, J. Sandbank, D. Zipori, and T. Lapidot, "G-CSF induces stem cell mobilization by decreasing bone marrow SDF-1 and up-regulating CXCR4," *Nat. Immunol.*, vol. 3, no. 7, pp. 687–694, Jul. 2002.

[293] W. Wang, X. Wang, A. C. Ward, I. P. Touw, and A. D. Friedman, "C/EBPalpha and G-CSF receptor signals cooperate to induce the myeloperoxidase and neutrophil elastase genes," *Leukemia*, vol. 15, no. 5, pp. 779–786, May 2001.

[294] T. H. Lee, J. Wang, and C.-H. Wang, "Double-walled microspheres for the sustained release of a highly water soluble drug: characterization and irradiation studies," *J. Controlled Release*, vol. 83, no. 3, pp. 437–452, 2002.

[295] E. C. Tan, R. Lin, and C.-H. Wang, “Fabrication of double-walled microspheres for the sustained release of doxorubicin,” *J. Colloid Interface Sci.*, vol. 291, no. 1, pp. 135–143, Nov. 2005.

[296] E. J. Pollauf and D. W. Pack, “Use of thermodynamic parameters for design of double-walled microsphere fabrication methods,” *Biomaterials*, vol. 27, no. 14, pp. 2898–2906, May 2006.

[297] Y. Xia, P. F. Ribeiro, and D. W. Pack, “Controlled protein release from monodisperse biodegradable double-wall microspheres of controllable shell thickness,” *J. Controlled Release*, vol. 172, no. 3, pp. 707–714, Dec. 2013.

[298] W. Yuan and Z. Liu, “Controlled-release and preserved bioactivity of proteins from (self-assembled) core-shell double-walled microspheres,” *Int. J. Nanomedicine*, p. 257, Jan. 2012.

[299] H. Tan and J. Ye, “Surface morphology and in vitro release performance of double-walled PLLA/PLGA microspheres entrapping a highly water-soluble drug,” *Appl. Surf. Sci.*, vol. 255, no. 2, pp. 353–356, Nov. 2008.

[300] L. E. Kokai, H. Tan, S. Jhunjhunwala, S. R. Little, J. W. Frank, and K. G. Marra, “Protein bioactivity and polymer orientation is affected by stabilizer incorporation for double-walled microspheres,” *J. Controlled Release*, vol. 141, no. 2, pp. 168–176, Jan. 2010.

[301] Q. Xu, S. E. Chin, C.-H. Wang, and D. W. Pack, “Mechanism of drug release from double-walled PDLLA(PLGA) microspheres,” *Biomaterials*, vol. 34, no. 15, pp. 3902–3911, May 2013.